ADSORPTION OF SULFUR DIOXIDE AND REDUCTION OF SULFATE ON ALUMINA AND ALKALI-ALUMINA AT HIGH TEMPERATURES

Thesis by

Sergio Edelstein

In Partial Fulfillment of the Requirements

for the Degree of

Doctor of Philosophy

California Institute of Technology

Pasadena, California

1987

(Submitted November 3, 1986)

To my mother,

who showed me the way.

Parve – nec invideo – sine me, liber, ibis in urbem...

Vade, liber, verbisque meis loca grata saluta...

Publius Ovidius Naso, *Tristia*, 8 AD.

ACKNOWLEDGEMENTS

I wish to express my gratitude to my thesis advisor, Dr. George R. Gavalas, who gave me support throughout the course of this project while allowing me the freedom to pursue my research interests.

I am also grateful to Dr. William Reynolds of Stanford University, who taught me all about STANJAN, his thermodynamic equilibrium program, and to Dr. Paula Grunthaner of the Jet Propulsion Laboratory, who was always ready to run *one more sample* at JPL's X-ray photoelectron spectroscopy facilities.

Part of the work presented in Section 10.1 was done in collaboration with Teri Weston. I would like to acknowledge Teri's assistance during the early stages of the project. The results presented in Chapter 3 were obtained using an experimental system constructed by Scott Northrop.

Many members of the staff at the Caltech Chemical Engineering and Chemistry Departments contributed to this project. In particular, I wish to thank Patrick Koen for his assistance with the electron microscope, George Griffith for his help with the experimental system, Tom Dunn for resuscitating the electronic equipment, and Donna Johnson for her help with the typing.

I gratefully acknowledge the financial support provided by the Union Oil Company Foundation, the Josephine de Karman Fellowship Trust, the National Science Foundation, and the California Institute of Technology.

I am indebted to my family in Argentina and my friends and colleagues, both at Caltech and in the world, who were a never-ending source of moral support.

I owe my greatest debt to Batia, for more things than I can express here. She made it all worthwhile.

ABSTRACT

Several interrelated problems in connection with the treatment of sulfur dioxide at temperatures between 700 and 800°C were studied. The interaction of SO_2 with Al_2O_3 was studied experimentally using B.E.T., thermogravimetry and temperature-programmed desorption. Adsorption takes place through a wide range of binding energies, with some SO_2 adsorbing irreversibly at temperatures below 800°C. The amount adsorbed depends on the surface history and thermal treatment. An adsorption isotherm based on a bimodal energy distribution provides an adequate description of the equilibrium process.

The chemical composition, sulfation and regeneration of an alkali-alumina sorbent for sulfur dioxide were studied using thermogravimetry, gas chromatography, and X-ray photoelectron spectroscopy. The active sorbent consists of a thin layer of sodium and lithium aluminates supported on alumina. The rate of sulfation is proportional to the SO_2 concentration in the gas, up to $[SO_2] \approx$ 5000 ppm. The activation energy of the sulfation is $E = 21.6$ kcal/mole. The sulfated sorbent was regenerated by reduction with CO at 700-800°C. Sulfur removal from the sorbent and distribution of gaseous products were measured at different alkali loadings, temperatures and CO concentrations. The reduction takes place in two consecutive stages through a complex reaction network in which the alumina support plays a decisive role, both as a reactant and as a catalyst. A simplified reaction network is used as a basis for a kinetic model that provides an adequate description of the reduction process at moderate sorbent loadings.

CONTENTS

LIST OF TABLES

LIST OF FIGURES

1. INTRODUCTION

The combustion of coal constitutes the major source of sulfur dioxide emissions into the atmosphere, with smaller contributions from petroleum combustion, ore smelting and petroleum refining [5,15]. Efforts to abate atmospheric pollution have led to research and development of a large number of desulfurization processes, following two basic approaches. The first is fuel desulfurization, which can be accomplished by physically cleaning or washing the coal prior to combustion, or through chemical desulfurization [10]. The second approach is the desulfurization of combustion gases, and is currently employed in various fluidized-bed combustion (FBC) and flue gas desulfurization (FGD) processes.

Nonregenerable FGD processes generally involve wet or dry scrubbing with alkaline slurries or a dry alkali powder. Typical reagents used are limestone, dolomite, lime, and soda ash. In order to avoid the solids disposal problem associated with nonregenerable processes, several regenerable sorbents have been proposed. Some of the materials that have been investigated are *alkalized alumina* (an active form of sodium aluminate) [1,14,16], molten alkali carbonates [11], calcium silicates [19], and metal oxides supported on alumina [2,4,17,18]. These sorbents react with SO_2 at temperatures between 400 and 800^oC to form stable sulfates :

$$2NaAlO_2 + SO_2 + \tfrac{1}{2}O_2 \rightarrow Na_2SO_4 + Al_2O_3$$

$$K_2CO_3 + SO_2 + \tfrac{1}{2}O_2 \rightarrow K_2SO_4 + CO_2$$

$$CaSiO_3 + SO_2 + \tfrac{1}{2}O_2 \rightarrow CaSO_4 + SiO_2$$

etc.

Regeneration can be accomplished by reducing the sulfated sorbent with CO or H_2. Under suitable conditions the reduction may lead to the production of elemental sulfur, a useful by-product which can be commercialized or converted to other sulfur products such as sulfuric acid. In most cases the detailed reaction pathways involved in the regeneration remain unknown or very poorly understood.

The direct reduction of SO_2 to elemental sulfur on alumina or alumina-based catalysts at temperatures between 400 and 600°C according to :

$$SO_2 + 2CO \rightarrow \frac{1}{2}S_2 + 2CO_2 \qquad (1.1)$$

has recently received increasing attention [7,12]. This attractive alternative would accomplish the simultaneous removal of SO_2 and NO_X [13] through a dry, simple process. Considerable effort has been devoted to understanding the mechanism of reaction 1.1 [8,9], as well as that of the Claus reaction [3,6] :

$$SO_2 + 2H_2S \rightarrow \frac{3}{2}S_2 + 2H_2O. \qquad (1.2)$$

This reaction constitutes a widely used commercial process for sulfur recovery from concentrated ($\geq 20\%$) H_2S streams at 200 to 250°C. In both cases the complex nature of the active sites on the alumina surface was found to play a decisive role.

The present thesis is centered around the use and regeneration of an alkali-alumina sorbent for the removal of SO_2 at high temperatures. Preliminary work

[18] indicated that this sorbent can be repeatedly regenerated by reduction with CO at temperatures between 700 and 800°C. The objectives of the present work were to study the effect of sorbent composition and operating conditions on the regeneration, and to gain insight into the detailed chemistry of the regeneration and the role of the alumina surface. The thesis was divided into two parts. In Part I (Chapters 2 through 6) the interaction of SO_2 with alumina is studied experimentally. This problem is relevant to the mechanism of sorbent regeneration and also of reactions 1.1 and 1.2 [3,6]. This part constitutes a self-contained unit, but its results are used in subsequent chapters.

In Part II (Chapters 7 through 11), the preparation, chemical composition, sulfation and regeneration of the sorbent are analyzed and discussed. Chapter 10 deals with the problem of sorbent regeneration: the nature of the species involved, reaction network and effect of operating conditions are discussed, and a simple kinetic model is proposed. The problems are presented in order of increasing complexity, which does not necessarily correspond to the one in which they were attacked.

Two microprocessor-based systems were developed to carry out the data acquisition and processing and to program and control the reaction temperature. These systems are described in the appendices.

REFERENCES

[1] Bienstock, D.J., Field, J.H., and Myers, J.G., *BuMines Rept. Invest. 7021*, July 1967.

[2] Dautzenberg, F.M., Naber, J.E., and van Ginneken, A.J.J., *Chem. Eng. Progr.*, **67**(8), 86, 1971.

[3] Deo, A.V., Dalla Lana, I.G., and Habgood, H.W., *J. Catal.*, **21**, 270, 1971.

[4] Groenendaal, W., Naber, J.E., and Pohlenz, J.B., *AIChE Symposium Series*, **72**(156),12, 1973.

[5] Hangebrauck, R.P., and Spaite, P.W., *The Oxides of Sulfur. Problems and Possible Methods of Control*, 6th Annual Sanitary and Water Resoruces Eng. Conf., June 1967.

[6] Karge, H.G., and Dalla Lana, I.G., *J. Phys. Chem.*, **88**(8), 1538, 1984.

[7] Khalafalla, S.E., Foerster, E.F., and Haas, L.A., *Ind. Eng. Chem. Prod. Res. Develop.*, **10**(2), 133, 1971.

[8] Khalafalla, S.E., and Haas, L.A., *J. Catal.*, **24**, 115, 1972.

[9] Khalafalla, S.E., and Haas, L.A., *J. Catal.*, **24**, 121, 1972.

[10] Meyers, R.A., *Coal Desulfurization*, Marcel Dekker, New York, 1977.

[11] Oldenkamp, R.D., and Margolin, E.D., *Chem. Eng. Progress*, **65**(11), 73, 1969.

[12] Querido, R., and Short, W.L., *Ind. Eng. Chem. Process Des. Develop.*, **12**(1), 10, 1973.

[13] Ryason, P.R., Harkins, J., *J. APCA*, **17**(12), 796, 1967.

[14] Schlesinger, M.D., and Illig, E.G., *Chem. Eng. Progr. Symposium Series*, **67**(115), 46, 1971.

[15] Singer, S.F., ed., *Global Effects of Environmental Pollution*, Springer-Verag, New York, 1970.

[16] Town, J.W., Paige, J.I., and Russell, J.H., *Chem. Eng. Progr. Symposium Series*, **66**(105), 260, 1970.

[17] Vogel, R.F., Mitchell, B.R., and Massoth, F.E., *Env. Sci. Tech.*, **8**(5), 432, 1974.

[18] Weston, T.A., *PhD Dissertation*, California Inst. of Tech., 1985.

[19] Yang, R.T., and Shen, M.S., *AIChE J.*, **25**(5), 811, 1979.

PART I

THE HIGH-TEMPERATURE ADSORPTION OF SULFUR DIOXIDE ON ALUMINA

2. BACKGROUND INFORMATION

In an effort to understand the mechanism of the Claus reaction several infrared studies on the interaction between SO_2 and Al_2O_3 have been conducted [1,3,4,5,8,9,11]. Even though up to five different types of sites for SO_2 adsorption have been identified [4], their exact nature has not yet been established with certainty. It is known, however, that the amount of SO_2 chemisorbed and its adsorption energy are strongly influenced by the pretreatment, acidity, and extent of hydration of the alumina surface.

2.1. The Alumina Surface

The term *alumina* designates the aluminum oxides and hydroxides. Aluminum hydroxide gels, some of which are amorphous, are usually obtained by precipitation from solutions of aluminum salts or alkali aluminates [12]. Aging of these gels leads to the formation of crystalized aluminum trihydroxides (gibbsite, bayerite, nordstrandite) and aluminum oxide hydroxides (boehmite, diaspore). The activated aluminas are obtained by elimination of H_2O of constitution from these hydrated aluminas through controlled heating. At least six different transition phases may be obtained in the heating process, namely χ-, η-, γ-, κ-, and θ-Al_2O_3. The sequence of phases is a function of the structure of the starting material, pressure, water vapor pressure, heating rate and particle size. Although these phases are thermodynamically unstable they have reasonably reproducible structures [18]. The best-known transition form is γ-Al_2O_3, which possesses a well-ordered O^{2-} sublattice. Corundum (or α-Al_2O_3)

is the stable form of anhydrous alumina, obtained by heating any of the transition phases to 1100-1200^oC. This transformation is irreversible, i.e., it is not possible to obtain transition aluminas by hydration of α-Al_2O_3.

While the stable hydroxides have little porosity and low surface area, evacuation and heating causes the development of pore structure and an increase in surface area, which reaches a maximum at approximately 400^oC [18]. The surface area of γ-Al_2O_3, for example, may be as high as 500 m^2/gram. Dehydration of transition aluminas is accompanied by loss of both surface area and pore volume. The surface area of α-Al_2O_3 is typically 2 to 4 m^2/gram.

The surface of transition aluminas exhibits a complex structure, characterized by the exposure of many different crystal planes [13] and by the presence of hydroxyl groups that can be eliminated by heating. This dehydroxylation process takes place through the combination of neighboring OH groups leading to the loss of H_2O and possibly to the formation of strained Al-O-Al linkages on the surface. Although the Al^{3+} and O^{2-} ions do have catalytic activity in some chemical reactions [15] , the hydroxyl groups and the defect sites created upon dehydroxylation are largely responsible for the high adsorptive and catalytic activity of transition aluminas.

These defect structures in the Al_2O_3 lattice appear to be concentrated at a relatively small number of sites [13], thus creating patches of localized catalytic activity. The chemical properties of these localized regions appear to be influenced by the presence of adjacent OH groups and underlying Al^{3+} ions.

Five different types of surface hydroxyl groups have been identified [13],

depending on the nature of their interaction with the Al_2O_3 substrate, giving rise to at least five distinct types of catalytic sites [2]. The catalytic activity is strongly influenced by the acidity of the surface. Abnormally exposed Al^{3+} ions may behave as strong Lewis acids, whereas the various types of surface hydroxyls constitute Brönsted acids of varying concentration and strength. Although α-Al_2O_3 is almost completely dehydroxylated it exhibits certain catalytic activity due to its high Lewis acidity.

The surface properties and, therefore, its catalytic activity are strongly influenced by the method of preparation of the alumina catalyst: the nature of the precursor, precipitation conditions, aging, and preheating and calcination temperatures are all factors to be taken into account. Current catalyst technology is concentrating on the control of these variables to obtain a catalyst with the desired characteristics. Efforts are being made to tailor the pore structure by controlling the kinetics of the dehydroxylation process (micropores) and the agglomeration technique (macropores) [17], and also to modify the acidity of existing transition aluminas [7,14].

2.2. Sulfur Dioxide Adsorption

The industrial importance of the Claus reaction, whose mechanism remains largely unknown, has motivated a substantial amount of work aimed at elucidating the structure of the alumina and the nature of the chemisorbed species. As most of that work has relied on infrared techniques progress in the area has been closely tied with the development of more refined equipment, such as

computer-supported [8] and Fourier transform [4] spectrometers.

The first thorough investigation of sulfur dioxide adsorption on γ-alumina was reported in 1971 by Deo *et al.* [5]. In an effort to understand the catalysis of the Claus reaction by alumina and zeolites they employed infrared spectroscopy to study the interaction of SO_2 and H_2S with those substrates at temperatures below $400°C$. They found that both reactants adsorb physically and chemically. According to their interpretation, physical adsorption takes place through hydrogen bonding between SO_2 or H_2S and the hydroxyl groups present on the alumina surface, as shown in Fig. 2.1(a). Chemisorption was attributed to the formation of a sulfate-like structure with surface O^{2-} ions (Fig. 2.1(b)). This chemisorbed species was considered to behave as an intermediate in the Claus reaction. Pretreatment of the alumina with $NaOH$ followed by exposure to SO_2 led to the irreversible formation of a *sulfation product*.

The heat of adsorption of SO_2 on heat-treated γ-Al_2O_3 at $150°C$ was measured by Glass and Ross [6]. Their results appeared to confirm the interpretation given by Deo *et al.* [5] (Fig. 2.1 (a) and (b)). A high heat of adsorption was encountered at low coverages, and was attributed to a strong interaction between the SO_2 molecules and defect sites created by the high temperature treatment.

Adsorption measurements at higher temperatures than those involved in the Claus reaction were reported by Chang [1], in connection with the sulfation of automotive emission control catalysts [16]. Using a BET technique he measured adsorption isotherms of a single sample at temperatures between 25 and

500^oC. Each run was preceded by a heat treatment at 700^oC. Chang's BET results suggest that the SO_2 uptake increases with increasing surface dehydroxylation at a given temperature, but decreases with increasing temperature. His data provide values of the isosteric heat of adsorption that are in general agreement with those of Glass and Ross [6]. In the same study Chang presents IR data that prove the existence of two forms of adsorbed SO_2. The species that adsorbs first is very firmly bound and only desorbs by heating at high temperatures. He suggests that this species is a surface SO_3^{2-}, although the IR spectra do not provide conclusive evidence. Oxidation of this species seems to lead to the formation of aluminum sulfate. The second species, more weakly bound, would be associated with the surface hydroxyls through hydrogen bonding, as described by Deo *et al.* [5] (Fig. 2.1(a)).

According to the models proposed by Deo *et al.* [5] and by Chang [1], surface dehydroxylation would cause an increase in the amount of SO_2 chemisorbed due to the formation of new active sites from their harbingers. At some point in the heating process the total surface area would start to decrease, causing the SO_2 uptake to reach a maximum. Karge *et al.* [9] showed that this maximum occurs at approximately 700^oC. They also identified the presence of two types of adsorbed species. In their interpretation SO_2 chemisorbs through the irreversible formation of a SO_2^- anion radical. Although hydrogen bonding also takes place, SO_2 would react preferentially with basic OH groups.

Direct evidence of the correlation between the total amount of SO_2 that adsorbs irreversibly and the extent of surface dehydroxylation was first presented by Lavalley *et al.* [10]. Their gravimetric results also provide conclusive

evidence that the SO_2 uptake increases with increasing temperature, contradicting Chang's results [1]. This issue will be addressed in Chapter 3. Ruling out the possibility of hydrogen bonding, Lavalley *et al.* proposed that adsorption takes place through the formation of a hydrogen sulfite species $-SO_3H$, as shown in Fig. 2.1(c) [10], and used this concept to provide a mechanism for the Claus reaction [11].

The use of probe molecules [8] and recent advances in IR spectroscopic techniques [3,4,8] have helped reveal new complications, such as for example the role of the Lewis acid and basic sites [4,8] and the possible existence of up to five different adsorbed species [4] (Fig. 2.1 (d) and (e)). Although many questions remain open, it is possible to draw some useful conclusions :

(i) Adsorption takes place through the formation of several surface species with varying binding energies, which can be divided into two groups : strongly chemisorbed, and weakly adsorbed SO_2.

(ii) The strongly chemisorbed species are associated with Lewis acid or basic sites existing on the surface or created upon dehydroxylation, and can only be desorbed by heating at high temperatures.

(iii) The weakly adsorbed species are associated with the existence of surface hydroxyls on the surface of transition aluminas.

Whereas the work carried out so far concentrated mainly on the nature of the SO_2-Al_2O_3 interaction, and measurements of uptake and heat of adsorptions were limited to temperatures below $500°C$, the objective of the present study was to determine adsorption isotherms, heat of adsorption, and adsorp-

tion/desorption kinetics at 700 to 800°C. In Chapter 3 equilibrium adsorption and heat of adsorption data are presented, and an adsorption isotherm is proposed. Chapter 4 centers around the adsorption/desorption dynamics. In Chapter 5 some results using temperature-programmed desorption are presented and discussed.

REFERENCES

[1] Chang, C.C., *J. Catal.*, **53**, 374, 1978.

[2] Cocke, D.L., Johnson, E.D., and Merrill, R.P., *Catal. Rev. Sci. Eng.*, **26**(2), 163, 1984.

[3] Datta, A., and Cavell, R.G., *J. Phys. Chem.*, **89**(3), 454, 1985.

[4] Datta, A., Cavell, R.G., Tower, R.W., and George, Z.M., *J. Phys. Chem.*, **89**(3), 443, 1985.

[5] Deo, A.V., Dalla Lana, I.G., and Habgood, H.W., *J. Catal.*, **21**, 270, 1971.

[6] Glass, R.W., and Ross, R.A., *Can. J. Chem.*, **50**, 2537, 1972.

[7] Homs, N., Ramírez de la Piscina, P., and Sueiras, J.E., *J. Catal.*, **89**, 531, 1984.

[8] Karge, H.G., and Dalla Lana, I.G, *J. Phys. Chem.*, **88**(8), 1538, 1984.

[9] Karge, H.G., Tower, R.W., Dudzik, Z., and George, Z.M., *VII International Congress on Catalysis*, Tokyo, 1980.

[10] Lavalley, J.C., Janin, A., and Preud'homme, J., *React. Kinet. Catal. Lett.*, **18**(1-2), 85, 1981.

[11] Lavalley, J.C., Lamotte, J., Saussey, H., and Preud'Homme, J., *Sulfur Letters*, **1**(3), 101, 1982.

[12] MacZura, G., Goodboy, K.P., and Koenig, J.J., *Aluminum Compounds*, Aluminum Company of America, Pittsburgh, 1978.

[13] Peri, J.B., *J. Phys. Chem.*, **69**(1), 211, 1965.

[14] Przystajko, W., Fiedorow, R., and Dalla Lana, I.G., *Appl. Catal.*, **15**, 265, 1985.

[15] Rosynek, M.P., and Strey, F.L., *J. Catal.*, **41**, 312, 1976.

[16] Taylor, K.C., *Ind. Eng. Chem. Prod. Res. Dev.*, **15**(4), 264, 1976.

[17] Trimm, D.L., and Stanislaus, A., *Appl. Catal.*, **21**, 215, 1986.

[18] Wefers, K., and Bell, G.M., *Oxides and Hydroxides of Aluminum*, Aluminum Company of America, Pittsburgh, 1972.

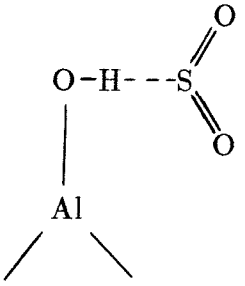

(a) Deo *et al.* [5].

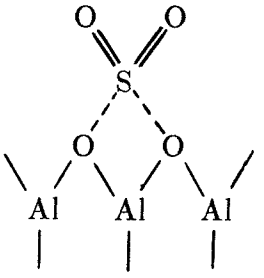

(b) Deo *et al.* [5].

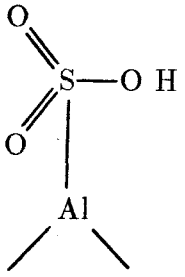

(c) Lavalley *et al.* [10].

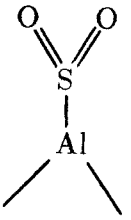

(d) Datta *et al.* [4].

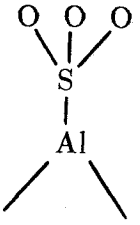

(e) Datta *et al.* [4].

Figure 2.1. Possible Nature of Adsorbed Sulfur Dioxide.

3. EQUILIBRIUM ADSORPTION

3.1. Experimental

3.1.1. Materials Two types of materials were used. γ-Al_2O_3 particles, $210 \leq d_p \leq 420\ \mu m$, were obtained by crushing and sieving UC-T-2432 γ-Al_2O_3 pellets (from United Catalysts Inc.). The second material was obtained by treating γ-Al_2O_3 powder with $NaOH$, following the procedure described in Ref. [3]. A slurry was prepared by mixing T-2432 powder with 2% by weight of $NaOH$, and adding H_2O. This slurry was dried and the resulting cake was crushed and sieved ($210 \leq d_p \leq 420\ \mu m$). The samples were degassed at $500°C$ for 24 hours and then exposed to oxygen at $700°C$ for 5 hours. Measurements of the adsorption of SO_2 on α-Al_2O_3 were not possible with the techniques described in Secs. 3.1.2 and 4.1 due to its low surface area.

After the pretreatment, BET N_2 adsorption isotherms of both materials were obtained, as described in Sec. 3.1.2, yielding a surface area of 102 m^2/gram for pure γ-Al_2O_3, and 69 m^2/gram for the *doped* material. The adsorbate was high purity SO_2, obtained from Matheson Research Grade lecture bottles.

3.1.2. Apparatus and Procedure The adsorption isotherms were obtained using a modified BET apparatus [7]. The adsorbate is admitted into a vacuum chamber of known volume at a known flow rate through a small orifice. In the experiments described here the gas flow rate was typically 3 to 5×10^{-4} moles/hour. The sample is located in a sample tube attached to the vacuum chamber. System pressures in the range 10^{-4} to 10^3 torr are measured using a

baratron gauge. The sample tube is surrounded by an electric furnace powered through a temperature controller, allowing operation at up to $1000°C$. The sample tube can also be immersed in a Dewar flask containing liquid N_2 for surface area determinations.

The baratron gauge was interfaced to a microcomputer equipped with a data-acquisition board for real time collection of pressure vs. time data. A set of computer programs was developed for data collection and file manipulation and reduction.

The samples were weighed, loaded in the sample tube, and degassed at low pressure ($\approx$ 0.01 torr). Pressures as low as 10^{-4} torr may be attained by means of a diffusion pump. Once the system reached thermal equilibrium at the desired temperature the chamber was isolated from the vacuum system and the adsorbate admitted while the pressure was recorded. Each run was repeated twice in order to ensure reproducibility of the results. The amount of gas adsorbed can be determined by the difference between the amount of gas which has passed through the orifice and the amount that occupies the dead volume :

$$n(P) = \int_0^t Q(t)\ dt\ -\ \frac{P(t)}{R} \int_V \frac{dV}{T}, \tag{3.1}$$

where :

Q : molar gas flow rate $(\frac{moles}{sec})$,

t : time (sec),

$P(t)$: system pressure (torr),

R : gas constant $\left(\frac{cm^3\ torr}{mole\ ^oK}\right)$, and

$\int_V \frac{dV}{T}$: effective volume/temperature $\left(\frac{cm^3}{^oK}\right)$.

Calibration runs with helium are required in order to determine the effective volume/temperature and the gas flow rate.

Using pressure vs. time data and information obtained from the calibration runs the adsorption isotherms were obtained using eq. 3.1. These data were then stored on magnetic disks for further calculations and plotting. A more detailed description of this system and its operation are given in Ref. [7].

In order to obtain true equilibrium isotherms it is essential that the gas flow rate be small enough when compared to the rate of adsorption so as to allow the pressure to be near equilibrium at all times. The occurence of slow physical or chemical processes involving some species present in the gas phase, such as intraparticle diffusion or slow chemical reactions [2] would also lead to errors in the resulting curves. In order to investigate these issues, the gas flow into the chamber was suddenly cut off at different points during several trial runs, and the pressure recorded for 1 hour thereafter. No noticeable pressure change was recorded in any of the runs, indicating that for all practical purposes the surface may be considered to be at equilibrium with the gas. Some of the runs described in Sec. 3.1.3 were duplicated using a lower gas flow rate. Again, the isotherms obtained at both flow rates were almost identical.

3.1.3. Results Fig. 3.1 shows a set of adsorption isotherms obtained by repeated exposure of a single γ-Al_2O_3 sample to SO_2 at pressures below 100

torr. The amount adsorbed has been divided by the sample weight. Every run was preceded by a 2-hour treatment under vacuum, at the temperature of the run. Curve (a) was obtained using a fresh sample at 700^oC. At 100 torr the total SO_2 uptake was approximately 28 μmole/gram, and the surface did not appear to be saturated. After run (a) the sample was degassed at 700^oC and 0.04 torr for 2 hours, and a new isotherm (b) was recorded. The total amount of SO_2 adsorbed was now 17 μmole/gram. Only 60% of the original adsorptive capacity was restored after degassing, indicating that either the surface properties were affected by the first exposure or some SO_2 has remained on the surface. In an effort to remove the remaining adsorbate by reduction to elemental sulfur the sample was exposed to pure CO at 300 torr and 700^oC for 3 hours. After this treatment a new run was performed at 700^oC. The resulting curve (c) indicates that only a small fraction of the adsorptive capacity has been recovered, while the uptake at low pressures has decreased. Finally, curves (d) and (e) were obtained at 750 and 800^oC, respectively.

A similar series of experiments was carried out with a $NaOH$-treated alumina sample. The corresponding isotherms at 700^oC before (a, b) and after (c) the CO treatment and those at 750 (d) and 800^oC (e) are presented in Fig. 3.2. A comparison with Fig. 3.1 reveals that the uptake has approximately doubled as a result of the alkali treatment. In this case 32% of the adsorptive capacity was lost after the first run. As before, the isotherm obtained after the treatment with CO (curve c) exhibited a reduction in the amount adsorbed at low pressures.

The effect of the temperature of pretreatment on the amount adsorbed

was examined. A fresh γ-Al_2O_3 sample was subjected to a 2-hour treatment under vacuum at 800^oC. The temperature was then lowered to 700^oC and the adsorption isotherm recorded (Fig. 3.3, curve a). The amount adsorbed at 100 torr was now 36 μmole/gram. Three more isotherms were obtained at 700 (b), 750 (c), and 800^oC (d), preceded by 2-hour treatments at 800^oC. In all the cases the amount adsorbed was higher than obtained previously (Fig. 3.1). At 800^oC (curve *d*) the surface exhibited approximately 90% of the original adsorptive capacity.

3.1.4. Discussion The amount of SO_2 adsorbed on γ-Al_2O_3 at 100 torr varied between 17 and 36 μmole/gram (10^{17} to 2.1×10^{17} molecules/m^2), depending on the temperature and surface pretreatment. These values are of the same order of magnitude as those reported by Chang [2] at temperatures below 500^oC. When treated with $NaOH$ alumina can adsorb as much as 60 μmole/gram, or 0.4% by weight. An estimate of the surface concentration of a SO_2 monolayer can be obtained by means of the Emmett-Brunauer equation :

$$C_s \approx 0.92 \left[\frac{N_A\ \rho}{M}\right]^{\frac{2}{3}}, \tag{3.2}$$

where :

C_s : surface concentration $\left(\frac{molecules}{m^2}\right)$,

N_A : Avogadro's number,

ρ : liquid density $\left(\frac{gram}{m^3}\right)$, and

M : molecular weight $\left(\frac{gram}{mole}\right)$.

In the case of SO_2 eq. 3.2 yields $C_s \approx 5 \times 10^{18}$ molecules/m^2. A calculation based on the spacing between O^{2-} and Al^{3+} ions on the (110) plane of the γ-Al_2O_3 lattice yields $C_s = 4.7 \times 10^{18}$ molecules/m^2 [1]. Thus, the fraction of the surface covered by SO_2 molecules is 0.02-0.04 for γ-Al_2O_3, and 0.08-0.10 for alkali-treated γ-Al_2O_3.

The adsorptive capacity of fresh γ-Al_2O_3 depends on the temperature of the thermal pretreatment. An increase in this temperature from 700 to 800^oC causes a 29% increase in the amount adsorbed at 100 torr (Figs. 3.1(a) and 3.3(a)). As higher temperatures are attained, more sites for chemisorption are formed by dehydroxylation at the expense of the disappearance of weaker sites constituted by surface OH groups. The net effect at temperatures above 300^oC is an increase in the total amount adsorbed [6].

The results obtained by Chang [2] would suggest that the amount adsorbed decreases with increasing temperatures. It is known, however, that as the temperature increases the surface is activated by dehydroxylation. This apparent contradiction is resolved by noting that a fraction of the adsorbed SO_2 chemisorbs very strongly, and can only be removed by heating at temperatures above 800^oC. As much as 30 to 40% of the SO_2 adsorbed at 700^oC may be present as a strongly chemisorbed species. While the total adsorptive capacity actually increases with increasing temperature, pretreatment at 700^oC only removes part of the previously adsorbed SO_2, causing a decrease in the observed uptake.

After the first exposure to SO_2 part of the adsorptive capacity can be

recovered by heating at 800^oC, due to desorption of some of the chemisorbed species (Fig. 3.3 (b),(c),(d)). The stability of that species may explain its resistance to reduction by CO according to :

$$SO_2^* + 2CO \rightarrow S^* + 2CO_2, \tag{3.3}$$

where the superscript * denotes chemisorbed species. Reaction 3.3 is known to proceed under the prevailing conditions [8] and may be taking place to a small extent, accounting for the slight increase in the amount adsorbed and the decrease in the availability of high-energy sites (Figs. 3.1 and 3.2 c). A second possibility that cannot be confirmed with this technique is that elemental sulfur is produced in substantial amounts, but remains attached to the surface.

According to Deo *et al.* [3], the effect of the $NaOH$ treatment on the γ-Al_2O_3 is the substitution of surface $-OH$ groups according to :

$$-OH \; + \; NaOH \; \rightarrow \; -ONa \; + \; H_2O.$$

In our case, the surface area decreased to 2/3 of its original value as a result of the $NaOH$ treatment (Sec. 3.1.1), while the adsorptive capacity was doubled (Fig. 3.2). These results suggest that the treatment is causing more drastic changes than the mere displacement of H^+ ions. The alkali treatment may actually comprise the formation of sodium aluminate :

$$Al_2O_3 + 2NaOH \rightarrow 2NaAlO_2 + H_2O.$$

When exposed to SO_2 this aluminate would then react to form sodium sulfite :

$$2NaAlO_2 + SO_2 \rightarrow Na_2SO_3 + Al_2O_3,$$

accounting for the enhancement of the adsorptive capacity, and also for the formation of the *chemisorbed species* reported by Deo *et al.* [3].

3.2. Adsorption Isotherm

The equilibrium data presented in Sec. 3.1.3 could not be adequately described by any of the well-known equilibrium isotherms. The Langmuir isotherm provided reasonable fit up to fractional coverages $\theta \approx 0.3$, and gave better results than the Freundlich, Temkin and Sips [11] equations. Whereas these equations assume that the distribution of adsorption energies is either monotonic (Freundlich, Temkin), or posesses only one maximum (Langmuir, Sips), in the case under study there are two groups of active sites involved, and possibly a wide range of binding energies. Assuming that all the strong sites have an energy of adsorption q_1, all the weak sites have an energy of adsorption q_2, both groups of sites behave independently, and that the traditional Langmuir assumptions apply to each type of sites, a simple bimodal isotherm can be written :

$$\theta = x\left[\frac{K_1 p}{1+K_1 p}\right] + (1-x)\left[\frac{K_2 p}{1+K_2 p}\right] \tag{3.4}$$

where :

θ : fractional coverage $\equiv \frac{n}{n_{sat}}$,

x : fraction of (strong) sites with energy q_1,

K_1, K_2 : equilibrium constants for sites of type 1 (strong) and 2 (weak), and

p : pressure.

The constants K_1 and K_2 are related to the heats of adsorption by :

$$K_1 = k_1 \; exp\left[\frac{q_1}{RT}\right], \qquad K_2 = k_2 \; exp\left[\frac{q_2}{RT}\right].$$

In order to rescale the data in terms of fractional coverage it is necessary to obtain an estimate of the maximum amount adsorbed, n_{sat}. This can be accomplished by extrapolation from the data at higher pressures :

$$\theta \equiv \frac{n}{n_{sat}} = x\left[\frac{1}{1+\frac{1}{K_1 p}}\right] + (1-x)\left[\frac{1}{1+\frac{1}{K_2 p}}\right] \approx$$

$$\approx 1 - \left[\frac{x}{K_1} + \frac{1-x}{K_2}\right]\frac{1}{p} \qquad (as\ p \to \infty).$$

Hence,

$$n = n_{sat} - n_{sat}\left[\frac{x}{K_1} + \frac{1-x}{K_2}\right]\frac{1}{p},$$

correct to order p^{-1}.

The data shown in Fig. 3.3 (b, c and d) are redrawn as n vs. $\frac{1}{p}$ in Fig. 3.4. The values of maximum coverage obtained by linear regression are : n_{sat} = 28.5, 32, and 35 μmole/gram, at 700, 750, and 800°C, respectively. Using these values, the coverage attained at 100 torr is $\theta \approx 0.92$.

Once the data have been rescaled as θ vs. p they can be used to obtain the parameters x, K_1 and K_2. After some algebraic manipulation eq. 3.4 can be rewritten as

$$\theta = \frac{p^2 + ap}{p^2 + bp + c}$$

$$\Rightarrow \; p^2(1-\theta) = bp\theta + c\theta - ap, \qquad (3.5)$$

where :

$$a \equiv \frac{(K_1 - K_2)x + K_2}{K_1 K_2},$$

$$b \equiv \frac{K_1 + K_2}{K_1 K_2},$$

$$c \equiv \frac{1}{K_1 K_2}.$$

The parameters a, b, and c could in principle be obtained by linear regression from the experimental data, solving the system of equations :

$$\begin{aligned}
\left(\sum p^2\right) a - \left(\sum p^2\theta\right) b - \left(\sum p\theta\right) c &= -\sum p^3 (1-\theta) \\
\left(\sum p^2\theta\right) a - \left(\sum p^2\theta^2\right) b - \left(\sum p\theta^2\right) c &= -\sum p^3\theta (1-\theta) \\
\left(\sum p\theta\right) a - \left(\sum p\theta^2\right) b - \left(\sum \theta^2\right) c &= -\sum p^2\theta (1-\theta) .
\end{aligned}$$

The solution of this system using the data shown in Fig. 3.3 led to unreallistic values of x, K_1 and K_2. This may be due either to the fact that eq. 3.4 cannot adequately describe the data, or to errors in the minimization of the error function by linear regression.

If $K_1 \gg K_2$ adsorption will take place preferentially on sites of type 1 at very low pressures and on sites of type 2 at very high pressures. In that case it may be possible to obtain the constants K_1 and K_2 from suitable asymptotic forms of eq. 3.4, an attractive alternative to a nonlinear regression approach. After some algebraic manipulation, eq. 3.4 can be recast in the following useful form :

$$\theta = K_2 p(1-\theta) + \left[\frac{K_1 - K_2}{K_1 + \frac{1}{p}}\right] x. \qquad (3.6)$$

If $K_1 = K_2$ (or, equivalently, $x = 0$) eq. 3.6 becomes the Langmuir isotherm :

$$\theta = Kp(1-\theta). \tag{3.7}$$

In the particular case $p \to 0$ eq. 3.6 approaches the Langmuir equation 3.7 after a Taylor expansion to order p, with

$$K \equiv (K_1 - K_2)x + K_2. \tag{3.8}$$

There are two cases of interest in which all sites of type 1 are occupied, with eq. 3.6 approaching the form :

$$\theta = K_2 p(1-\theta) + \phi. \tag{3.9}$$

The first such case occurs when all sites of type 1 have an infinite binding energy (i.e., $\phi \equiv x$). The second case corresponds to $p \to \infty$, with :

$$\phi \equiv \left[\frac{K_1 - K_2}{K_1}\right] x. \tag{3.10}$$

A comparison between the experimental data from Fig. 3.3(d) and eqs. 3.7 and 3.9 is shown in Fig. 3.5. The data follow the Langmuir equation only at very low coverages ($\theta < 0.3$), and eq. 3.9 when $\theta > 0.5$. The uncertainty in the value of $p(1-\theta)$ at high coverages causes scatter in the data above $\theta \approx 0.8$. The constant K_2 is obtained by linear regression from the slope of the data points at high pressures (eq. 3.9), while K_1 and x are calculated from the intercept of those points (ϕ), and the slope of the low pressure data (K), together with

eqs. 3.8 and 3.10 :

$$K_1 = \frac{K - K_2}{\phi},$$

$$x = \frac{K - K_2}{K_1 - K_2}.$$

Table 3.1 lists the values of K_1, K_2 and x obtained by linear regression from the data at 700, 750 and 800^oC. Using these constants eq. 3.4 fits the data on Fig. 3.3 within $\pm 5\%$. The values of these constants vary as much as 10% as a result of small changes in the value of n_{sat} obtained by extrapolation.

3.3. Heat of Adsorption

Assuming that the Langmuir assumptions hold for all sites with a given binding energy q, the surface coverage is given by :

$$\theta = \int_0^\infty N(q) \left\{ \frac{k\ p\ exp\left[\frac{q}{RT}\right]}{1 + k\ p\ exp\left[\frac{q}{RT}\right]} \right\} dq, \qquad (3.11)$$

where $N(q)$ is the distribution function of adsorption sites with respect to the adsorption energy, which satisfies :

$$\int_0^\infty N(q)dq = 1.$$

In principle, it would be possible to obtain the distribution function $N(q)$ from θ vs. p data by inversion of the integral 3.11. Although this task poses great numerical difficulties, it is possible to carry out the inversion using Stieltjes transforms, when a mathematical expression $\theta = f(p)$ is given [11]. Some

mathematical techniques have been developed [9,10] to simplify the inversion when $q_{min} \gg RT$. Unfortunately, in our case the temperatures are high and a substantial amount of SO_2 adsorbs with fairly low binding energies, rendering this approach inapplicable.

While the distribution function associated with eq. 3.4 is simply

$$N(q) = x\ \delta(q - q_1) + (1 - x)\ \delta(q - q_2),$$

the true function $N(q)$ is probably a superposition of two broad peaks (see Sec. 2.2 and Chapter 5). The adsorption energies q_1 and q_2 could be found by linear regression from

$$ln\ K_i = ln\ k_i + \frac{q_i}{RT} \qquad (i = 1, 2)$$

using K_1, K_2 and T from Table 3.1. The values of q_1 and q_2 obtained using this procedure vary widely with K_1, K_2 and x, which in turn depend strongly on n_{sat}. Furthermore, it is found that K_1 and K_2 are not linear functions of T^{-1}.

A widely used approach is the use of the Clausius-Clapeyron equation

$$q(\theta) = RT^2 \left(\frac{d\ ln\ p}{dT}\right)_\theta \tag{3.12}$$

to calculate the isosteric heat of adsorption from experimental θ vs. p data. The function $q(\theta)$ is usually found to decrease with increasing θ [4]. Even though isotherm 3.4 does not take into account any adsorbate-adsorbate interaction it

does predict a decrease in the isosteric heat of adsorption with surface coverage :

$$q(\theta) = -\frac{RT^2}{p}\frac{\left(\frac{\partial\theta}{\partial T}\right)_p}{\left(\frac{\partial\theta}{\partial p}\right)_T}$$

$$= -\frac{RT^2}{p}\left[\frac{\left(\frac{\partial\theta}{\partial K_1}\right)_p \frac{dK_1}{dT} + \left(\frac{\partial\theta}{\partial K_2}\right)_p \frac{dK_2}{dT}}{\left(\frac{\partial\theta}{\partial p}\right)_T}\right]$$

$$= \frac{xK_1q_1\left[1+K_2p\right]^2 + (1-x)\,K_2q_2\left[1+K_1p\right]^2}{xK_1\left[1+K_2p\right]^2 + (1-x)\,K_2\left[1+K_1p\right]^2}.$$

Given that $K_1 > K_2$ and $q_1 > q_2$ this expression decreases monotonically with p and, therefore, with θ.

The isosteric heat of adsorption as a function of surface coverage was calculated using eq. 3.12 and the data shown in Fig. 3.3. The derivative

$$\left(\frac{\partial\, ln\, p}{\partial T}\right)_\theta$$

was approximated by means of a least-squares regression at every value of θ. The resulting curve is shown in Fig. 3.6. The values of q below $\theta = 0.25$ and above $\theta = 0.9$ were not included as the corresponding least-squares correlation coefficients were very low. The heat of adsorption remains approximately constant at about 18 kcal/mole up to $\theta \approx 0.5$. It then starts to decrease steadily, reaching 8 kcal/mole at $\theta \approx 0.9$. These values are lower than those reported by Glass and Ross [5] and by Chang [2] at lower temperatures. At low coverages the SO_2 molecules adsorb preferentially on sites with a high energy of adsorption. Therefore, Fig. 3.6 only shows the isosteric heat of adsorption of the *weak* sites.

REFERENCES

[1] Andersson, S., Pompe, R., and Vannerberg, N., *Appl. Catalysis*, **16**, 49, 1985.

[2] Chang, C.C., *J. Catal.*, **53**, 374, 1978.

[3] Deo, A.V., Dalla Lana, I.G., and Habgood, H.W., *J. Catal.*, **21**, 270, 1971.

[4] Emmett, P.H., *Catalysis*, **III**, Reinhold Publishing Co., New York, 1955.

[5] Glass, R.W., and Ross, R.A., *Can. J. Chem.*, **50**, 2537, 1972.

[6] Lavalley, J.C., Janin, A., and Preud'homme, J., *React. Kinet. Catal. Lett.*, **18**(1-2), 85, 1981.

[7] Northrop, S.P., *M.S. Thesis*, California Inst. of Tech., 1986.

[8] Querido, R., and Short, W.L., *Ind. Eng. Chem. Process Des. Develop.*, **12**(1), 10, 1973.

[9] Roginsky, S.Z., *Comptes Rendus*, **45**(2), 61, 1944.

[10] Roginsky, S.Z., *Comptes Rendus*, **45**(5), 194, 1944.

[11] Sips, R., *J. Chem. Phys.*, **16**(5), 490, 1948.

Table 3.1. Constants for the Two-Site Isotherm.

Temperature	K_2	ϕ	K	K_1	x
^oC	$torr^{-1}$		$torr^{-1}$	$torr^{-1}$	
700	0.064	0.15	0.12	0.37	0.18
750	0.069	0.16	0.13	0.38	0.20
800	0.071	0.17	0.14	0.41	0.20

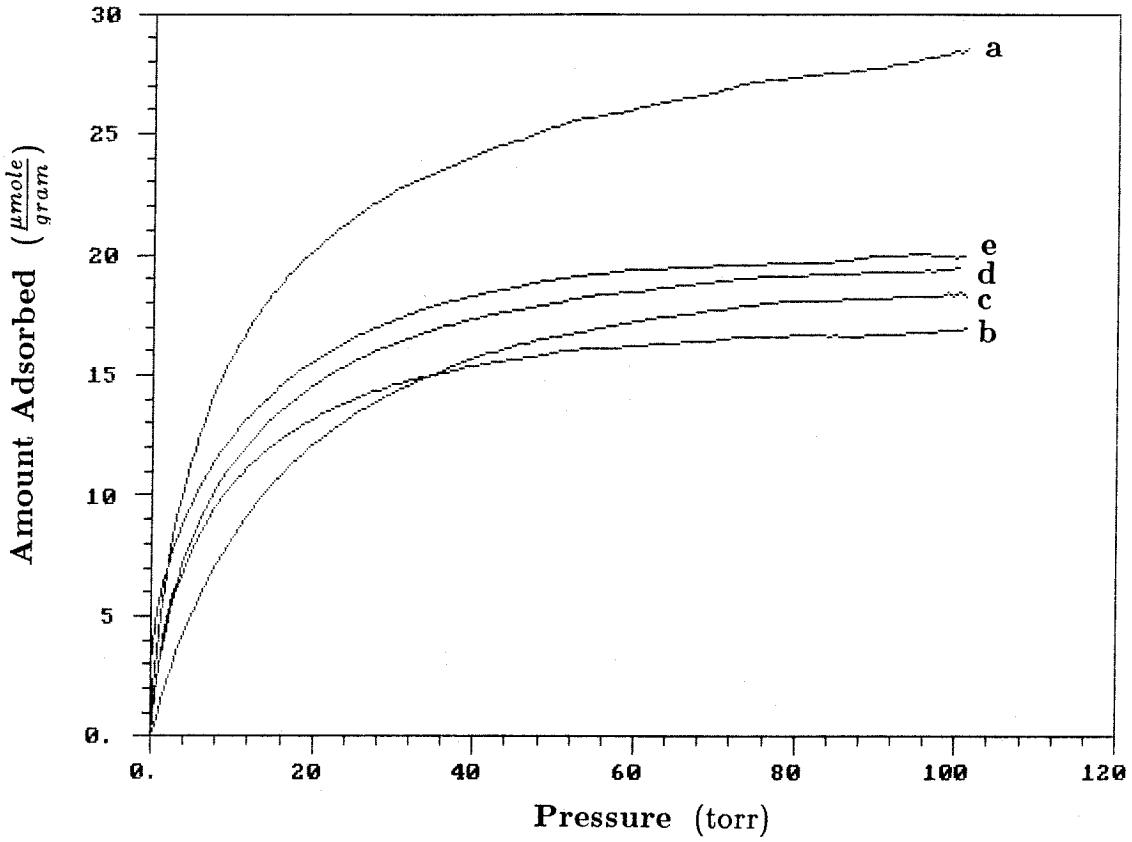

Figure 3.1. SO_2 Adsorption Isotherms on γ-Al_2O_3 at :
(a,b,c) 700, (d) 750, and (e) 800^0C.

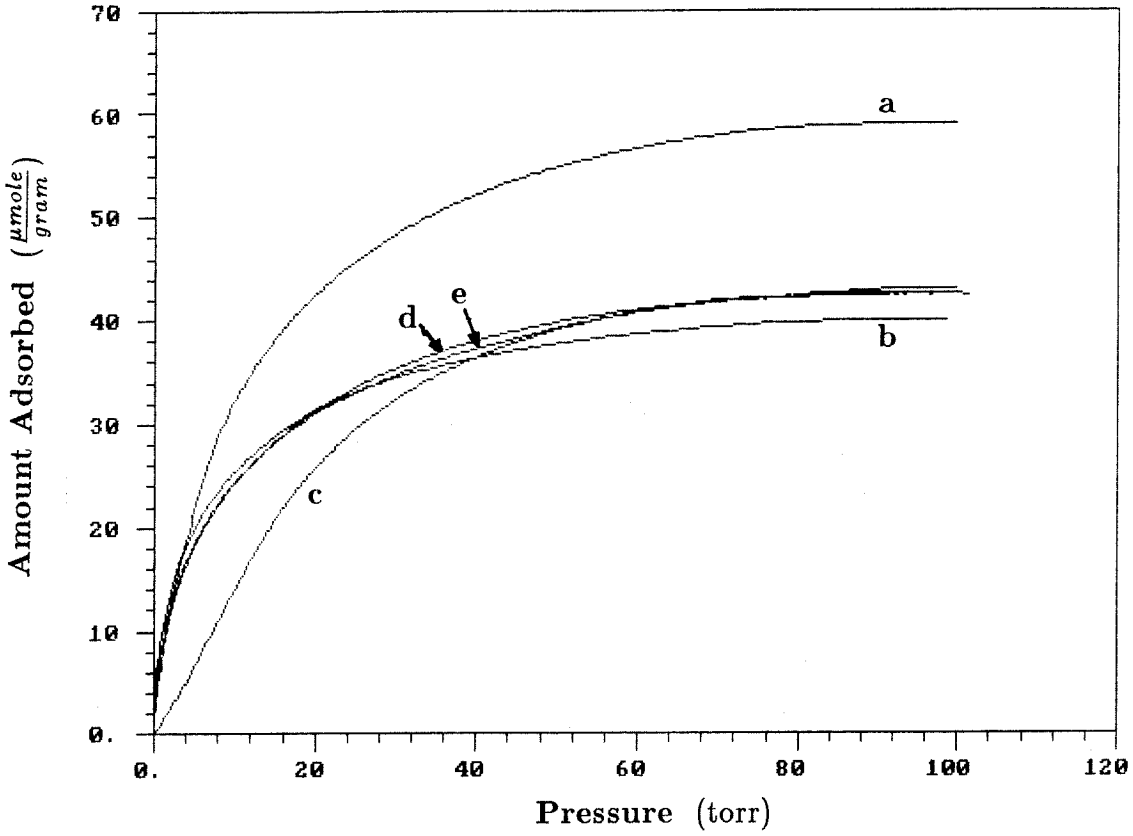

Figure 3.2. SO_2 Adsorption Isotherms on $NaOH$-treated γ-Al_2O_3 at : (a,b,c) 700, (d) 750, and (e) 800^0C.

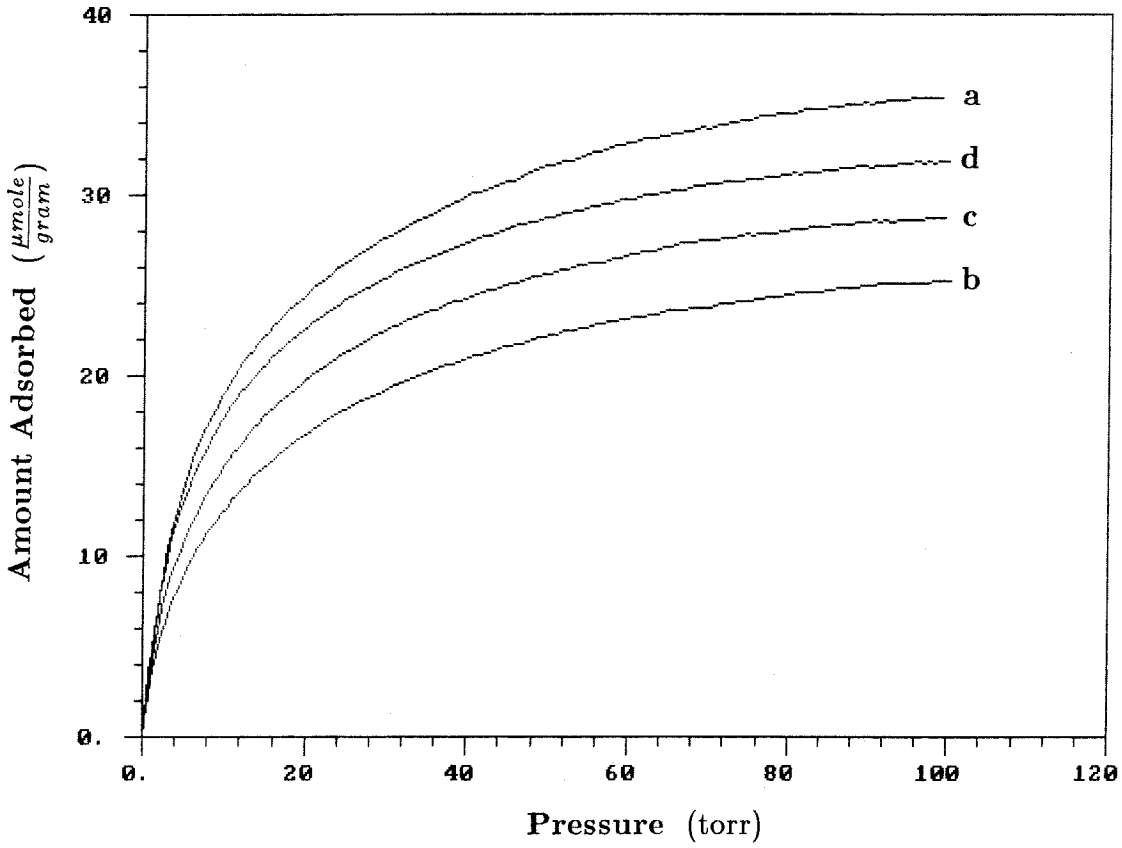

Figure 3.3. SO_2 Adsorption Isotherms on γ-Al_2O_3 at : (a,b) 700, (c) 750, and (d) 800°C, with Pretreatments at 800°C.

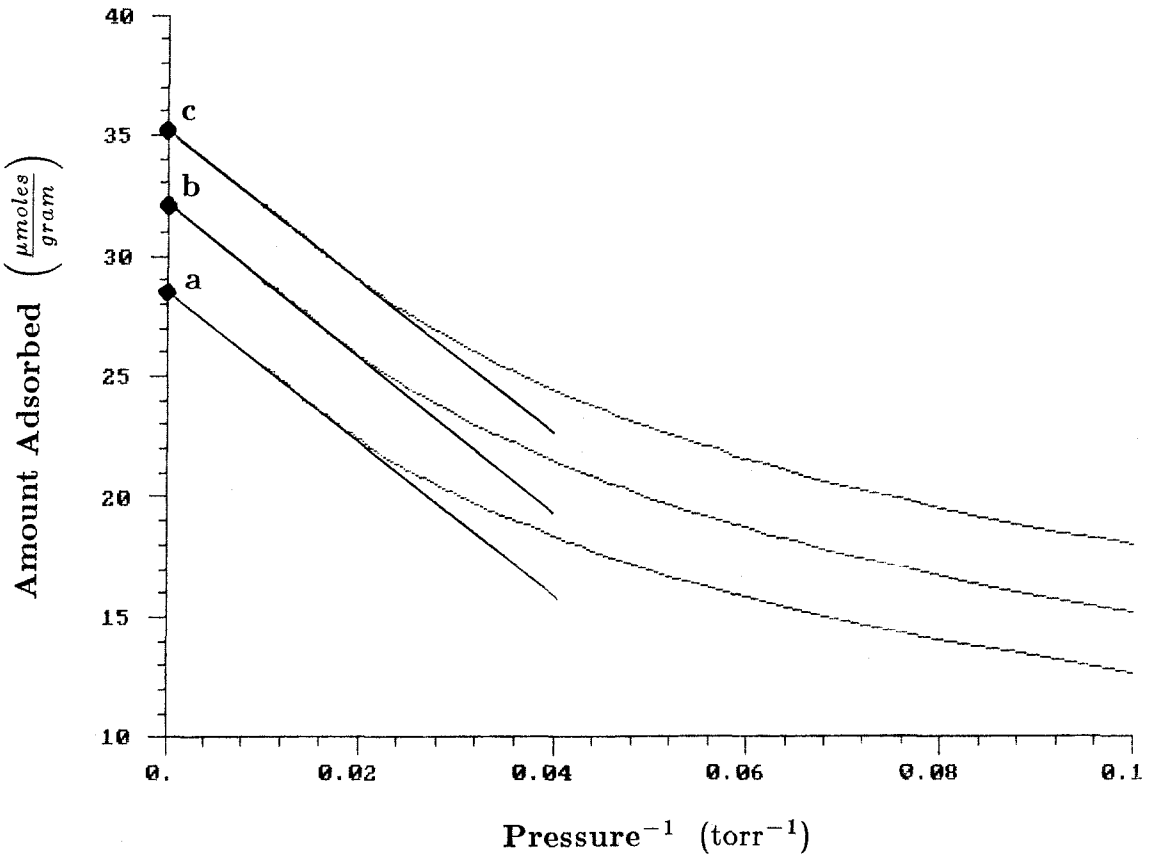

Figure 3.4. Extrapolated Values of the Maximum Amounts Adsorbed at : (a) 700, (b) 750, and (c) 800^0C.

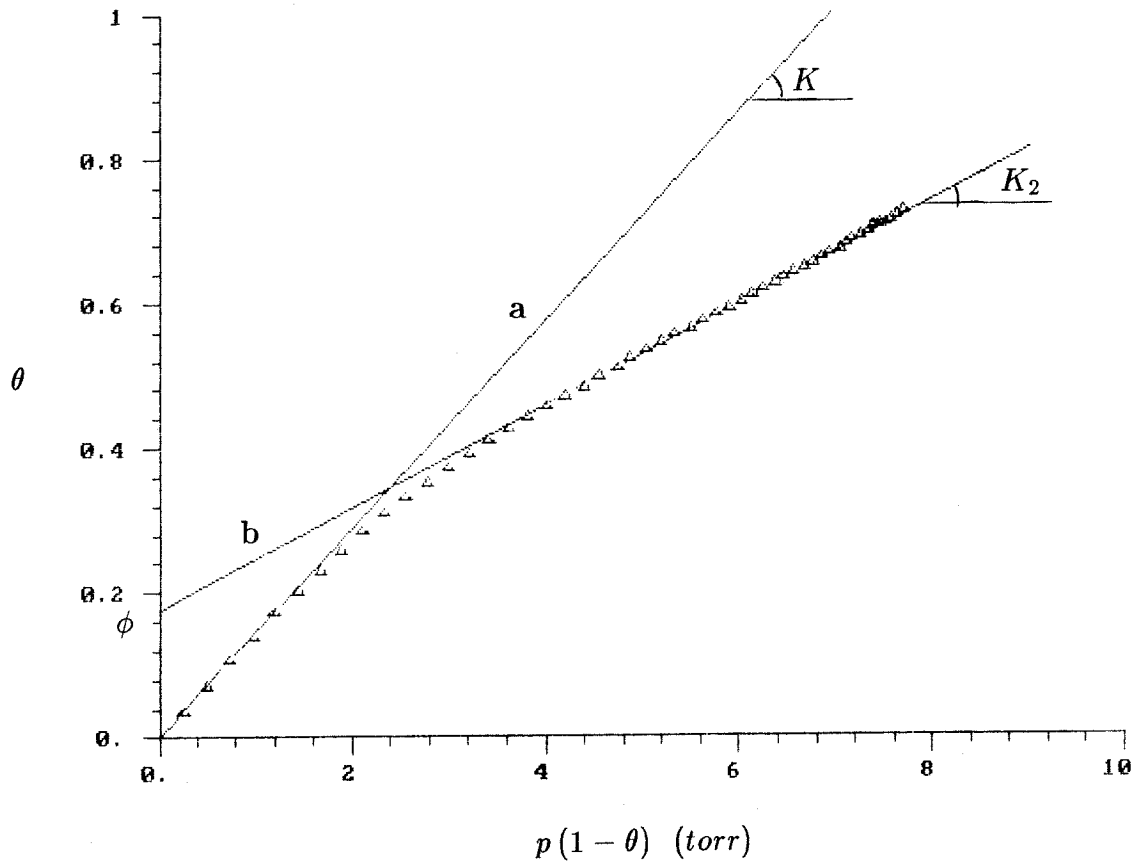

Figure 3.5. Comparison Between the Data at 800^0C and (a) the Langmuir Isotherm, (b) Eq. 3.9.

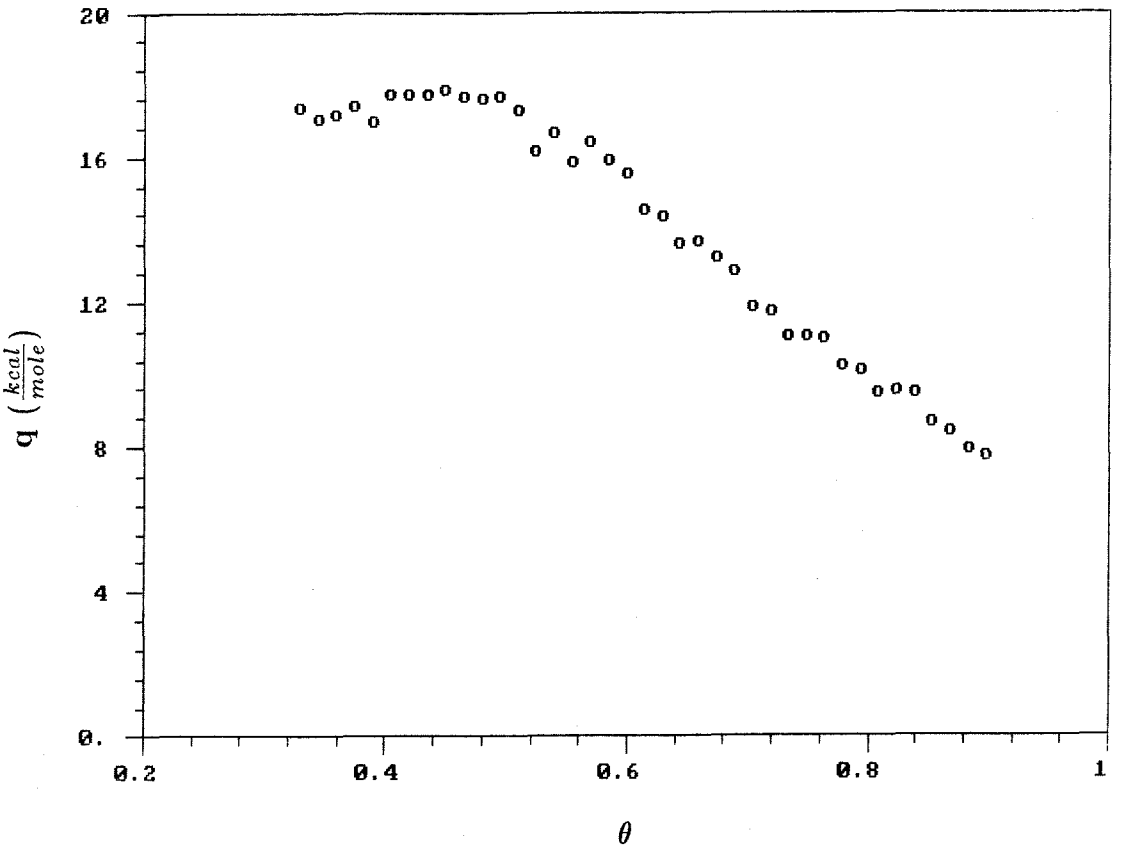

Figure 3.6. Isosteric Heat of Adsorption.

4. ADSORPTION AND DESORPTION KINETICS

4.1. Experimental System and Procedure

The isothermal adsorption and desorption of SO_2 on γ-Al_2O_3 and $NaOH$-treated γ-Al_2O_3 were studied using the system depicted in Fig. 4.1. The sample weight was measured as a function of time using a Du Pont 951 Thermogravimetric Analyzer (TGA). This instrument provides analog outputs proportional to the weight and rate of weight change of samples below 200 mg., with an approximate accuracy of $\pm 10\mu g$. The TGA reaction chamber consists of a cylindrical quartz tube surrounded by a furnace assembly and housing a horizontal balance arm and platinum sample pan. Power to the furnace is controlled by a temperature programmer, allowing operation at temperatures between ambient and 1000^oC (see Sec. 5.2 and Appendix B). A Type K thermocouple located inside the reaction chamber near the sample pan measures the sample temperature, while a Platinel II thermocouple imbedded in the furnace assembly measures the heater temperature for control purposes.

Prepurified N_2 was used as an inert diluent for the desorption experiments. The adsorbate was a mixture of 20% SO_2 and 80% N_2. Air was also available for sample pretreatment. The gases flowed from pressurized cylinders through pressure regulators, H_2O and O_2 traps, a set of valves and pressure gauges, a multiport valve and into the TGA through a side arm. A purge stream of N_2 diluent was fed continuously from the rear end of the reaction chamber to protect the balance mechanism from corrosive gases. The flow rates of both streams were measured using calibrated mass flowmeters.

The exit gases from the TGA were sent into a Miran-IA gas analyzer, manufactured by Foxboro Co. This analyzer is a single-beam, variable filter infrared spectrometer equipped with a gas cell, and was used to monitor the SO_2 absorption band at 7.4 μm. The instrument was calibrated to measure SO_2 concentrations in the exit stream between 0.5% and 10%.

A data acquisition system was assembled and programmed to collect and process the data from the TGA and the IR spectrometer. Data files containing weight, rate of weight change, temperature and gas concentration vs. time were created at run time and sent to a remote mainframe computer for reduction and plotting. This system is described in Appendix A.

The materials used were the same as in the equilibrium experiments (Sec. 3.1.1). A 30-50 mg. sample was spread evenly on the sample pan forming a thin, even layer, to minimize diffusional resistances in the particle bed. The gas pressure and flow rates were then adjusted to the desired total flow rate and adsorbate concentration and to ensure a total pressure of 3 psig in the TGA. The samples were pretreated at a constant temperature of $700°C$ for 5 hours under an air stream, and then heated to the temperature of the run. Before each run the samples were exposed to a stream of pure N_2 for 2 hours. At time $t = 0$ a gas stream containing SO_2 with the desired concentration was admitted into the TGA using the multiport valve, while the weight and the output from the IR spectrometer were logged every 10 seconds. Once the weight reached a plateau, SO_2 was desorbed by switching back to a flow of pure N_2. Both adsorption and desorption were carried out at a constant temperature. This procedure was repeated with various samples and at different temperatures,

duplicating each run. The concentration curves from the gas analyzer had the same general shape as the thermogravimetric data. However, they were always somewhat higher, probably due to SO_2 desorption from the TGA walls. The IR data were also noisier due to the low SO_2 concentrations in the exit stream. Only thermogravimetric results will be presented here.

4.2. Heat and Mass Transfer in the TGA

Two questions of concern are :

(i) the possibility that diffusion of SO_2 to and from the gas stream may decrease the overall rate of adsorption and desorption, and

(ii) the error involved in the measurement of the sample temperature.

Under typical operating condition the gas flow inside the TGA is laminar, with $Re \approx 5$ to 10. For a gas containing mostly N_2 and assuming that the sample behaves as a flat plate parallel to the direction of the flow a boundary layer calculation leads to

$$Nu_H \approx Nu_M \approx 1,$$

where Nu_H and Nu_M are the Nusselt numbers for heat and mass transfer. Calculations based on other geometries lie within 20% of this value. The corresponding mass transfer coefficient is $k_M \approx 2$ cm/sec, and the characteristic time for external mass transfer is only a fraction of a second. On the other hand, adsorption and desorption times are of the order of several minutes to 1 hour (Sec. 4.3), indicating that external diffusion is much faster than ad- and desorption. A set of experiments was carried out to measure the overall rate

of adsorption at a given temperature and with varying gas flow rates. No appreciable difference was found between runs, confirming that the measurements correspond to the true rates of adsorption and desorption.

When the furnace temperature is 700-800°C the gas stream enters the TGA at ambient temperature, is slightly heated by convection from the chamber walls and sample pan, and leaves the reaction chamber at 60-120°C. Both the sample and the thermocouple are heated by radiation from the heating element and cooled by convection to the gas stream, and are likely to be at similar temperatures. Heat transfer calculations and temperature measurements show that the rate of heat transfer to the gas is much lower than that from the furnace, so that the sample temperature is only 30 to 60°C lower than the heater temperature.

4.3. Results and Discussion

Fig. 4.2 shows the adsorption and desorption cycles of SO_2 on γ-Al_2O_3 and $NaOH$-treated γ-Al_2O_3 samples at 750°C with $[SO_2]$ = 15%, corresponding to a SO_2 partial pressure of 137 torr. These samples had not been exposed to SO_2 before the runs. Adsorption takes place very rapidly in both cases, reaching 90% of the maximum uptake in less than 5 minutes. The amount of SO_2 adsorbed on pure alumina after 70 minutes was 36% higher than in the equilibrium experiments. In the case of treated alumina that amount was 30% higher. This enhancement is probably caused by the presence of O_2 traces in the gas stream [1,5].

Out of the total amount of SO_2 adsorbed 18% remained bound to the γ-Al_2O_3 surface after 2 hours of exposure to N_2. That amount was 29% in the case of the $NaOH$-treated sample. In both cases desorption was slow : after 1 hour of exposure to the N_2 stream 9% of the adsorbate that would eventually desorb was still attached to the pure Al_2O_3 surface. In the case of the alkali-treated Al_2O_3 that figure was 15%.

4.3.1. Isothermal Adsorption The effects of a previous exposure to SO_2 and the operating temperature on the adsorption kinetics are illustrated in Fig. 4.3. Curve (a) shows the amount adsorbed on a fresh sample at 700^oC, as a function of time. The run was repeated after desorption under N_2 for 5 hours at 700^oC (curve (b)). The temperature was then raised to 800^oC, SO_2 was let to desorb for 5 hours, and SO_2 was admitted at that temperature (curve (c)).

The initial exposure to SO_2 causes a 36% decrease in the adsorptive capacity after 1 hour. After the first exposure the adsorption process takes place in two steps. During the first minute 25% of the total uptake adsorbs very rapidly. After the first minute the adsorption becomes slow (curve b). Both the rate of adsorption during the second step and the amount adsorbed after a one-hour exposure to SO_2 become slightly higher at 800^oC (curve c). The amount adsorbed during the second exposure at 700^oC was only 80% of the amount desorbed during the N_2 purge that followed the first exposure. These observations indicate that the effect of the first exposure to SO_2 is not only the blockage of strong sites but also a modification of the adsorptive properties of the surface.

In order to interpret these results it is useful to formulate a simple mathematical description of the adsorption/desorption process. If all the adsorption sites had constant activation energies for adsorption and desorption, and assuming that both processes are of first order, the adsorption rate would be given by :

$$\begin{aligned} \frac{d\theta}{dt} &= k_a\,(1-\theta)\,p - k_d\theta \\ &= k_a p - (k_a p + k_d)\,\theta, \end{aligned} \tag{4.1}$$

$$\theta = \theta_0 \qquad at\ t = 0$$

where $k_a = k_a^o\ exp\left[-\frac{E_a}{RT}\right]$, $k_d = k_d^o\ exp\left[-\frac{E_d}{RT}\right]$. E_a and E_d are the activation energies for adsorption and desorption, related by

$$E_d - E_a = q.$$

At constant temperature, the solution of eq. 4.1 is

$$\theta = \frac{Kp}{1+Kp} - \left[\frac{Kp}{1+Kp} - \theta_0\right]\ exp\left\{-\left(Kp+1\right)k_d t\right\}, \tag{4.2}$$

where

$$K \equiv \frac{k_a}{k_d}.$$

At steady state eq. 4.2 approaches the Langmuir isotherm. In the cases presented in Fig. 4.3 we have $\theta_0 = 0$ and $\frac{Kp}{1+Kp} \approx 1$, since we are on the plateau of the isotherm (Figs. 3.1 and 3.3). Thus, eq. 4.2 reduces to

$$ln\,(1-\theta) = -k_a p t. \tag{4.3}$$

The data from Fig. 4.3 are redrawn as $ln\,(1-\theta)$ vs. t in Fig. 4.4. The assumption of a constant activation energy for adsorption does not hold in the case of a fresh sample, particularly at low coverage (a). On the other hand that assumption becomes more plausible in the cases of curves (b) and (c), after the initial period of rapid adsorption. When first exposed to SO_2 a large proportion of the sites exhibit a low activation energy for adsorption. The effect of the first exposure is to block those sites, leaving weaker sites with a narrower energy distribution available for reversible adsorption and desorption. This explanation, however, fails to account for the large fraction of the sites that exhibit a low rate of adsorption after the first exposure (Fig. 4.3 (b) and (c)). An approximate value for the activation energy obtained from curves (b) and (c) is $E_a \approx 1$ kcal/mole.

4.3.2. Isothermal Desorption As discussed in Sec. 4.2, readsorption can be neglected during desorption under N_2. Setting $p = 0$ and $\theta_0 = 1$ in eq. 4.2, we obtain

$$ln\ \theta = -k_d t. \tag{4.4}$$

Fig. 4.5 shows three $ln\ \theta$ vs. t curves for a single γ-Al_2O_3 sample at three different temperatures. The sample had been exposed to SO_2 at 700^oC prior to the runs, and subjected to intermediate heatings at 800^oC between runs. The difference between the first and second runs at 700^oC was not very significant. As expected, the desorption rate increases with increasing temperatures. Eq. 4.4 provides an adequate description only at low coverage, when SO_2 desorbs from sites with large values of E_d. Linear regression of the slopes of curves (a),

(b) and (c) at low coverage yields an upper bound for the activation energy, $E_d < 22$ kcal/mole. Thus, $q = E_d - E_a < 21$ kcal/mole for the weaker sites, in agreement with Fig. 3.6.

REFERENCES

[1] Andersson, S., Pompe, R., and Vannerberg, N., *Appl. Catalysis*, **16**, 49, 1985.

[2] Bird, R.B., Stewart, W.E., and Lightfoot, E.N., *Transport Phenomena*, John Wiley & Sons, New York, 1976.

[3] Emmett, P.H., *Catalysis*, **III**, Reinhold Publishing Co., New York, 1955.

[4] Schlichting, H., *Boundary-Layer Theory*, McGraw-Hill, New York, 1979.

[5] Summers, J.C., *176th National Meeting of the American Chemical Society*, Miami Beach, 1978.

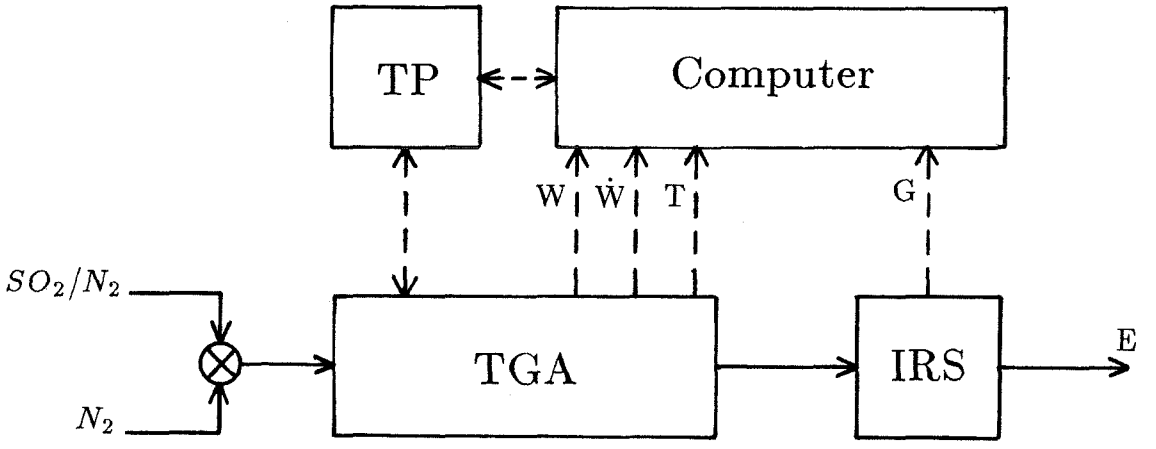

TGA : Thermogravimetric Analyzer

IRS : Infrared Spectrometer

TP : Temperature Programmer

E : Exhaust gases

W : Weight signal

$\dot{W}$: Rate of weight change signal

T : Temperature signal

G : SO_2 concentration signal

Figure 4.1. Block Diagram of the Experimental System.

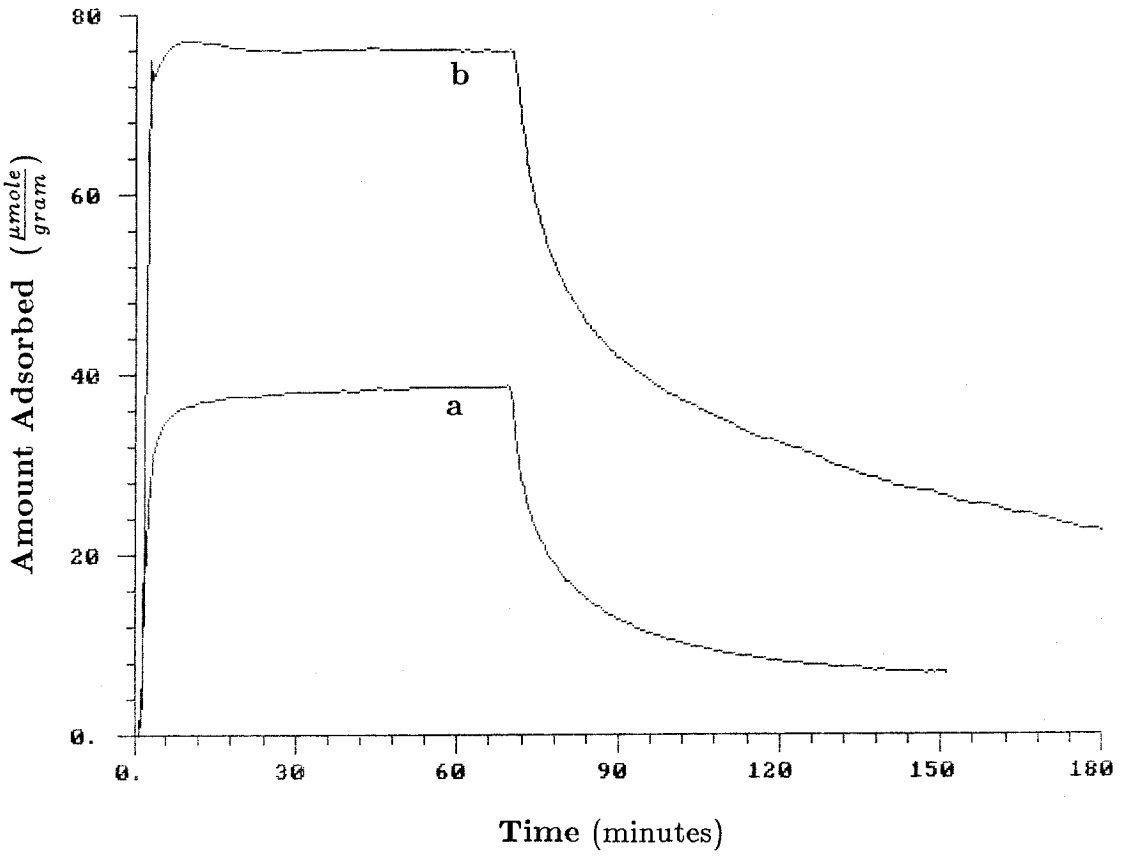

Figure 4.2. Adsorption and Desorption of SO_2 on (a)γ-Al_2O_3 and (b)$NaOH$-treated γ-Al_2O_3 at 750^oC with 15% SO_2.

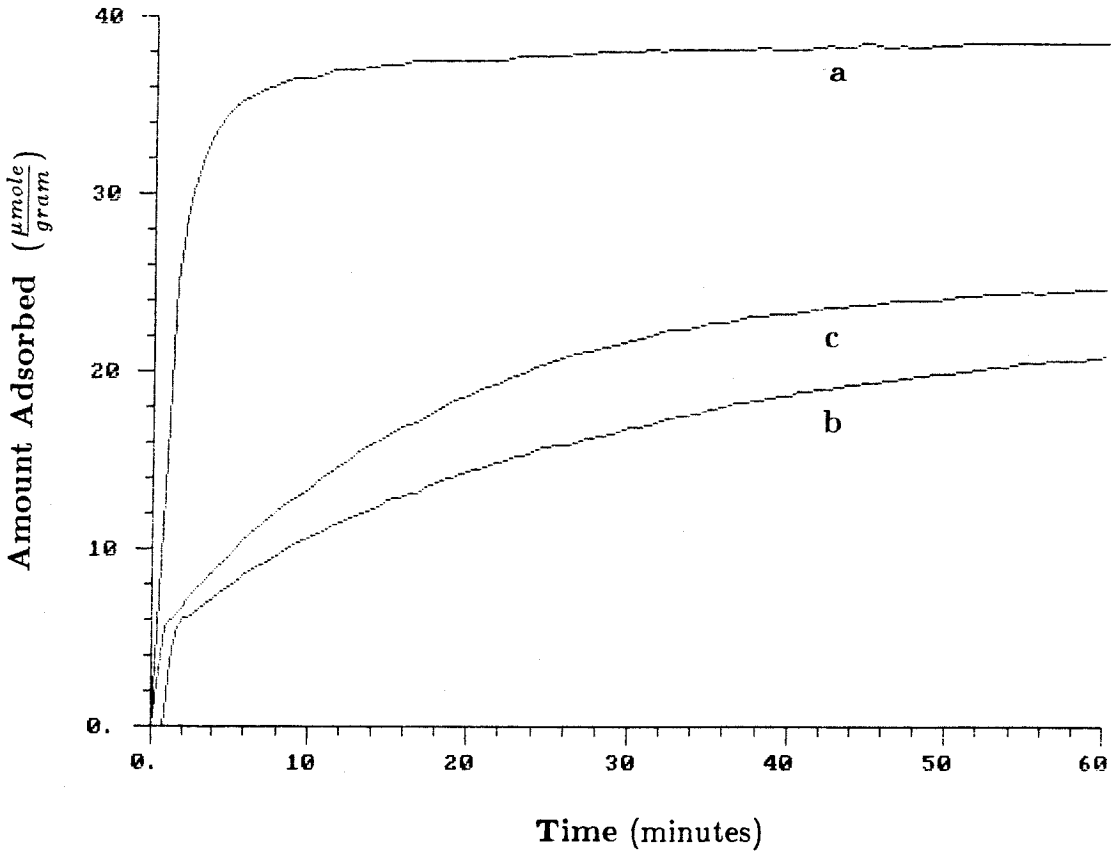

Figure 4.3. SO_2 Adsorption on γ-Al_2O_3 at :
(a,b) 700, (c) 800^0C, with 15% SO_2.

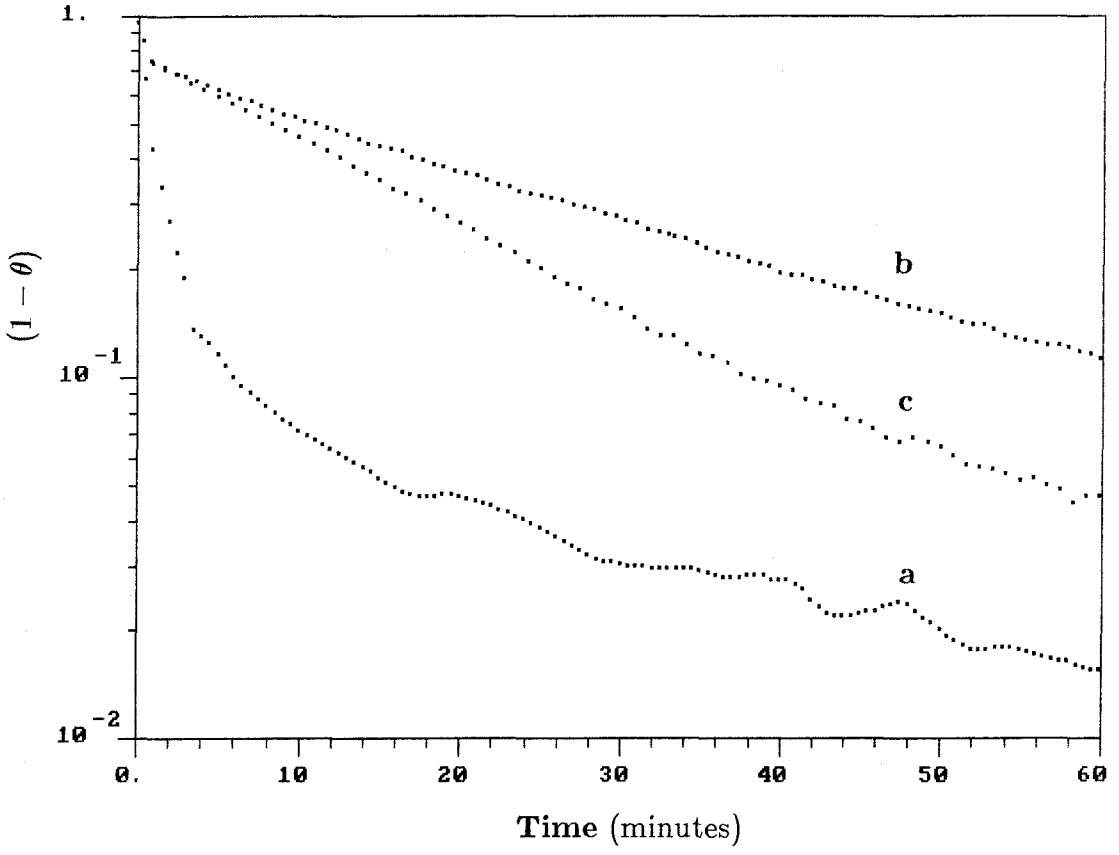

Figure 4.4. SO_2 Adsorption on γ-Al_2O_3 at :
(a,b) 700, (c) 800^0C, with 15% SO_2.

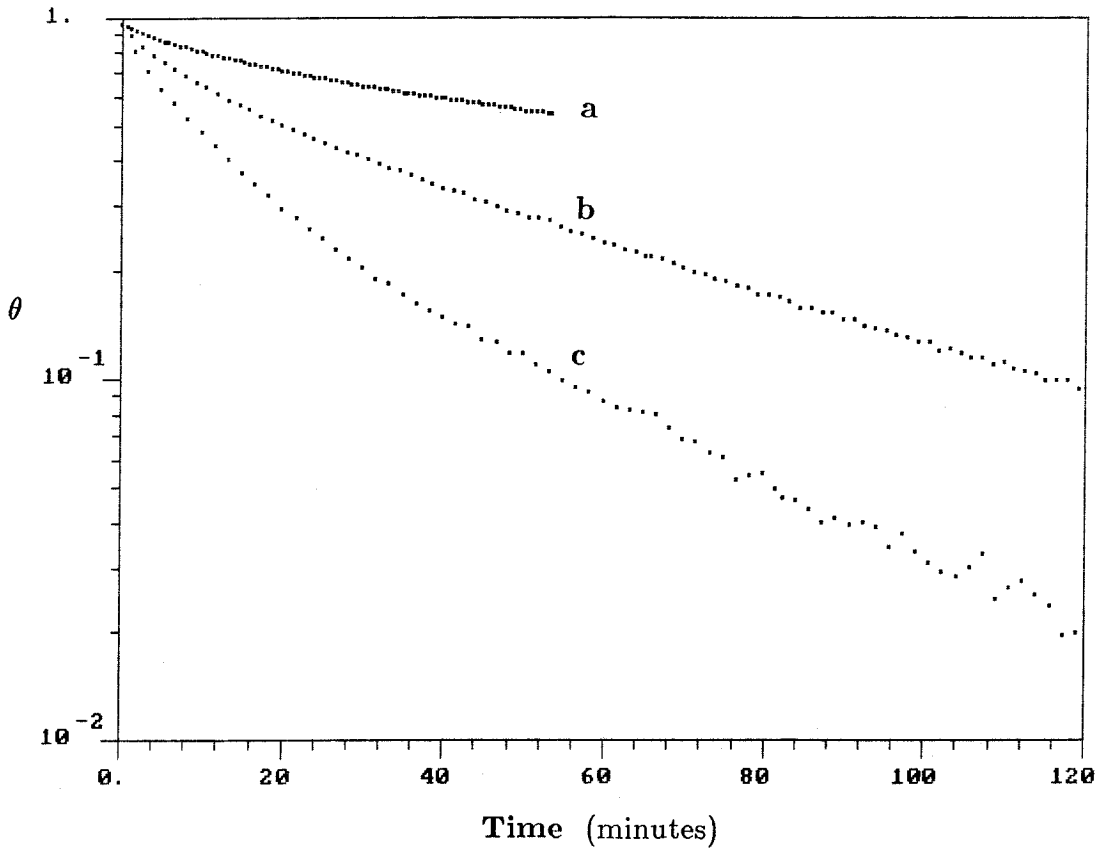

Figure 4.5. SO_2 Desorption from γ-Al_2O_3 at :

(a) 700, (b)750, and (c) 800^0C.

5. TEMPERATURE-PROGRAMMED DESORPTION

5.1. Introduction

Temperature-programmed desorption (TPD) is a technique wherein an adsorbed gas is released from a surface by a continuous increase of the surface temperature. Because the amount desorbed is measured over a wide range of temperatures, thermal desorption spectra provide information about chemisorption phenomena that would require several isothermal experiments.

The method was originally called *flash filament technique*, and was used to measure N_2 adsorption on tungsten. In the early stages the adsorbate was preadsorbed on a metal surface in a vacuum system and rapidly desorbed (i.e., *flashed*) by heating, while the pressure was recorded using a sensitive gauge [1,2,9,10,11]. It was soon recognized that the information obtained from the pressure bursts could be used to identify different adsorbed species, and even quantify their binding energies [9-11]. Through later improvements it became possible to study desorption from nonmetals and surface reactions, and more sensitive detectors such as thermistor sensors, thermal conductivity detectors and mass spectrometers were used [6].

Redhead [19] and Carter [3], working independently and simultaneously, developed a simplified mathematical analysis to determine the order of the desorption process, the activation energy of desorption and the initial site population from the desorption spectra obtained under typical temperature schedules. It was found that the temperature at which the desorption peak reaches its

maximum value, T_p, may shift as a result of surface heterogeneity, second-order desorption, or readsorption. On the other hand, in the simplest case of first-order kinetics T_p is independent of the initial coverage. It became apparent that the existence of a continuous distribution of binding energies renders the interpretation of the spectra very difficult [16]. In recent years the mathematical theory of temperature-programmed desorption has been greatly refined [4,5,8,13,25,26] and applied to many problems of practical interest [4,6,24]. Reviews of applications of the method and its theory are given in Refs. [6], [17], and [21].

In the present work TPD was used to study the adsorption of SO_2 on γ-Al_2O_3. Given the high surface area of the substrate and its considerable adsorptive capacity it was possible to measure the amount desorbed as a function of temperature using a thermogravimetric technique.

5.2. Experimental Method

The experimental system was the same as the one used for the isothermal adsorption/desorption experiments (Sec. 4.1 and Fig. 4.1). The temperature programmer allows isothermal operation, a temperature increase at constant heating rates between 1 and 100 $^{\circ}C$/min, or a pre-programmed heating schedule (see Appendix B). Several blank runs revealed an apparent weight increase with temperature, mainly due to thermal expansion of the balance arm. The total increase was less than 28 μg and was found to be almost independent of the heating rate. An average file from these runs was stored and substracted from

the data files.

As before, the substrates were pure and $NaOH$-treated aluminas (Sec. 3.1.1). A mixture of SO_2/N_2 and pure N_2 were used as adsorbate and diluent, respectively (Sec. 4.1). A thin bed of 40 to 60 mg. of sample particles was placed on the sample pan and pretreated under air and N_2 for 7 hours at $700°C$. The total system pressure was kept at 3 psig at all times. After the sample pretreatment the system was cooled under N_2 to the initial temperature of the run, usually 200 to $500°C$. Once thermal equilibrium was reached, SO_2 was admitted into the system and the weight increase recorded. Adsorption was allowed to proceed until no further weight change was observed. At that point the SO_2 stream was replaced by a pure N_2 stream and a linear temperature increase was programmed, with final temperatures between 900 and $1000°C$, and heating rates of 4 to 12 $°C$/min. The effects of SO_2 readsorption may become significant when the pumping speed is very small or the heating rate is very large. The above heating rates were chosen to minimize the effects of SO_2 readsorption, according to the criterion derived by Chan and Weinberg [5]. Weight, rate of weight change, sample temperature and exit gas concentration were recorded using the data acquisition system described in Appendix A.

After the completion of the experiments the raw data were reduced to files containing values of the rate of desorption vs. temperature. The data were smoothed and numerically differentiated using a 15-point, weighted coefficient routine [20,23]. This procedure provided spectra that were less noisy than the $\dot{W}$ signal from the TGA. Again, the IR data were somewhat noisy and subject to error due to desorption from the TGA internal walls. TPD spectra

were obtained with various values of initial coverage, initial temperature, and heating rate.

5.3. Results and Discussion

A typical TPD spectrum from an initially saturated (i.e., $\theta_0 = 1$) γ-Al_2O_3 surface is shown in Fig. 5.1. Preadsorption was carried out at $T_0 = 500°C$ and desorption took place between that temperature and $1000°C$, with a heating rate $\beta = 8\ °C/\text{min}$. Some SO_2 desorbs immediately after switching to N_2, but most of it desorbs in one single, broad peak at temperatures between 700 and $1000°C$, with a maximum desorption rate at $825°C$.

The position and shape of this peak exhibited great reproducibilty under different heating rates, initial temperatures, and initial amounts preadsorbed. Fig. 5.2 (curve a) shows a desorption spectrum obtained using a γ-Al_2O_3 sample with $T_0 = 300°C$, $\beta = 4\ ^0/\text{min}$, and $\theta_0 = 0.7$. The peak shown in Fig. 5.1 was plotted again for comparison (curve b). A larger percentage of the total SO_2 desorbs now at lower temperatures, between 300 and $500°C$. The high-temperature peak appears slightly shifted to the low-temperature region ($T_P = 800°C$).

TPD spectra obtained from the alkali-treated material appeared to vary widely with the sample batch and initial temperature. The peaks were broad and the temperature of maximum desorption rate T_P varied between 750 and $850°C$. A typical spectrum is shown in Fig. 5.3. The treated sample (a) exhibited a broader peak than the untreated one (b). Desorption began at

650^oC and did not appear to have ended at 1000^oC. In this particular case the maximum rate occured at $T_P = 780^oC$. Some desorption at the lowest end of the spectrum is observed in both cases.

The TPD spectra confirm the existence of two groups of adsorption sites, covering a broad range of binding energies. Weakly held SO_2 desorbs at temperatures below 550^oC, while complete desorption requires heating to 900-1000^oC. TPD/mass spectrometry studies on used Claus catalysts are in qualitative agreement with the spectra shown in Fig. 5.2 [7,15].

The skewness of the TPD peaks was measured following the definition given by Chan *et al.* [4] :

$$\chi = \left[\frac{T_1 + T_2 - 2T_P}{T_2 - T_1}\right] \times 100,$$

where χ = skewness parameter, T_1, T_2: lowest and highest temperatures at $\frac{1}{2} \times$ peak height, T_P = temperature at which the desorption rate is maximum. The skewness parameters varied between -16 and -20. Assuming that the criteria derived for the case of constant activation energy hold in our case, these values would indicate that desorption is a first-order process [4].

A calculation of the activation energy E_d from the peak width $\Delta W = T_2 - T_1$ based on the analysis by Chan *et al.* [4] yields E_d = 26-30 kcal/mole. Since the analysis assumes E_d = constant, these values can be interpreted as a mean activation energy for desorption from the strong sites.

REFERENCES

[1] Apker, L.,*Ind. Eng. Chem.*, **40**(5), 846, 1948.

[2] Becker, J.A., and Hartman, C.D., *J. Phys. Chem.*, **57**, 153, 1953.

[3] Carter, G., *Vacuum*, **12**, 245, 1962.

[4] Chan, C.M., Aris, R., and Weinberg, W.H., *Appl. Surface Sci.*, **1**, 360, 1978.

[5] Chan, C.M., and Weinberg, W.H., *Appl. Surface Sci.*, **1**, 377, 1978.

[6] Cvetanović, R.J., and Amenomiya, Y., *Advances in Catalysis*, **17**, 103, Academic Press, New York, 1967.

[7] Dalla Lana, I.G., Karge, H.G., and George, Z.M., *9th North American Meeting of The Catalyst Society*, Houston, 1985.

[8] Demmin, R.A., and Gorte, R.J., *J. Catal.*, **90**, 32, 1984.

[9] Ehrlich, G., *J. Phys. Chem.*, **60**, 1388, 1956.

[10] Ehrlich, G., *J. Chem. Phys.*, **34**(1), 29, 1961.

[11] Ehrlich, G., *J. Chem. Phys.*, **34**(1), 39, 1961.

[12] Ehrlich, G., *Advan. Catalysis*, **14**, 255, 1963.

[13] Falconer, J.L., and Madix, R.J., *J. Catal.*, **48**, 262, 1977.

[14] Golze, M., and Grunze, M., *Vacuum*, **31**(10-12), 697, 1981.

[15] Goodboy, K.P., Downing, J.C., and Fleming, H.L., *Sulfur and Carbon Deposition on Claus Catalyst Examined*, Aluminum Company of America, Pittsburgh, 1985.

[16] Grant, W.A., and Carter, G., *Vacuum*, **15**(1), 13, 1965.

[17] King, D.A., *Surface Sci.*, **47**, 384, 1975.

[18] Menzel, D., *Chemistry and Physics of Solid Surfaces*, R. Vanselow and R. Howe, eds., Springer-Verlag, New York, 1982.

[19] Redhead, P.A., *Vacuum*, **12**, 203, 1962.

[20] Savitzky, A., and Golay, M.J.E., *Anal. Chem.*, **36**(8), 1627, 1964.

[21] Schmidt, L.D., *Catal. Rev. Sci. Eng.*, **9**, 115, 1974.

[22] Soler, J.M., and García, N., *Surface Sci.*, **124**, 563, 1983.

[23] Steinier, J., Termonia, Y., and Deltour, J., *Anal. Chem.*, **44**(11), 1906, 1972.

[24] Taylor, J.L., and Weinberg, W.H., *Surface Sci.*, **78**, 259, 1978.

[25] Taylor, J.L., and Weinberg, W.H., *Surface Sci.*, **78**, L508, 1978.

[26] Wittrig, T.S., Ibbotson, D.E., and Weinberg, W.H., *Appl. Surface Sci.*, **4**, 234, 1980.

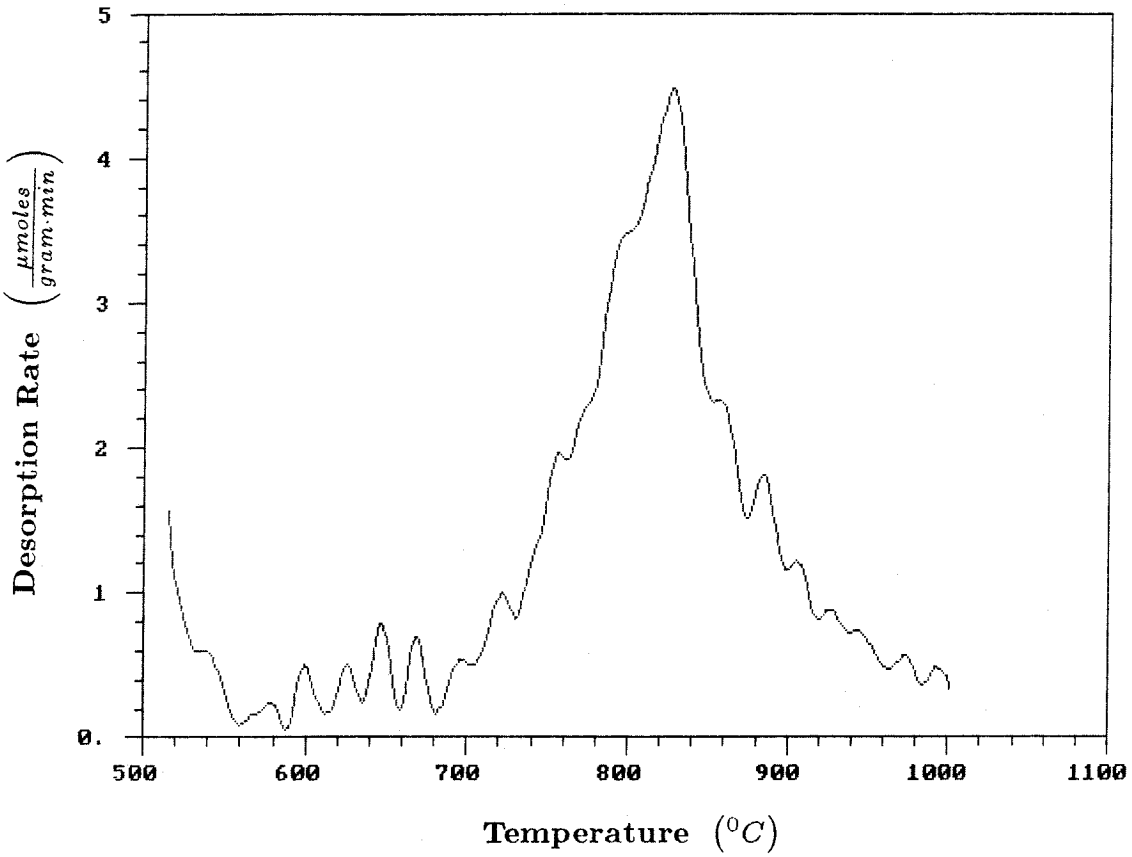

Figure 5.1. TPD Spectrum from $SO_2/\gamma\text{-}Al_2O_3$,
$T_0 = 500°C$, $\theta_0 = 1$, $\beta = 8\ \frac{°C}{min}$.

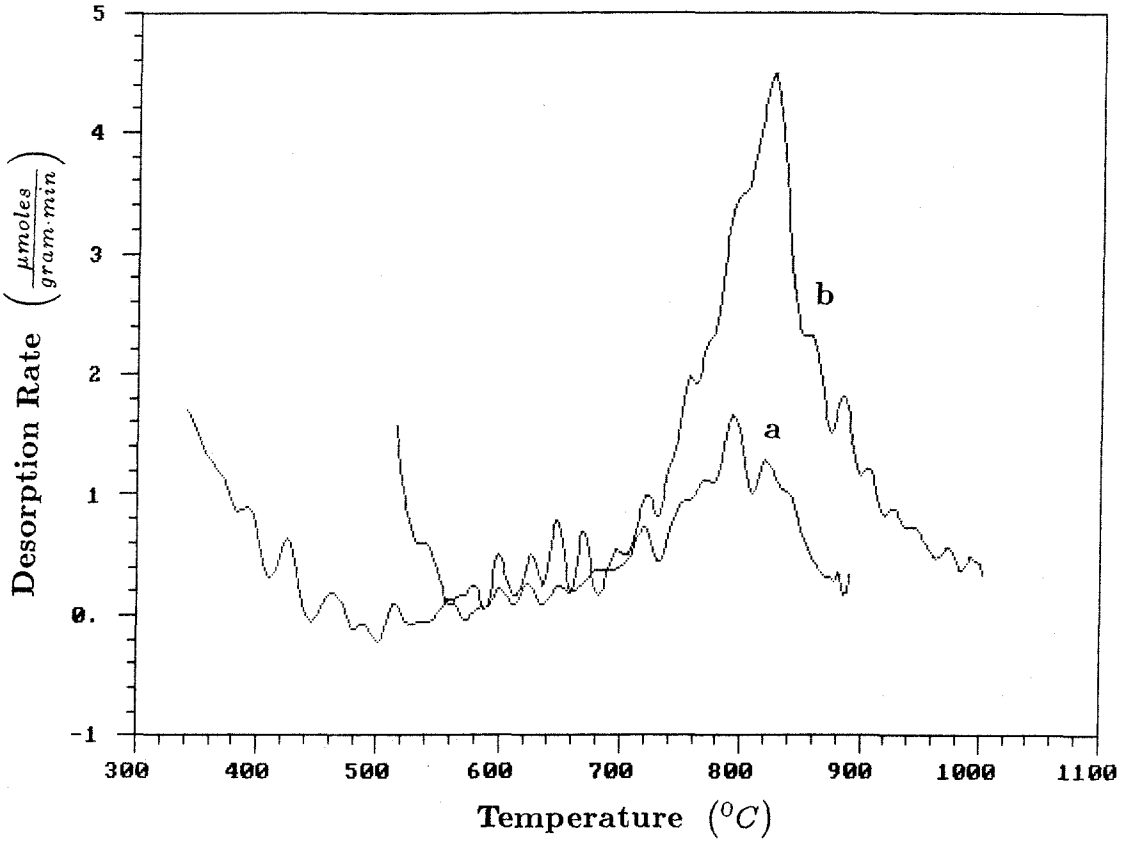

Figure 5.2. TPD Spectra from $SO_2/\gamma\text{-}Al_2O_3$, (a) $T_0 = 300°C$, $\theta_0 = 0.7$, $\beta = 4\ \frac{°C}{min}$, (b) $T_0 = 500°C$, $\theta_0 = 1$, $\beta = 8\ \frac{°C}{min}$.

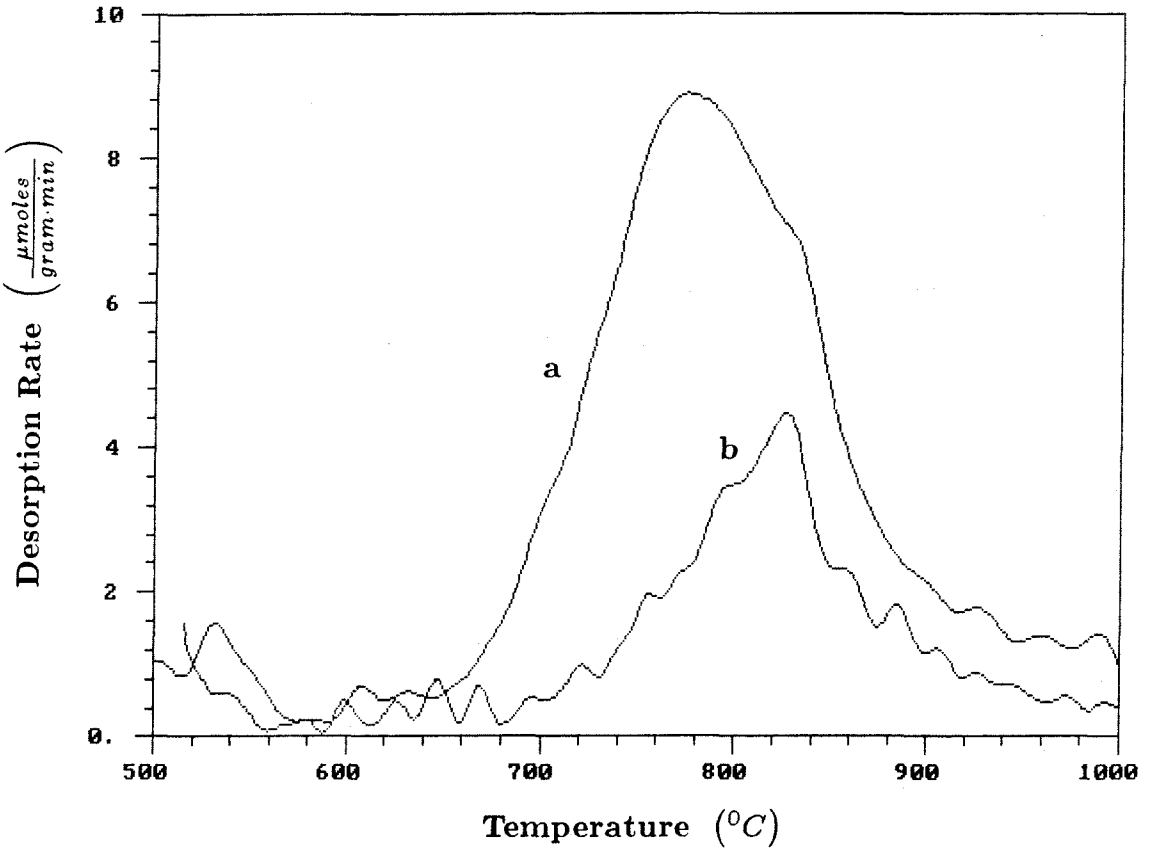

Figure 5.3. TPD Spectra for (a) $NaOH$-treated γ-Al_2O_3, (b) γ-Al_2O_3. $T_0 = 500^0C$, $\theta_0 = 1$, $\beta = 8\ \frac{^0C}{min}$.

6. CONCLUSIONS AND RECOMMENDATIONS

The results presented in Secs. 3.1.3, 4.3 and 5.3 confirm the existence of two types of adsorbed species at 700-800°C, in agreement with IR observations at lower tempertures [2,4]. Depending on the surface treatment and operating conditions, 20 to 40% of the adsorbed SO_2 may be present as a strongly chemisorbed species below 800°C. Complete desorption of this species requires heating to 900-1000°C. The remaining SO_2 adsorbs more weakly, with adsorption energies between 8 and 21 kcal/mole.

Both the equilibrium and adsorption experiments show a loss of adsorptive capacity after the first exposure to SO_2. This is partly due to blockage of the strong sites. Adsorption on the remaining sites, however, is much slower after the first exposure, indicating that the adsorptive properties of the surface have been modified. Several electron-donor adsorbates have been reported to attach very strongly to special sites present in γ- and η-Al_2O_3 [7]. These sites, which have been designated *X-sites*, consist of aluminum cations adjacent to basic OH groups, and exhibit strong Lewis acidity. IR studies revealed that adsorption on X-sites strongly perturbs the neighboring OH groups [7]. In the case of SO_2, FTIR studies have shown that the most strongly chemisorbed species result from unidentate $S \rightarrow Al$ bonds, while the weakly held species is directly attached to the hydroxyls. It is then reasonable to conclude that strong adsorption of SO_2 on the X-sites would alter the adsorptive properties of the weaker sites.

The adsorptive capacity of the alumina surface was found to be very sen-

sitive to its history and thermal treatment. The effect of the temperature is threefold. As the temperature increases the amount of SO_2 adsorbed per unit surface area increases as a result of surface activation and desorption of previously adsorbed SO_2, whereas the specific surface area decreases. The net effect depends on the extent and kinetics of these competitive processes. The surface area of γ-Al_2O_3 decreases rather slowly below 150 m^2/gram [1], and did not change significantly during the time span of our equilibrium experiments. On the other hand, an increase in the temperature of the thermal treatment caused a substantial enhancement in the adsorptive capacity.

The treatment of γ-Al_2O_3 with $NaOH$ causes a sharp increase in its adsorption capacity, as a result of the formation of sodium aluminate on the surface. Although desorption from the treated alumina comprises the decomposition of the sulfite, the overall desorption rate did only appear to be slightly smaller than that of pure γ-Al_2O_3. The fraction of adsorbate that remains on the surface at 700-800^oC is comparable in both cases.

Several questions remain open for further investigation :

(i) *The role of* O_2 : It has been suggested that the SO_2 uptake may increase substantially in the presence of oxygen [1,8]. Some chemisorbed species could become more stable upon oxidation to sulfate, particularly in the case of alkali-treated alumina :

$$Na_2SO_3 + \frac{1}{2}O_2 \rightarrow Na_2SO_4.$$

At high SO_2 concentrations, the formation of aluminum sulfate becomes

possible [2] :

$$Al_2O_3 + 3SO_2 + \frac{3}{2}O_2 \rightarrow Al_2(SO_4)_3.$$

(ii) *The effect of changes in the alumina structure* : As the calcination of a transition alumina proceeds at a given (constant) temperature, its specific surface area, hydroxyl content, and γ-Al_2O_3/α-Al_2O_3 ratio decrease. All these processes can be followed as a function of time using BET N_2 adsorption, thermogravimetry and X-ray diffractometry, respectively. By measuring the SO_2 adsorption at different stages of the process it would be possible to correlate changes in the adsorptive properties with changes in the structure of the alumina.

(iii) *The reaction of strongly chemisorbed SO_2 with CO* : It was found that the chemisorbed species could not be removed by reduction with CO. The possibility that reduction does take place, leading to the formation of chemisorbed sulfur needs to be investigated (e.g. FTIR spectroscopy).

(iv) *The effect of SO_2 on the surface properties* : The effect of the strongly held species on the adsorptive properties of the remaining sites should be studied using FTIR spectroscopy.

(v) *The heat of adsorption of the strongly chemisorbed species* : Although the equilibrium isotherm 3.4 gives an adequate description of the equilibrium adsorption, the values of the parameters are more sensitive to the regression technique than to the temperature, precluding the calculation of q_1 and q_2 from K_1 and K_2. Similarly, calculations of the isosteric heat of adsorption were not possible at very low coverage, when adsorption on the *strong*

sites is more likely to occur. Glass and Ross [6] showed that the heat of adsorption of SO_2/Al_2O_3 can be measured calorimetrically, and can be as high as 85 kcal/mole.

REFERENCES

[1] Andersson, S., Pompe, R., and Vannerberg, N., *Appl. Catalysis*, **16**, 49, 1985.

[2] Chang, C.C., *J. Catal.*, **53**, 374, 1978.

[3] Datta, A., Cavell, R.G., Tower, R.W., and George, Z.M., *J. Phys. Chem.*, **89**(3), 443, 1985.

[4] Deo, A.V., Dalla Lana, I.G., and Habgood, H.W., *J. Catal.*, **21**, 270, 1971.

[5] Fink, P., *Z. Chem.*, **7**, 324, 1967.

[6] Glass, R.W., and Ross, R.A., *Can. J. Chem.*, **50**, 2537, 1972.

[7] Knözinger, H., and Ratnasamy, P., *Catal. Rev.-Sci. Eng.*, **17**(1), 31, 1978.

[8] Summers, J.C., *176th National Meeting of the American Chemical Society*, Miami Beach, 1978.

PART II

STUDY OF A HIGH-TEMPERATURE SULFUR DIOXIDE SORBENT

7. INTRODUCTION AND BACKGROUND

Although more complex in nature, regenerable flue gas desulfurization (FGD) processes eliminate the problems associated with the handling and disposal of the sulfated sorbent, and may produce elemental sulfur as a by-product. The U.S. Bureau of Mines has conducted an extensive study of the use of *alkalized alumina* as a dry, regenerable sorbent for SO_2 [2,15,16,19]. This material is an alkali deficient sodium aluminate obtained by coprecipitation of aluminum sulfate and sodium carbonate, followed by calcination of the dawsonite. The sorbent can be repeatedly regenerated with natural gas, hydrogen [2], carbon monoxide [16] or propane [19] at 600-730^oC. Reduction by carbon monoxide at 680^oC removes only 30% of the sulfur [16]. The rigors of recirculation through moving and fluidized beds cause severe losses of the sorbent by attrition [19], specially at high concentrations of sodium in the solid [16]. Attrition losses were found to be substantially lower when the sorbent was prepared by impregnation [13].

Limited effort has been devoted to using calcium-containing bulk materials as regenerable sorbents. Regeneration of lime or limestone sorbents employed in FBC and lime injection processes is very difficult due to the high chemical stability of the calcium sulfate [4]. Some calcium silicates are reactive towards SO_2 and reduction of the sulfation products is more favorable thermodynamically than the reduction of calcium sulfate [22].

One of the problems associated with the use of bulk dry sorbents is that both sulfation and regeneration may proceed at low rates at moderate temper-

atures. Only a small portion of a material obtained by coprecipitation may be available for reaction on the pore surface. Since the rest of the active component is buried within the support material the overall rate of reaction is limited by slow diffusional processes. In order to improve the mass transfer characteristics several processes using supported [9,17,18] or unsupported [14] molten salts have been proposed. Regeneration of a sorbent consisting of a mixture of molten alkali carbonates, for example, was reported to proceed very rapidly at $427°C$ [14]. The use of an unsupported melt, however, would pose serious corrosion problems to process equipment.

The rate of mass transfer to and from the sorbent can be substantially increased by distributing the active material as a thin layer over the pore surface of a support, such as silica or alumina. Although the capacity of such system per unit volume of sorbent may or may not be greater than that of the corresponding bulk material, the reactivity is significantly higher [20]. Screening of a number of metals and metal oxides supported on alumina showed that Na_2O has a particularly high reactivity towards SO_2, and a higher sorption capacity than alkalized alumina [20]. A process using alumina-supported copper oxide has already been commercialized [6,10]. Regeneration of this sorbent can be carried out with H_2 or a H_2/CO mixture at $400°C$ in a fixed [6,10] or fluidized bed [1,23].

The present work concentrates on the behavior of a sorbent consisting of a mixture of Na and Li aluminates supported on porous alumina. Preliminary work on Na, Li, and Na-Li mixtures supported on alumina showed that these sorbents can be repeatedly regenerated using CO at 700-800$°C$ [21]. Reduction

in that temperature range leads to formation of gaseous S_2, COS and SO_2, and possibly sulfide, aluminate and/or carbonate, through a complex network of catalytic and noncatalytic chemical reactions. The rate of sulfur removal and the selectivity towards elemental sulfur are higher when both Na and Li are present, probably due to the presence of a molten layer on the surface of the support. The mixture of sodium and lithium sulfates is molten at 700-800°C. Silica supported sorbents do not react with SO_2, and sulfated γ-Al_2O_3 sorbents decompose irreversibly. Therefore, α-Al_2O_3 was found to be the most suitable support for these sorbents [7,21].

The main objective of this investigation was to elucidate the nature of the species and chemical reactions involved in the regeneration stage, with emphasis on the effect of sorbent, support, temperature, CO concentration, and sorbent loading on the product selectivity and kinetics. Thermogravimetry, temperature-programmed reaction, gas chromatography, scanning electron microscopy, and X-ray photoelectron spectroscopy were the experimental techniques employed. The preparation and chemical composition of the sorbent, and its reaction with SO_2 and O_2 are discussed in Chapters 8 and 9, respectively. The problem of sorbent regeneration is addressed in Chapter 10, the most extensive one. The chemical reactions involved in the reduction of the supported sulfates are discussed in detail, and a simple kinetic model is proposed.

REFERENCES

[1] Best, R.J., and Yates, J.G., *Ind. Eng. Chem. Process Des. Dev.*, **16**(3), 347, 1977.

[2] Bienstock, D., Brunn, L.W., Murphy, E.M., and Benson, H.E., *BuMines Inf. Circ. 7836*, 1958.

[3] Borgwardt, R.H., *AIChE J.*, **31**(1), 103, 1985.

[4] Chen, J.M., and Yang, R.T., *Ind. Eng. Chem. Fundam.*, **18**(2), 134, 1979.

[5] Cho, M.H., and Lee, W.K., *J. Chem. Eng. Japan*, **16**(2), 127, 1983.

[6] Dautzenberg, F.M., Naber, J.E., and Van Ginneken, A.J., *Chem. Eng. Prog.*, **67**(8), 86, 1971.

[7] Gavalas, G.R., Edelstein, S., Flytzani-Stephanopoulos, M., and Weston, T.A., *AIChE J.*, in press.

[8] Glasson, D.R., O'Neill, P., and Srodzinski, R. *Adsorption at the Gas-Solid and Liquid-Solid Interface*, J. Rouquerol and K.S.W. Sing (editors), Elsevier, Amsterdam, 1982.

[9] Glueck, A.R., *AIChE Symposium Ser.*, **70**(137), 231, 1974.

[10] Groenendaal, W., Naber, J.E., and Pohlenz, J.B., *AIChE Symposium Series*, **72**(156), 12, 1976.

[11] Hedges, S.W., Diffenbach, R.A., and Fauth, D.J., *AIChE 1985 Winter National Meeting*, Chicago, 1985.

[12] McCrea, D.H., Forney, A.J., and Myers, J.G., *J. Air Pollut. Control Assoc.*, **20**(12), 819, 1970.

[13] Medellin, P.M., Weger, E., and Duduković, M.P., *Ind. Eng. Chem. Process Des. Dev.*, **17**(4), 528, 1978.

[14] Oldenkamp, R.D., and Margolin, E.D., *Chem. Eng. Progress*, **65**(11), 73, 1969.

[15] Russell, J.H., Town, J.W., and Kelly, H.J., *BuMines Rep. Inv. 7415*, 1970.

[16] Schlesinger, M.D., and Illig, E.G., *Chem. Eng. Prog. Symposium Series*, **67**(115), 46, 1971.

[17] Sealock, L.J., Lyke, S.E., Hallen, R.T., and Roberts, G.L., *Battelle Pacific Northwest Laboratories Progr. Rep.*, January 1983.

[18] Stegen, G.E., *Proceedings of the Second Annual Contractors' Meeting on Contaminant Control in Hot Coal Derived Gas Streams*, Morgantown, 1982.

[19] Town, J.W., Paige, J.I., and Russell, J.H., *Chem. Eng. Prog. Symposium Series*, **66**(105), 260, 1970.

[20] Vogel, R.F., Mitchell, B.R., and Massoth, F.E., *Env. Sci. Tech.*,**8**(5), 432, 1974.

[21] Weston, T.A., *PhD Dissertation*, California Inst. of Tech., 1985.

[22] Yang, R.T., and Shen, M.S., *AIChE J.*, **25**(5), 811, 1979.

[23] Yeh, J.T., Demski, R.J., Strakey, J.P., and Joubert, J.I., *Env. Progr.*, **4**(4), 223, 1985.

8. SORBENT PREPARATION AND CHARACTERIZATION

8.1. Sorbent Preparation

Various samples consisting of supported and unsupported mixtures of sodium and lithium salts were used in the sulfation and reduction experiments. A description of the samples is given in Table 8.1. All sorbent materials were obtained by precipitation from solutions containing 60% Na and 40% Li (molar), the composition of the $Na_2SO_4 + Li_2SO_4$ eutectic. In all samples except $ST1$, $ST2$, $AC1$ and AL the salts were deployed over the pore surface of a support by impregnation. The sorbents designated ST were prepared in the sulfated form, whereas those termed AC were obtained from a solution of alkali acetates. The latter are more soluble than the former, thus facilitating the impregnation of high loading sorbents. Two samples consisting of supported alkali sulfides ($SD\alpha$) and carbonates ($CT\alpha$) were prepared for specific experiments.

The porous supports used were SP-100 χ-Al_2O_3 from Alcoa Chemicals (sample $AC\chi$), T-2432 γ-Al_2O_3 from United Catalysts (sample $ST\gamma$), and AL-3980 α-Al_2O_3 from Harshaw/Filtrol (all other samples). One sorbent ($AC\alpha1$) was made by impregnation of 4 mm diameter AL-3980 pellets. In all other cases the pellets were ground and sieved prior to impregnation. The size of the particles is indicated in the third column of Table 8.1. Samples $AC\alpha1$ and $ST\alpha1$ to 3 have approximately the same loading, but different particle sizes. The rest of the samples have the same range of particle sizes : $210 \leq d_p \leq 420\ \mu m$.

Because the particles were not suitable for X-ray photoelectron spectros-

copy (XPS) experiments, two samples ($AC1$ and $ST2$) were prepared by precipitation on nonporous, smooth Al_2O_3 films. Plates of *ADS*-996 *microrel* substrate supplied by Coors Ceramics were cut into 1 cm^2 squares. A dilute solution with a known concentration of the corresponding salt was spread evenly on the substrate using a microsyringe. The samples were then dried at $90°C$. The procedure was repeated several times to ensure homogeneity in the surface concentration.

A pure eutectic mixture ($ST1$) was prepared by precipitation and drying from a $Na_2SO_4 + Li_2SO_4$ solution, for use in unsupported reduction experiments. Na and Li aluminates (sample AL) were obtained by reacting equimolar quantities of α-Al_2O_3 and the alkali carbonates :

$$Al_2O_3 + M_2CO_3 \rightarrow 2MAlO_2 + CO_2, \qquad (8.1)$$

where $M = Na,\ Li$. The alumina particles were ground and sieved to $d_p \leq 400$ mesh, to ensure complete conversion to aluminate [2]. The reacting mixture was placed in a Leco furnace at $1000°C$, for 24 hours. The aluminates were then crushed and stored.

Impregnation of samples $AC\alpha 1$ and 2 was carried out using a standard excess solution technique. Since the resulting loading was somewhat unpredictable [13], all other samples were impregnated using an incipient wetness method, either under vacuum ($ST\alpha 4$, $AC\alpha 3$, $AC\kappa$, $ST\gamma$), or at atmospheric pressure ($ST\alpha 1$ to 3, $CT\alpha$, $SD\alpha$). In both cases a measured amount of the impregnating solution was slowly added to a known amount of dry particles, while the sample was stirred vigorously. The impregnation was stopped when

the solution completely filled the pores, indicated by particle clustering. The samples were dried at $90°C$ and weighed. The process was repeated until the desired loading was achieved. Impregnation under vacuum resulted in a 15 to 25% enhancement in the loading. After the impregnation was completed, the samples were washed and dried at $90°C$. The sorbents prepared in the sulfated form were calcined at $700°C$ for 5 hours in the Leco furnace.

The sorbent loadings based on the sulfated form are listed in the last column of Table 8.1. The loadings of the samples prepared by excess solution impregnation were calculated from the weight change upon sulfation of the calcined samples. That amount differed by 20-30% from a calculation based on the concentration of the impregnating solution, and assuming no adsorption of the solutes during impregnation. The loadings of the samples prepared using the incipient wetness techique were obtained from the volume of the impregnated solution and from the weight change upon impregnation. The loadings of the samples prepared from M_2CO_3 and CH_3-COOM were also obtained from the weight increase associated with the sulfation of the calcined samples according to :

$$2MAlO_2 + SO_2 + \frac{1}{2}O_2 \rightarrow M_2SO_4 + Al_2O_3. \qquad (8.2)$$

The sorbent loading is :

$$\lambda = 16.81\left(\frac{W_f - Wi}{W_f}\right),$$

where λ = sorbent loading (mmole M_2SO_4/gram), W_i, W_f = sample weight before and after sulfation (mg). The sorbent loadings obtained using these

three methods agreed within ±10%. Barium sulfate precipitation and atomic absorption analyses [13] of some of the samples were also in agreement with those values.

8.2. Sorbent Characterization

Given the small size of the particles, the open pore structure of α-Al_2O_3, and the fact that the samples were dried prior to impregnation, both the liquid imbibition and the diffusion of the solutes into the particles during impregnation are very fast, leading to a homogeneous concentration of solute over the entire pore volume [9]. The drying process causes the precipitation of small $NaLiSO_4$ crystallites, which melt at $T = 630°C$ [11]. The molten mixture wets the pore surface forming a thin layer.

The BET N_2 surface area of the sorbent materials was determined before and after impregnation, using the technique described in Sec. 3.1.2. The surface area of the γ-Al_2O_3 particles before impregnation was 95 m^2/g, and that of sample $ST\gamma$ was 86 m^2/g. The χ-Al_2O_3-supported sample $AC\chi$ exhibited a more dramatic decrease in surface area, from 153 to 59 m^2/g. The surface area of the α-Al_2O_3-supported sorbents varied between 4.5 and 5.2 m^2/g, and was almost unaffected by the impregnation process.

The effect of impregnation with $Na/Li\ SO_4$ on the physical structure of the α-Al_2O_3 support was examined qualitatively using scanning electron microscopy (SEM). Fresh and impregnated pellets of α-Al_2O_3 were split in half, mounted on aluminum discs and coated with a thin layer ($\approx$ 100 Å) of gold

to prevent charging. The internal surface of the pellets was examined under a ETEC-Autoscan scanning electron microscope. The micrographs shown in Fig. 8.1 indicate that the texture of the α-Al_2O_3 surface was not altered by the impregnation and heat treatment. The surface area measurements and SEM observations indicate that while the stable structure of α-Al_2O_3 remains unchanged after the impregnation and heat treatment, the more unstable transition aluminas may undergo structural changes and, possibly, pore blockage.

Calcination of the acetates and carbonates and reduction of the sulfates lead to the formation of alkali oxides or, more likely, aluminates and/or carbonates which constitute the active sorbent. Assuming a homogeneous distribution of alkali aluminate over the entire pore surface, the active layer of a medium-loading sorbent ($ST\alpha1$, $AC\alpha1$, $CT\alpha$) is only 20 molecules thick ($\approx$100 Å). In the cases of low ($ST\alpha4$) and high ($AC\alpha3$) loadings the thicknesses are 10 and 300 Å, respectively. As shown in Fig. 8.2, the active layer occupies a small fraction of the pore volume.

8.2.1. Acetate and Carbonate Decomposition In order to obtain information about the sorbent composition from the weight loss that accompanies the regeneration it is necessary to know what fraction of the active sorbent, if any, is in the carbonate form.

Any pure alkali oxides formed during reduction would react with CO_2 produced or present in the gas stream to form more stable carbonates, as predicted by the thermodynamic data shown in Fig. 8.3 (c) and (d). However, pure solid alkali carbonates decompose in the presence of Al_2O_3 at $T > 700°C$ if the CO_2

partial pressure is less than 1 atm. (Fig. 8.3 (a) and (b)). Since the Na_2CO_3-Li_2CO_3 eutectic has almost the same composition as the sulfates (58/42), with a eutectic temperature of $510°C$ [5], the carbonate mixture would be molten at the operating temperatures of the sorbent.

The decomposition of alumina-supported alkali carbonates and acetates was studied using the TGA system and method described in Secs. 4.1 and 5.2. Fig. 8.4 shows temperature-programmed decomposition spectra obtained by heating samples $CT\alpha$ and $AC\alpha 2$ under pure N_2 at a constant heating rate $\beta = 8\ °C/\text{min}$. In both cases the decomposition is complete at $750°C$. The total weight losses agree well with those calculated from the corresponding sample loadings (Table 8.1), assuming complete conversion to aluminate. Duplicate runs at $\beta = 4\ °C/\text{min}$ yielded similar results. The rate of carbonate decomposition becomes significant at $400°C$, and attains two maxima at 480 and $640°C$. Based on previous studies on similar systems [3,6,8] it can be concluded that these two peaks correspond to the decomposition of Li_2CO_3 and Na_2CO_3, respectively.

The decomposition of the alkali acetates begins at $200°C$. The shape of the spectrum suggests that carbonate formation according to :

$$2CH_3 \cdot COOM + 4O_2 \rightarrow M_2CO_3 + 3CO_2 + 3H_2O, \qquad (8.3)$$

first takes place at $200 < T < 300°C$, followed by :

$$M_2CO_3 + Al_2O_3 \rightarrow 2MAlO_2 + CO_2. \qquad (8.4).$$

The area under the first peak accounts for 61% of the total weight loss, compared to 57% predicted by reactions 8.3 and 8.4.

The reaction of $MAlO_2/Al_2O_3$ with CO_2 was examined. A sample of supported carbonates ($CT\alpha$) was decomposed by heating at $800°C$ and then exposed to a gas stream containing CO_2 ($p_{CO_2} = 532\ torr$) and N_2 at temperatures between 200 and $800°C$. Formation of carbonates was only observed in the range $400 < T < 500°C$. The rate of reaction was very low : 2×10^{-4} moles/mole·min at $400°C$. The lack of reactivity at high temperatures may be due to thermodynamic limitations (Fig. 8.3). This explanation is consistent with the fact that both supported ($CT\alpha 2$, calcined) and unsupported (AL) aluminates began to react with pure CO_2 at $T = 600°C$ and $p = 750\ torr$ in the BET system described in Sec. 3.1.2. Although carbonate formation is thermodynamically favorable at lower temperatures the reaction may be kinetically limited.

The isothermal decomposition of the supported carbonates ($CT\alpha 2$) was observed by heating the sample to $500°C$ under CO_2 and then switching over to N_2. A shown in Fig. 8.5., the decomposition rate is high, but does not proceed to completion. Only 30% of the carbonates decomposes at that temperature. The reaction of alumina with molten carbonate is known to be controlled by diffusion through the aluminate product [2]. In our case, however, the aluminate layer is very thin (Fig. 8.2). Fig. 8.4 provides a more plausible explanation : only the lithium carbonate decomposes at a significant rate at $500°C$.

Taking into account that CO_2 is present in small concentrations during sorbent regeneration, the above observations indicate that the sorbent consists primarily of supported alkali aluminates at $700 < T < 800°C$, although the possibility of transient accumulations of (sodium) carbonate cannot be ruled

out. It is not possible to determine at this point whether there is a sharp interface between the aluminate layer and the alumina substrate, or there exists a transition region with some penetration of sodium oxide into the alumina lattice. Both sodium oxide and lithium oxide are known to form stable compounds with alumina, with molar ratios varying between 1:1 and 1:11. The so-called *beta-aluminas*, for example, represent a group of sodium aluminates with composition $Na_2O \cdot 5Al_2O_3$ to $Na_2O \cdot 11Al_2O_3$ and similar crystalline structure. Lithium oxides form similar compounds, termed *lithium zeta*, with composition $Li_2O \cdot 5Al_2O_3$ to $Li_2O \cdot 8Al_2O_3$. Formation of these phases, however, has only been reported at temperatures above $1000°C$ [4,10,12].

REFERENCES

[1] Barin, I., and Knacke, O., *Thermochemical Properties of Inorganic Substances*, Springer-Verlag, Berlin, 1973.

[2] Christie, J.R., Darnell, A.J., and Dustin, D.F.,

[3] Cobb, J.W., *J. Soc. Chem. Ind.*, **29**, 399, 1910. *J. Phys. Chem.*, **82**(1), 33, 1978.

[4] DeVries, R.C., and Roth, W.L., *J. Am. Ceram. Soc.*, **52**(7), 364, 1969.

[5] Eitel, W., and Skaliks, W., *Z. anorg. u. allgem. Chem.*, 183, 270, 1929.

[6] Gavalas, G.R., Edelstein, S., Flytzani-Stephanopoulos, M., and Weston, T.A., *AIChE J.*, in press.

[7] *JANAF Thermochemical Tables*, 2nd ed., NSRDS-NS-37, 1971.

[8] Kovalenko, V.I., and Bukin, H.G., *Russ. J. Inorg. Chem.*, **23**(2), 158, 1978.

[9] Lee, S.Y., and Aris, R., *Catal. Rev.-Sci. Eng.*, **27**(2), 207, 1985.

[10] Lejus, A.M., *Rev. Hautes Temp. Refract.*, I, 53-95, 1964.

[11] Nacken, A.A., *Neues Jahrb. Mineral. Geol.*, Beilage Bd., 24A, 34, 1910.

[12] Wefers, K., and Bell, G.M., *Oxides and Hydroxides of Aluminum*, Aluminum Company of America, Pittsburgh, 1972.

[13] Weston, T.A., *PhD Dissertation*, California Inst. of Tech., 1985.

Table 8.1. Composition of Sorbents.

Sample	Salts	Support	Sorbent Loading	
			$\frac{mmole\ M^+}{m^2}$	$\frac{mg\ M_2SO_4}{gram}$
$ST\alpha 1$	$Na/Li\ SO_4$	α-Al_2O_3 (-35+65)	0.582	130.8
$ST\alpha 2$	$Na/Li\ SO_4$	α-Al_2O_3 (-65+80)	0.556	125.6
$ST\alpha 3$	$Na/Li\ SO_4$	α-Al_2O_3 (-120+150)	0.536	121.7
$ST\alpha 4$	$Na/Li\ SO_4$	α-Al_2O_3 (-35+65)	0.050	12.8
$AC\alpha 1$	$Na/Li\ Ac$	α-Al_2O_3 pellets	0.490	112.4
$AC\alpha 2$	$Na/Li\ Ac$	α-Al_2O_3 (-35+65)	0.539	122.2
$AC\alpha 3$	$Na/Li\ Ac$	α-Al_2O_3 (-35+65)	1.814	319.1
$AC1$	$Na/Li\ Ac$	Al_2O_3 film	0.576	—
$AC\chi$	$Na/Li\ Ac$	κ-Al_2O_3 (-35+65)	0.099	377.1
$CT\alpha$	$Na/Li\ CO_3$	α-Al_2O_3 (-35+65)	0.577	129.8
$SD\alpha$	$Na/Li\ S$	α-Al_2O_3 (-35+65)	0.595	133.3
$ST\gamma$	$Na/Li\ SO_4$	γ-Al_2O_3 (-35+65)	0.018	107.3
$ST1$	$Na/Li\ SO_4$	none	—	—
$ST2$	$Na/Li\ SO_4$	Al_2O_3 film	0.521	—
AL	$Na/Li\ AlO_2$	none	—	—

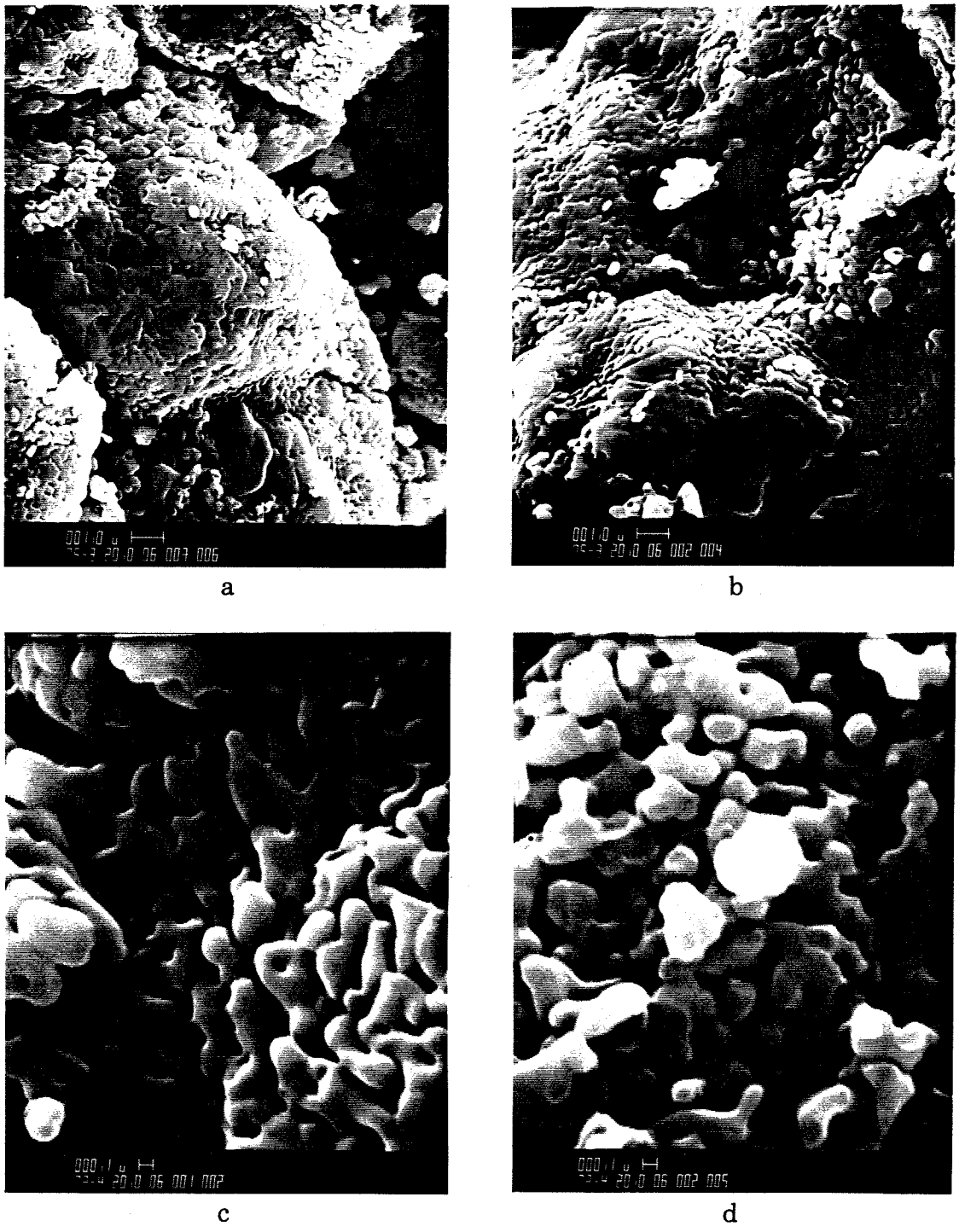

a b

c d

Figure 8.1. Scanning Electron Micrographs of α-Al_2O_3 Sorbent (a,c) Before, and (b,d) After Impregnation; (a,b) 4500X, (c,d) 18000X.

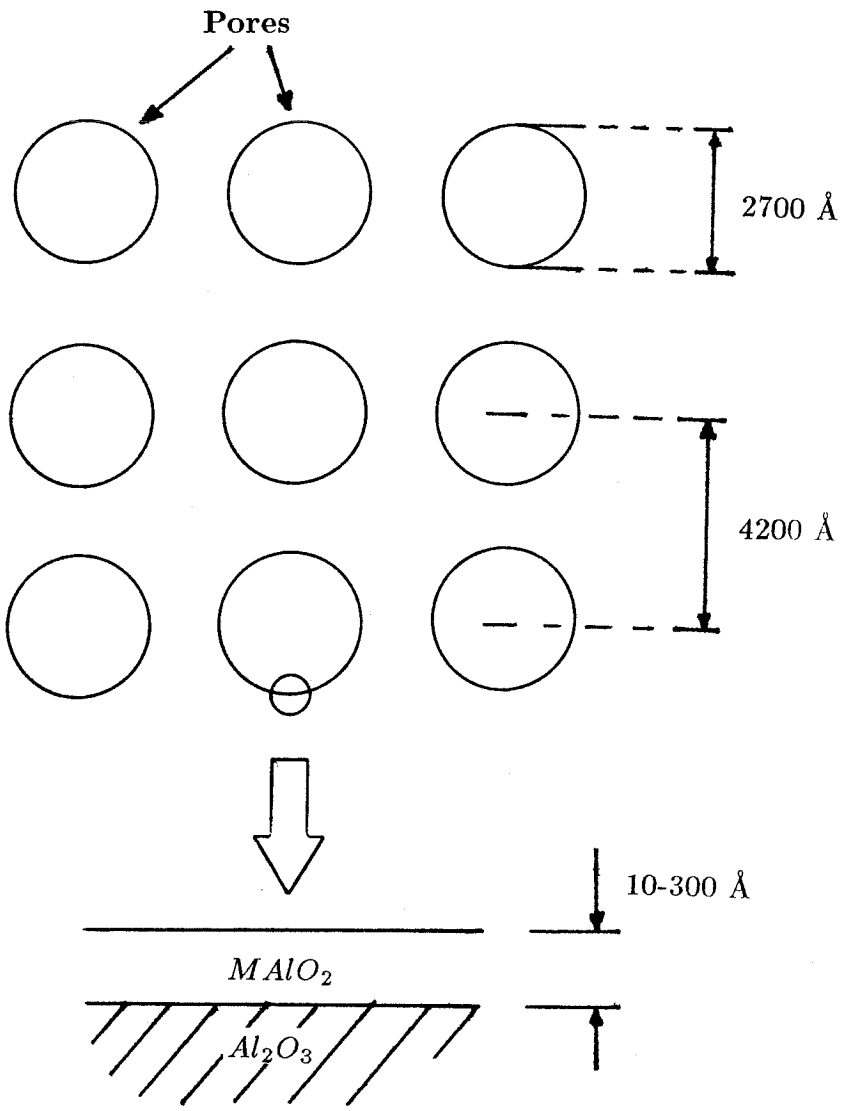

Figure 8.2. Physical Structure of the α-Al_2O_3-Supported Sorbent.

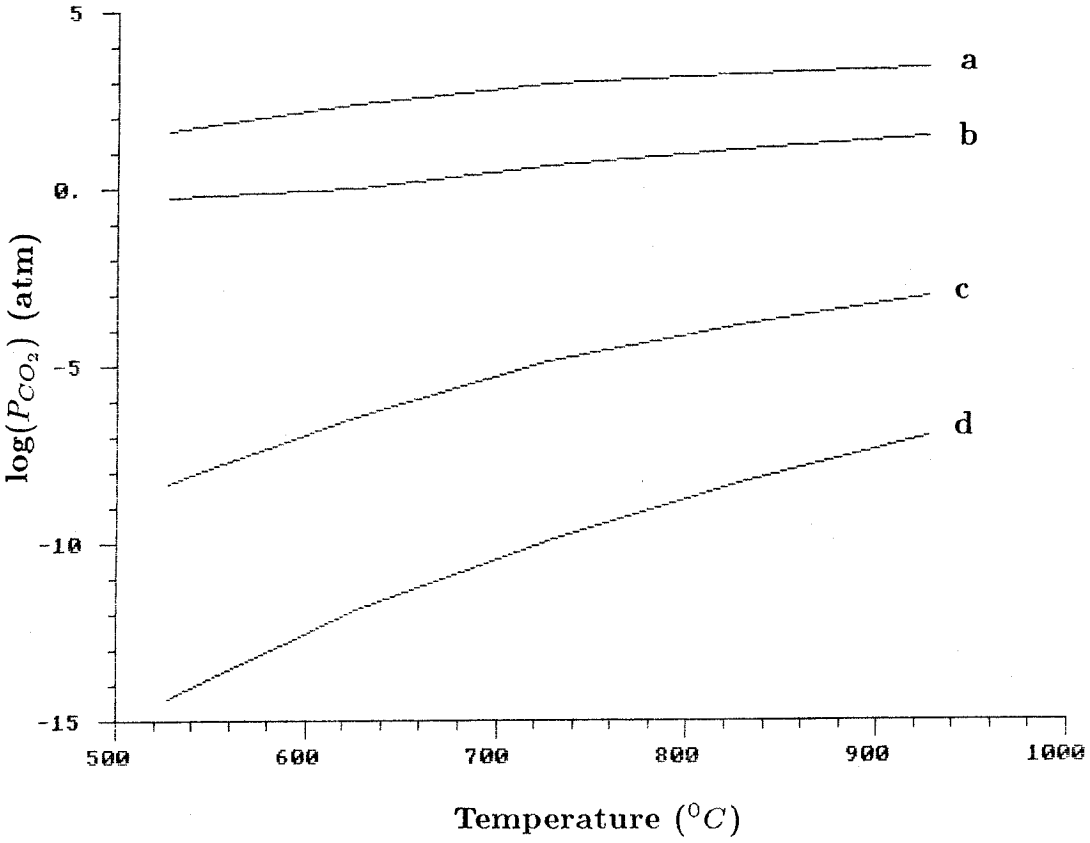

(a) $Li_2CO_3 + \alpha\text{-}Al_2O_3 = 2LiAlO_2 + CO_2$

(b) $Na_2CO_3 + \alpha\text{-}Al_2O_3 = 2NaAlO_2 + CO_2$

(c) $Li_2CO_3 = Li_2O + CO_2$

(d) $Na_2CO_3 = Na_2O + CO_2$

Figure 8.3. Decomposition of Alkali Carbonates.

(Data from JANAF [7] and Barin and Knacke [1])

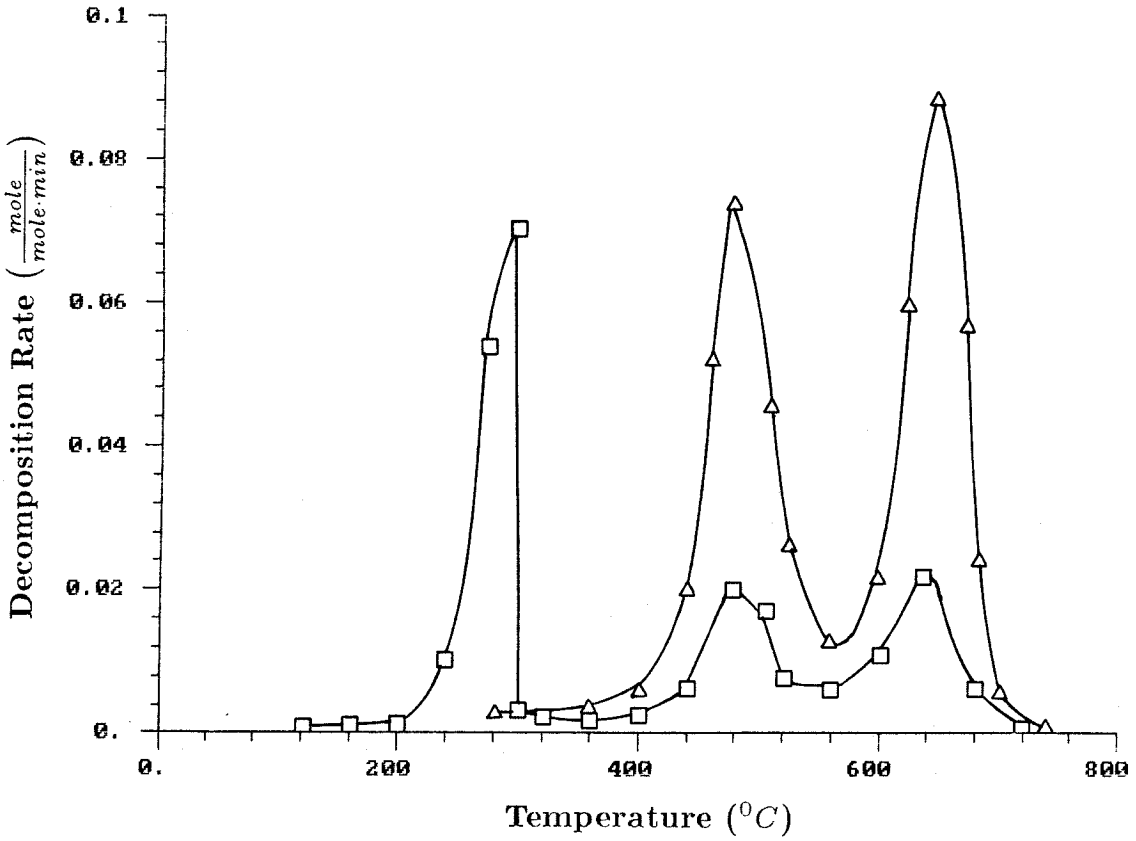

Figure 8.4. Temperature-Programmed Decomposition of Alkali Carbonates (△) and Acetates (□).

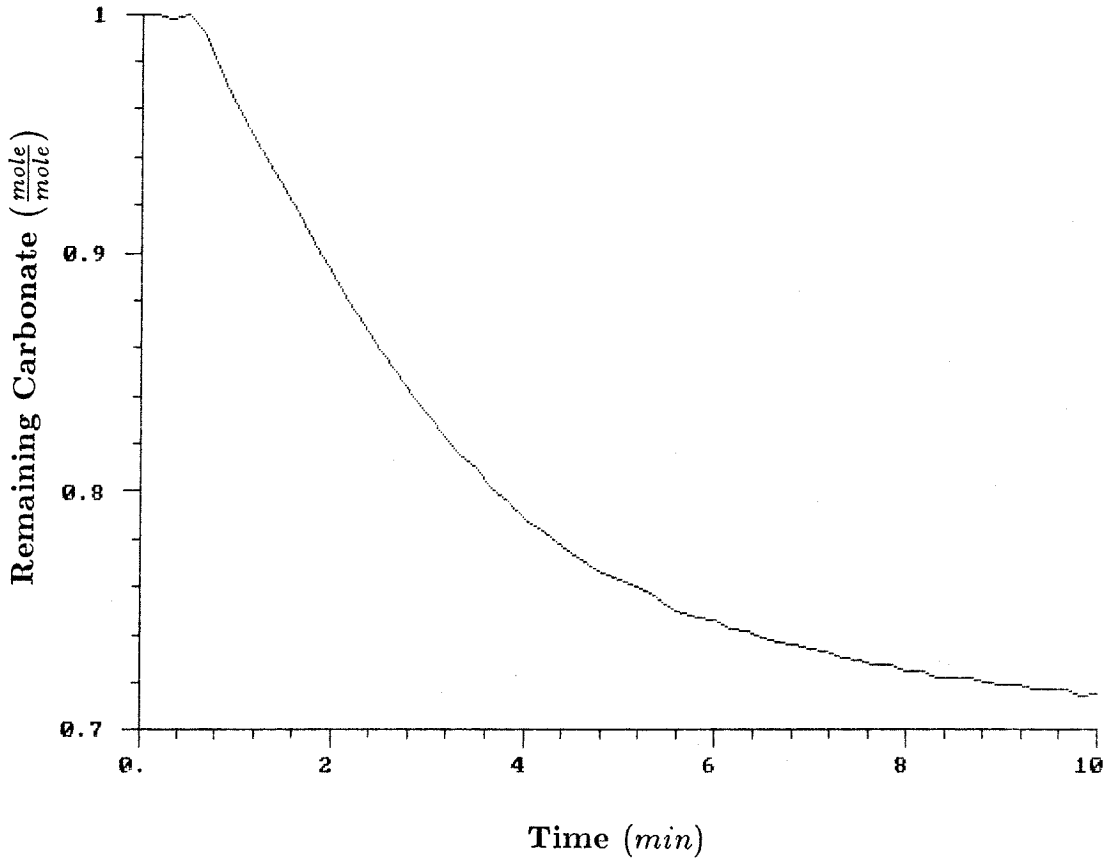

Figure 8.5. Carbonate Decomposition at 500^0C.

9. SORBENT SULFATION

At temperatures above $230°C$ the alkali aluminates react with SO_2 and O_2 to form alkali sulfates [4] :

$$2MAlO_2 + SO_2 + \frac{1}{2}O_2 \rightarrow M_2SO_4/Al_2O_3, \qquad (9.1)$$

where $M = Na,\ Li$. Sulfite formation according to :

$$2MAlO_2 + SO_2 \rightarrow M_2SO_3 + Al_2O_3$$

is only significant at temperatures below $230°C$ [4]. If carbonates are present, sulfation encompasses the evolution of CO_2 :

$$M_2CO_3 + SO_2 + \frac{1}{2}O_2 \rightarrow M_2SO_4 + CO_2. \qquad (9.2)$$

Reactions 9.1 and 9.2 are very favorable thermodynamically (Fig. 9.1). In our case, most of the active sorbent is in the aluminate form at 700-800$°C$ and, therefore, reaction 9.1 is the prevailing one. The sulfation of alumina-supported sodium aluminate was found to proceed at a considerable rate at $343°C$ [6]. The reaction rate is proportional to the SO_2 concentration and six times greater than the rate of sulfation of alkalized alumina [6], indicating that deploying the aluminate over the alumina surface increases the reactivity at that temperature. Sulfation of the supported sorbent entails pore diffusion of SO_2, diffusion through a growing layer of alkali sulfates, and reaction at the receding $M_2SO_4/MAlO_2$ interface. The sulfate layer is only a few hundred Å thick and is probably molten at the operating temperatures of the sorbent. Hence, all diffusion processes are expected to be fast under the given conditions.

9.1. Kinetics of Sulfation

The rate of sulfation of sorbents $ST\alpha$1-4, $AC\alpha$1-3, $AC\chi$, and $ST\gamma$ (Table 8.1) was measured thermogravimetrically at 700, 750 and 800^oC, and $[SO_2]$ = 800, 2500, 5000, and 10000 ppm, using the experimental technique described in Sec. 4.1. The sorbents prepared from alkali acetates were calcined for 3 hours in a Leco furnace at 800^oC. Those prepared in the sulfated form were first calcined and then reduced with CO for 1 hour at 800^oC. The reacting gas was a mixture of 1% SO_2 in air, which provided an excess of O_2. This stream was diluted with enough N_2 to attain the desired SO_2 concentration in the TGA chamber.

In all cases the reaction proceeded to completion. Some excess SO_2 was retained by the sorbent and eliminated during the N_2 purge that followed the sulfation. The amount retained increased with increasing loading, suggesting that the excess SO_2 may be dissolved in the sulfate melt. The results for sorbent $ST\alpha$1 (loading λ = 1.01 mmole M_2SO_4/ gram) are shown in Fig. 9.2. The rate of sulfation increases with increasing temperature and SO_2 concentration. The extent of sulfation attained after 30 minutes with $[SO_2]$ = 2500 ppm is 80% at 700^oC and 97% at 800^oC. The initial rate of sulfation is proportional to the concentration of SO_2 in the gas stream up to $[SO_2] \approx 5000\ ppm$. The sulfation rate of calcined sorbent $AC\alpha$2 under similar conditions was approximately the same as that of reduced sorbent $ST\alpha$1 (Fig. 9.2), and was not affected by successive sulfation/reduction cycles. No difference was observed between the sulfation rates of sorbents $AC\alpha$1 and $ST\alpha$1 to 3, indicative of the absence of

intraparticle diffusional limitations.

No decomposition of sulfated sorbents supported on α-Al_2O_3 or χ-Al_2O_3 was observed during the N_2 purge that followed the sulfation at 700-800°C. However, γ-Al_2O_3-supported sorbent $ST\gamma$ decomposed partially and irreversibly at temperatures above 450°C.

The effect of sorbent loading on the rate of sulfation is illustrated in Fig. 9.3. After a 10-minute exposure to SO_2 (2500 ppm) at 800°C, low-loading sorbent $ST\alpha4$ (0.10 mmole/gram of sorbent) was completely sulfated, medium-loading sorbent $ST\alpha1$ (1.01 mmole/gram of sorbent) reached 93% sulfation, and high-loading sorbent $AC\alpha3$ (2.47 mmole/gram of sorbent) reached 75% sulfation. The initial rates of reaction are 0.42, 0.54, and 0.50 mmole/g sorbent·min, respectively.

9.2. Discussion

The sulfation rate of the sorbent under study is compared to that of calcined lime and a commercial monocalcium silicate in Fig. 9.4 (data from [7]). The temperature was 800°C in the case of $Na/Li\ AlO_2/Al_2O_3$ and 900°C in the cases of CaO and $CaSiO_3$. The SO_2 concentration was 2500 ppm in all three cases. In the case of the alkali-alumina sorbent, conversion is defined as :

$$X\ (\%) \equiv \frac{[SO_4^{2-}]}{\lambda} \times 100,$$

where $[SO_4^{2-}]$ and λ are the sulfate concentration in the sorbent and the loading, in mmole SO_4^{2-}/gram. While the alkali-alumina sorbent attained 92%

conversion after 40 minutes, the calcium oxide and silicate only reached 16 and 36%, respectively. The volume expansion caused by sulfation of bulk materials such as calcium oxide and silicates leads to slow pore diffusion and, eventually, pore blockage [5]. On the other hand, the total capacity per unit weight of both types of sorbents is similar : after 30 minutes of exposure alkali-alumina sorbents can hold 16% SO_2 by weight, approximately the same as the bulk materials.

The previous results suggest that under the prevailing conditions all diffusional limitations are negligible, and the sulfation is controlled by reaction 9.1. Thus, the overall rate of sulfation is given by :

$$r = \frac{d\left[SO_4^{2-}\right]}{dt} = k\ \left[SO_2\right]\ a_R = k^o\ e^{-E/RT}\ \left[SO_2\right]\ a_R,$$

where a_R is the exposed surface area of aluminate, available for reaction, in m^2/gram $(a_R \leq a)$. In most cases, the experimental rate of sulfation remained approximately constant in the range $\left\{0 < \left[SO_4^{2-}\right] < 0.4\lambda\ to\ 0.6\lambda\right\}$, after which the rate began to decrease as the exposed aluminate area diminished. This interpretation is consistent with the fact that the initial rate of sulfation of sorbents of medium and high loadings differed by only 10% (Fig. 9.3).

The activation energy for sulfation can be obtained from :

$$ln\ r_o = ln\left\{k^o a_o\left[SO_2\right]\right\} - \frac{E}{RT},$$

where $r_o \equiv \left[\frac{d\left[SO_4^{2-}\right]}{dt}\right]_{t=0}$, and $a_o \equiv \left[a_R\right]_{t=0}$.

A linear regression calculation from the experimental data yields $E = 21.6$ kcal/mole.

REFERENCES

[1] Barin, I., and Knacke, O., *Thermochemical Properties of Inorganic Substances*, Springer-Verlag, Berlin, 1973.

[2] Dennis, J.S., and Hayhurst, A.N., *Chem. Eng. Sci.*, **41**(1), 25, 1986.

[3] *JANAF Thermochemical Tables*, 2nd ed., NSRDS-NS-37, 1971.

[4] Russell, J.H., Town, J.W., and Kelly, H.J., *BuMines Rep. Inv. 7415*, 1970.

[5] Simons, G.A., and Garman, A.R., *AIChE J.*, **32**(9), 1491, 1986.

[6] Vogel, R.F., Mitchell, B.R., and Massoth, F.E., *Env. Sci. Tech.*, **8**(5), 432, 1974.

[7] Yang, R.T., and Shen, M.S., *AIChE J.*, **25**(5), 811, 1979.

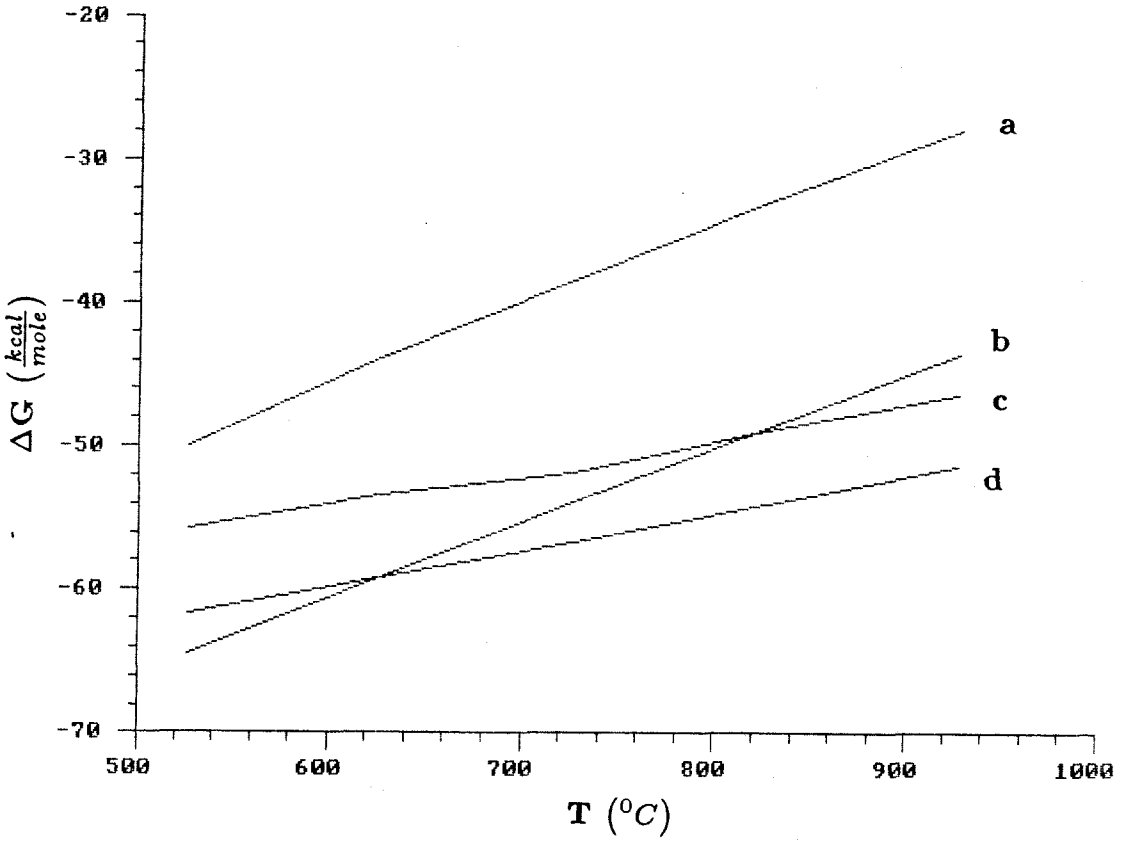

(a) $2LiAlO_2 + SO_2 + \frac{1}{2}O_2 = Li_2SO_4 + \alpha\text{-}Al_2O_3$

(b) $2NaAlO_2 + SO_2 + \frac{1}{2}O_2 = Na_2SO_4 + \alpha\text{-}Al_2O_3$

(c) $Li_2CO_3 + SO_2 + \frac{1}{2}O_2 = Li_2SO_4 + CO_2$

(d) $Na_2CO_3 + SO_2 + \frac{1}{2}O_2 = Na_2SO_4 + CO_2$

Figure 9.1 Standard Free-Energy Changes for the Sulfation Reactions. (Data from JANAF [3] and Barin and Knacke [1])

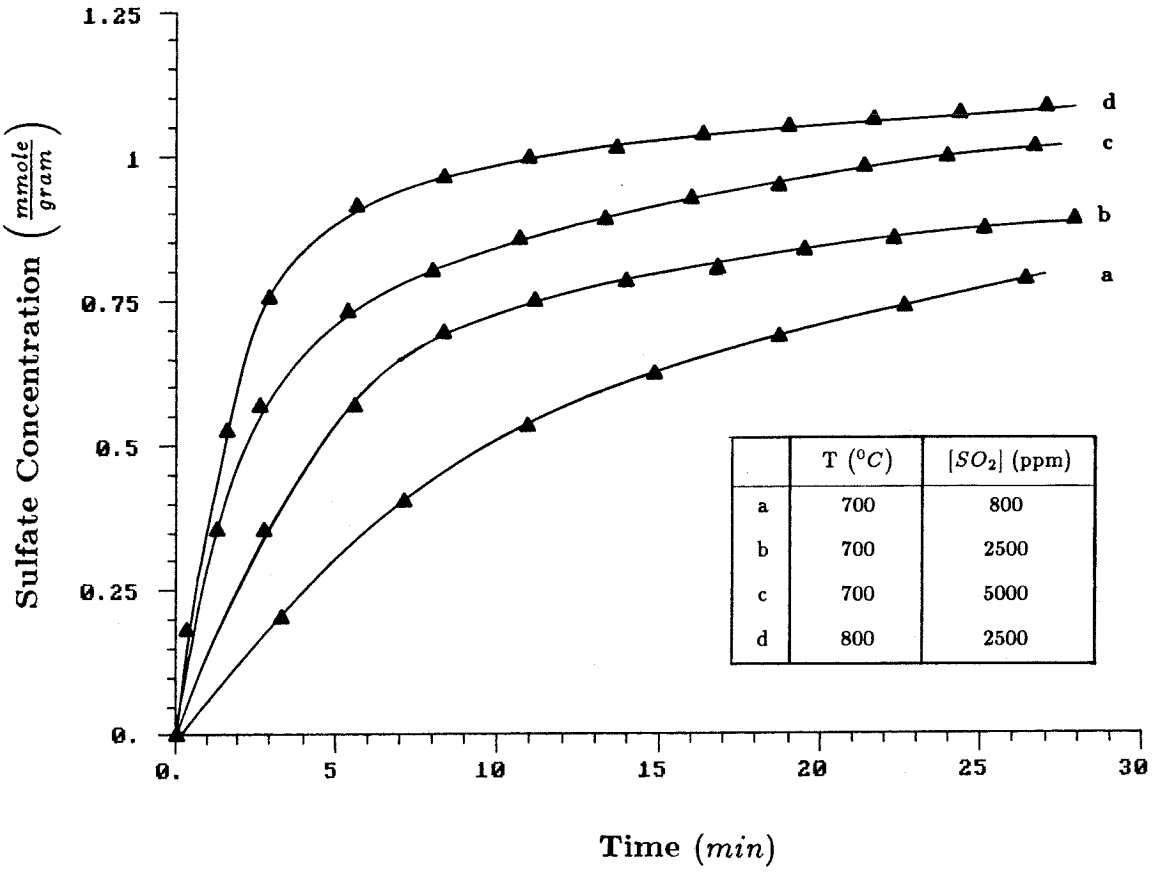

Figure 9.2 Effect of the Temperature and SO_2 Concentration on the Rate of Sulfation (Sorbent $ST\alpha 1$: $\lambda = 1.01$ mmole/gram).

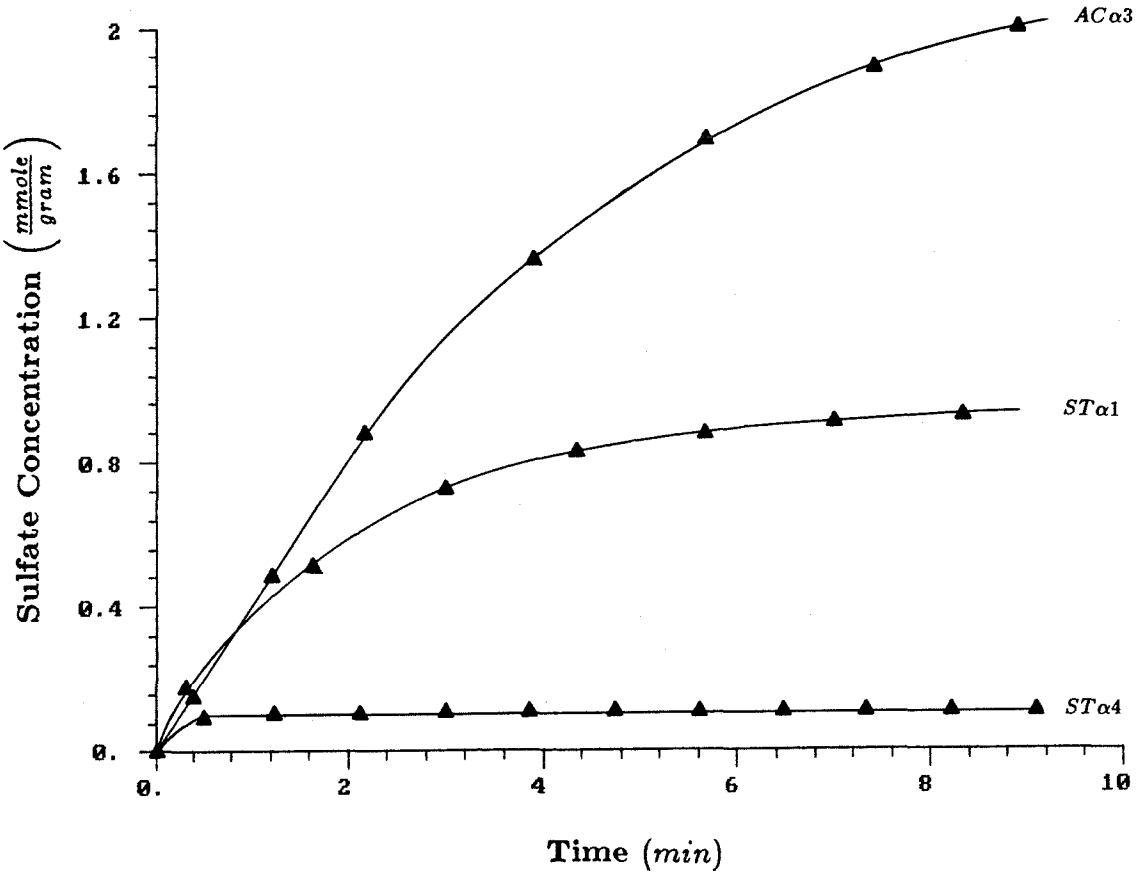

Figure 9.3 Effect of Sorbent Loading on the Rate of Sulfation

$(T = 800°C,\ [SO_2] = 2500\ ppm,\ \lambda(ST\alpha 4) = 0.10,$

$\lambda(ST\alpha 1) = 1.01,\ \lambda(AC\alpha 3) = 2.47$ mmole/gram).

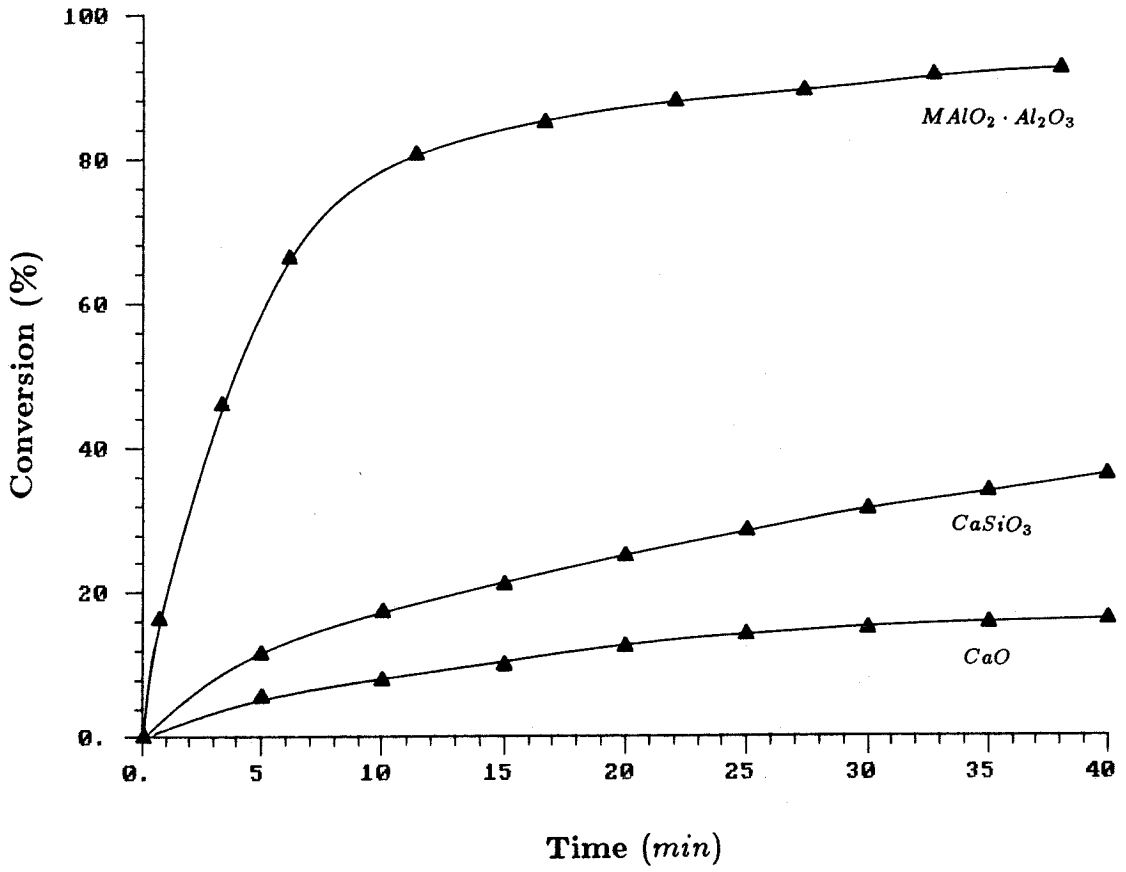

Figure 9.4 Comparison between the Sulfation Rates of $Na - Li\ AlO_2/Al_2O_3$, $CaSiO_3$, and CaO ($[SO_2] = 2500\ ppm$) [7].

10. SORBENT REGENERATION

10.1. Chemistry of Regeneration†

ABSTRACT

The high-temperature removal of SO_2 by sorbents consisting of sodium and lithium salts supported on α-Al_2O_3 has been investigated with emphasis on the chemistry of regeneration. The sulfated sorbents were regenerated by reduction with CO at 700-800°C in a thermogravimetric analyzer and a packed-bed microreactor. Sulfur removal from the sorbent and distribution of gaseous products were measured at different alkali loadings, temperatures, and CO concentrations. The results are interpreted in terms of a network of reactions wherein alumina is important as a catalyst and as a reactant. During regeneration sulfate is converted to aluminate and sulfide, the fraction of aluminate defining the extent of regeneration. The rate and extent of sulfur removal increase with the ratio of alumina to alkali and are higher in the presence of lithium. The product gas consists of SO_2, COS, and elemental sulfur, the latter compound constituting up to 35% of the sulfur removed.

---

† *Alkali-Alumina Sorbents for High-Temperature Removal of* SO_2, by G. R. Gavalas, Sergio Edelstein, M. Flytzani-Stephanopoulos and T. A. Weston, *AIChE Journal*, in press.

INTRODUCTION

Dry desulfurization of flue gas from coal combustion or sulfide roasting can be carried out using nonregenerable (throwaway) or regenerable sorbents. Limestone and dolomite are essentially the only economical sorbents for throwaway use. These sorbents are employed in calcined form in industrial fluidized boilers and will certainly be utilized when utility fluidized combustion boilers become commercial. Application to pulverized coal boilers is also being investigated in a variety of configurations.

Regenerable sorbents eliminate the extensive solids disposal requirement associated with throwaway sorbents and, under suitable conditions, produce elemental sulfur as a salable by-product. So far the only regenerable sorbents that have been investigated in some depth are alumina-supported copper oxide (Groenendaal *et al.*, 1976; McCrea *et al.*, 1970; Cho and Lee, 1983) and "alkalized alumina" (Bienstock *et al.*, 1958; Town *et al.*, 1970; Schlesinger and Illig, 1971). Alumina-containing sorbents are also being seriously considered for SO_2 removal in catalytic cracking regenerators (Wall, 1984). Limited effort has been devoted to using calcium-containing materials such as calcium silicates (Yang and Shen, 1979) as regenerable sorbents.

The regeneration of sulfated sorbents requires reduction by hydrogen or carbon monoxide and produces a mixture of gaseous sulfur compounds including SO_2, COS (or H_2S) and S_2. This off-gas will have to be treated further, e.g., by the Claus process, for final sulfur recovery. The cost of using a regenerable sorbent depends largely on the composition of the off-gas, as well as on the

resistance of the sorbent to attrition, especially when used in fluidized reactors.

Among regenerable sorbents, so-called alkalized alumina has been extensively investigated for *in situ* SO_2 removal in fluidized coal combustion (Bienstock *et al.*, 1958; Town *et al.*, 1970; Schlesinger and Illig, 1971). This material is an alkali-deficient sodium aluminate obtained by calcination of sodium aluminum carbonate. Reduction of the sulfated sorbent at 680^oC with hydrogen removed over 80% of the sulfur in the form of H_2S. Reduction by carbon monoxide at 680^oC produced COS and removed only about 30% of the sulfur in the solid (Schlesinger and Illig, 1971). Successive sulfation-regeneration cycles resulted in sorbent attrition as high as 2.5% per cycle depending on the form of the sorbent and the operating conditions employed. The costs associated with regeneration, final sulfur recovery, and sorbent loss by attrition discouraged further development of this sorbent, at least for application to fluidized combustion.

Instead of using the alkali and alumina components in the form of a homogeneous compound, i.e., sodium aluminate, one can deploy the alkali in supported form, i.e., as a thin film over the pore surface of the alumina. Although at reaction temperatures the two components combine to form aluminate, this compound might be confined to a layer near the pore surface, at least when the alumina employed is of the less reactive alpha form.

The purpose of this work was to investigate sorbents consisting of sodium, lithium, or sodium-lithium mixtures supported on α-Al_2O_3. Sulfur dioxide

removal by such sorbents involves the oxidative sulfation

$$M_2O + (SO_2, O_2) \rightarrow M_2SO_4 \quad (1)$$

and the reductive regeneration

$$M_2SO_4 + (COorH_2) \rightarrow M_2O, M_2S + (S_2, SO_2, COS \text{ or } H_2S, CO_2 \text{ or } H_2O) \quad (2)$$

where M is the alkali metal and M_2O represents oxide, carbonate, or aluminate. Sulfation is very rapid and proceeds to completion, but regeneration is complex, involving catalytic and noncatalytic reactions influenced by slow desorption steps. The focus of this work was on elucidating the reaction network and the role of the alkali and alumina components in regeneration.

The results show the profound role of alumina as a reactant and catalyst during regeneration. Increasing the alumina surface area per unit mass of alkali results in faster and more complete regeneration. It is also found that sorbents containing lithium or sodium-lithium mixtures are superior to those containing sodium alone in terms of rate and extent of regeneration. Sulfur is removed as SO_2, COS, and elemental sulfur, S_2. The fraction of elemental sulfur in the sulfur gases decreases with the alkali to alumina ratio and the CO concentration, and increases with the temperature. Under the conditions of a thermogravimetric analyzer experiment this fraction reached 0.35 with 10% CO. As the concentration of CO is lowered SO_2 and S_2 increase at the cost of COS. When produced in substantial yield, elemental sulfur can be removed by condensation and COS and SO_2 can be recycled to the regeneration stage obviating the need for further sulfur recovery steps. A conceptual fluidized combustion

scheme incorporating this concept has been described by Gavalas *et al.* (1985). To be economical, the sorbent must possess good resistance to attrition in successive sulfation-regeneration cycles. The present study did not consider the mechanical properties of the sorbents.

EXPERIMENTAL

Sorbents

Table 1 lists the composition of the sorbents investigated. The sorbents were prepared by impregnation of the porous support, which had previously been ground and sieved. One sorbent ($NL\alpha 2$) was also made by impregnation of 4-mm diameter cylinders of α-Al_2O_3. All sorbents except $NL\alpha 2$ and $NL\alpha 3$ were prepared in sulfated form. Those two sorbents were prepared by impregnation with a solution of alkali acetates, followed by calcination at 800^oC. The Na_2SO_4/α-Al_2O_3 sorbents were prepared by impregnation either at incipient wetness or in excess solution. All other sorbents were prepared using the incipient wetness technique. Most sorbents were analyzed for sodium and lithium by atomic absorption spectroscopy and some were analyzed for sulfate by barium precipitation. The surface area of a few sorbents was measured by the BET method. Results show little difference in total surface area between sorbent and support material. Typical values are 4-5 m^2/g for α-Al_2O_3 sorbents and 90-100 m^2/g for γ-Al_2O_3 sorbents. At reaction temperatures of 700-800^oC, sodium sulfate and lithium sulfate are both solid, while the sodium-lithium sulfate mixture is molten.

Apparatus

Experiments were carried out with a thermogravimetric analyzer (TGA) and a packed-bed reactor. A DuPont 951 thermogravimetric analyzer interfaced to a data acquisition system was used for continuous logging of the weight, the rate of weight change, and the temperature during reaction. The TGA was furnished with a temperature programmer, allowing linear temperature increase or isothermal operation. Gaseous reactants were introduced through a side arm directly into the TGA reaction chamber, while nitrogen diluent flowing through the bulb housing the balance mechanism insured that no corrosive gases would contact the balance mechanism. The flow rates of both gas streams were measured with mass flowmeters. The elemental sulfur in the gaseous product was removed by a glass wool filter placed in the exit line of the TGA. The remaining gas phase products were collected by means of a multiport sampling valve and analyzed with a Varian series 3700 gas chromatograph equipped with a flame photometric detector. SO_2 and COS were separated isothermally at 60^oC using a Supelco 183 cm $\times$ 0.318 cm Chromosil 310 column with a helium carrier flow rate of 30 cm^3/min. Due to the small size of the samples, the elemental sulfur produced could not be measured directly.

The other experimental system was a packed-bed reactor consisting of a 0.8 cm ID quartz tube mounted vertically in an electric tube furnace. The sample was held in place by a quartz frit and quartz wool. The temperature of the bed was monitored with a thermocouple inserted within a thermal well imbedded in the solid sample. The flow of reactant gases was measured using calibrated gas flowmeters. Elemental sulfur was condensed in traps immersed in an ice

bath, and could be measured by weighing. All lines between the reactor and the sulfur traps were heated to prevent condensation of sulfur. Gaseous products were analyzed using a Hewlett-Packard 5750 gas chromatograph equipped with a flame photometric detector and a Supelco 183 cm × 0.318 cm Chromosil 310 column. The column was used isothermally at $60°C$ with a helium carrier flow rate of 60 cm^3/min.

Procedure

The majority of the experiments involved the reduction of sulfated sorbents, either freshly prepared by impregnation or after one or more cycles of reduction and resulfation. The reducing gas compositions were 2.5% CO 0.15% CO_2, 6% CO-0.3% CO_2, and 10% CO-0.5% CO_2 in N_2. The CO_2 was added in sufficient concentration to prevent carbon deposition. After reduction the sorbents were resulfated using a mixture of 1% SO_2-10% air in N_2.

The sample size in the TGA experiments was 30 to 40 mg. A platinum pan was used for supported-sorbent measurements and a gold-coated platinum crucible was used for a few reference experiments with unsupported alkali salts. The samples were heated to the desired temperature in N_2 and the weight loss during the heating period was monitored to observe any sulfate decomposition. During reduction the weight loss of the sorbent was monitored continuously and gas samples were taken and analyzed for SO_2 and COS. The analysis of each sample required approximately 4 min. At the beginning of the reduction period, the product gas composition was found to change rapidly within the 4-min time span of a gas chromatogram. Therefore, samples were initially

collected every 15 to 30 sec using a multiport valve. During the remainder of the period samples were injected on-line. The collected samples were analyzed at the conclusion of the reduction period.

The sulfur and oxygen contents of the sorbent at the end of a reduction period were determined by measuring the weight gain when the reduced sorbent was exposed to oxygen. All oxygen-deficient sulfur species present were thus oxidized to sulfate. The sorbent was then fully resulfated by exposure to SO_2 and air, and another experiment with different reduction time could be performed. Interpretation of the successive weight changes provides the amount of sulfur, in any form, removed from the sorbent during reduction. Comparison of the total sulfur removed with the total amounts of SO_2 and COS produced, found by integration of gas analysis data, yields the amount of elemental sulfur produced during a reduction period.

For the microreactor experiments 1.5 to 2 g samples were used. As concentrations of the product gas exiting the reactor were at times in excess of those the detector was able to handle, the exit stream was diluted with N_2 prior to injection into the chromatograph. Elemental sulfur collected in the traps was measured gravimetrically after the conclusion of the reduction.

In both the TGA and microreactor experiments the reductions were carried out at 700, 750, or 800°C and at a pressure slightly above atmospheric.

RESULTS

Thermogravimetric Experiments

Sulfate and Carbonate Decomposition

Figure 1 shows the standard free-energy change for the decomposition of sodium and lithium sulfate and sodium carbonate by reaction with alumina. While the decomposition of the sulfates to form aluminates is highly unfavorable, the carbonate decomposition is favorable at temperatures between 700 and 800^oC. In agreement with these predictions, no decomposition of sulfated sorbents supported on α-Al_2O_3 was observed during the sample preheating in a stream of nitrogen. However, all sorbents supported on γ-Al_2O_3 decomposed partially and irreversibly. In each case, decomposition became evident at 450^oC and continued with further heating. Sulfation after reduction renewed only the sulfate lost during reduction, but not that lost during heating in nitrogen prior to reduction.

The interpretation of the thermogravimetric experiments used to determine the oxygen content of the sorbent requires making a distinction between carbonate and aluminate formed during reduction. To estimate the rate of conversion of carbonate to aluminate, samples of alumina impregnated with various carbonates were heated in the TGA at a constant rate of 100^oC/min until reaching 700^oC, after which the temperature was held constant at 700^oC. The results are shown in Figure 2. In agreement with the equilibrium calculations, sodium-lithium carbonate and lithium carbonate were completely converted at 700^oC. The rate of aluminate formation in these cases was comparable to the

rate at which carbonate would be formed during reduction. Sodium carbonate begins reaction with alumina between 650 and 700°C. When γ-Al_2O_3 impregnated with sodium-lithium carbonate was heated in N_2, decomposition began at temperatures about 100°C lower than that encountered with α-alumina.

Reduction Experiments

Reduction of a Na_2SO_4/α-Al_2O_3 sorbent ($N\alpha3$) at 700 and 800°C with 10% CO yielded the results shown in Figure 3. The weight was adjusted for the amounts of metal present in the sorbent to represent weight loss per initial weight of sulfate. Reduction takes place in two stages at both 700 and 800°C. During the first stage the weight decreases very slowly with SO_2 as the chief gaseous product. After approximately 1 min at 800°C or 3 min at 700°C, SO_2 is replaced by COS as the major gaseous product, accompanied by an acceleration of the weight loss. This general pattern repeated itself for all sorbents and reaction conditions, both in the TGA and the microreactor. Figure 4 shows similar results for the sorbent containing a sodium-lithium mixture. Under the same temperatures and CO concentrations, the mixed-alkali sorbent is reduced more rapidly than the sorbent containing pure sodium. Figure 5 shows the weight-loss curves of sorbents prepared with different alkali loadings. As the alkali loading increases, the reduction rate decreases and the transition from SO_2 to COS production becomes more gradual.

The effect of reductant concentration is depicted in Figure 6. As the CO concentration decreases, the reduction becomes slower and the period of SO_2 production is prolonged. The duration of this period increases dramatically

at CO concentrations below 5%, and for 1% CO switchover to COS was not observed. A longer SO_2 production period was also observed when (1) α-Al_2O_3 rather than γ-Al_2O_3 was used to prepare the sorbent, (2) Li was one of the alkali constituents, (3) the alkali loading was higher, (4) the temperature was lower, and (5) when the sorbent had been sulfated at high temperatures prior to reduction.

The cumulative yield of various products after 20 min at 700 and 800°C with 10% CO is shown in Table 2 for several sorbents. Sulfur removal from the sorbent (extent of regeneration) is favored by higher temperature, by using α-Al_2O_3 rather than γ-Al_2O_3, and by using lithium as one of the alkali components. The yield of elemental sulfur in the gaseous products is favored by higher temperature, by using a sodium-lithium mixture rather than sodium or lithium, by using α-Al_2O_3 rather than γ-Al_2O_3, and by decreasing the alkali loading.

Reduction-Oxidation Experiments

The reduction of Na_2SO_4/α-Al_2O_3 and $NaLiSO_4/\alpha$-Al_2O_3 sorbents was examined in greater detail by following sorbent composition as a function of time during reduction. By interrupting the reduction at different times and measuring the weight increase associated with oxidation in air and subsequent exposure to SO_2 and air, the total sulfur and total oxygen in the sorbent could be determined as discussed earlier. The results of the reduction at 800°C with 10% CO of a Na_2SO_4/α-Al_2O_3 sorbent and of a $NaLiSO_4/\alpha$-Al_2O_3 sorbent are shown in Figures 7 and 8, respectively. During the first stage of reduction,

oxygen is removed from the sorbent at a higher rate than is sulfur. During the second stage, the oxygen content remains almost constant while sulfur continues to decline at a substantial rate. Differences in the reduction of the two sorbents are more prominent in the initial period, during which the sulfur content of the sodium-lithium sorbent ,Figure 8, decreases to a much greater extent than that of the sodium sorbent ,Figure 7. The rate of sulfur loss during the second half of the reduction appears to be approximately the same for both sorbents. At $700°C$ similar variations between the two sorbents are exhibited, but sulfur removal during the later period is much slower than at $800°C$.

Microreactor Experiments

Sorbents with various alkali components and supports were reduced at different temperatures and CO concentrations using the microreactor system. Gas production exhibited behavior similar to that in the TGA experiments in that the major gas product switched from SO_2 to COS, the switchover time varying with reaction conditions. Significant amounts of elemental sulfur were produced during the nitrogen purge that followed the reduction.

Sorbents containing lithium-sodium mixtures supported on SiO_2 and ZrO_2 were also studied in the microreactor. SO_2 was the major gas product during the entire reduction of the silica sorbent. Very little sulfur was produced during the N_2 purge and, more important, the reduced sorbent was unable to reabsorb SO_2, thus making silica an unacceptable support. ZrO_2 on the other hand exhibited a pattern similar to that of α-alumina.

Infrared Spectrometry

Samples were prepared by reduction in the TGA for the desired length of time, cooling in nitrogen, grinding, and forming a mull that was pressed between KBr windows. Fourier-transform infrared spectrometry (FTIR) was carried out on a Mattson Sirius 100 instrument using a TGS detector. Each spectrum was generated by averaging 512 scans in the range 400-4000 cm^{-1}. The spectra were reduced by subtraction of the spectrum of the alumina substrate and the reduced spectra were compared to known absorption bands (Weston, 1985). Shifting baselines and variations in mull preparation caused difficulty in extracting quantitative information. In view of the large fraction of alumina in the sorbent (approximately 90%) and the strong absorption of alumina in the spectral region below 900 cm^{-1}, the spectra contained useful information mainly in the region above 900 cm^{-1}. A typical series of spectra for sorbent $NL\alpha 1$ ($NaLiSO_4/\alpha$-Al_2O_3) reduced for different periods is shown in Figure 9. The region above 900 cm^{-1} contains strong absorption bands for SO_4^{2-} around 1150 cm^{-1}. An SO_3^{2-} band around 980 cm^{-1} appears in the 1-min sample but is absent from the other samples.

DISCUSSION

Background Information

In this subsection we review thermodynamic data and experimental results from the literature useful to the interpretation of our results.

Homogeneous reactions

Figure 10 shows the free energy of various reduction reactions. While reduction of sulfate to sulfite is marginally feasible, reduction of sulfate or sulfite to sulfide is highly favorable thermodynamically. In previous work, reduction of bulk (unsupported) sodium sulfate by CO at $900°C$ gave a mixture of sulfide, carbonate, and smaller amounts of polysulfides (Ahlgren *et al.*, 1967). The reaction time was on the order of 1 h under mass-transfer-limited conditions. Sodium sulfate dissolved in molten sodium carbonate was reduced with H_2 and CO at 600 to $840°C$ also producing sulfide and possibly polysulfides (Oldenkamp and Margolin, 1969; Birk *et al.*, 1971). The reaction time was on the order of 1 h at $840°C$ and 6 h at $700°C$. Reduction with hydrogen was approximately three times faster than reaction with carbon monoxide.

Although sulfite has not been identified in these previous studies, it is a likely intermediate in sulfate reduction. This compound could then be reduced further or disproportionate. An early study of sulfite disproportionation (Foerster and Kubel, 1924) showed conversion to sulfate and sulfide according to the stoichiometric reaction

$$4Na_2SO_3 = Na_2S + 3Na_2SO_4 \qquad (3)$$

with reaction time on the order of 0.5 h at $700°C$. In the presence of SiO_2, sodium sulfite formed sodium silicate, with the release of SO_2 (Manring *et al.*, 1967). Reactions of sodium sulfide and sodium sulfite dissolved in the ternary eutectic Na_2SO_4-K_2SO_4-Li_2SO_4 were studied at $600°C$ by Dearnaley *et al.* (1983). The disproportionation of sulfite in this eutectic followed the stoichiom-

etry of reaction 3 but the rates were significantly higher than for the pure sulfite. Disproportionation of sulfite in the presence of SO_2 produced sulfate (but not sulfide) and elemental sulfur. The measured product distribution was explained by the reactions

$$SO_2 + 2SO_3^{2-} = \frac{1}{2}S_2 + 2SO_4^{2-} \tag{4}$$

$$2SO_2 + S^{2-} = S_2 + SO_4^{2-} \tag{5}$$

Under the conditions used in our TGA experiments, the reduction of unsupported sulfate would follow the sequence

$$SO_4^{2-} + CO = SO_3^{2-} + CO_2 \tag{6}$$

$$4SO_3^{2-} = S^{2-} + 3SO_4^{2-} \tag{7}$$

leading to sulfide as the final product. Direct reduction of sulfite to sulfide,

$$SO_3^{2-} + 3CO = S^{2-} + 3CO_2 \tag{8}$$

is favorable thermodynamically, as shown in Figure 10, but has not been studied directly.

Heterogeneous reactions

In the presence of alumina, the sulfite formed by Eq. 6 could decompose by the reaction

$$SO_3^{2-} + Al_2O_3 = SO_2 + 2AlO_2^- \tag{9}$$

Figure 11 shows the Gibbs free energy of the reaction between sodium sulfite and alumina with SO_2 produced in the gas phase. The Gibbs free energy of

reaction 9 will be substantially more negative if SO_2 is produced in chemisorbed form. In the presence of CO_2, sulfite could be converted to carbonate, which in turn could form aluminate,

$$SO_3^{2-} + CO_2 = SO_2 + CO_3^{2-} \tag{10}$$

$$CO_3^{2-} + Al_2O_3 = CO_2 + 2AlO_2^- \tag{11}$$

Relevant equilibria are listed in Figures 1 and 11.

The sulfur dioxide produced by reaction 9 reacts further with carbon monoxide to form elemental sulfur and carbonyl sulfide according to

$$SO_2 + 2CO = \frac{1}{2}S_2 + 2CO_2 \tag{12}$$

$$\frac{1}{2}S_2 + CO = COS \tag{13}$$

Khalafalla and Haas (1972), studied the mechanism of reaction 12 catalyzed by γ-Al_2O_3 at temperatures of 450-600°C and suggested chemisorption of SO_2 on Brönsted sites as the first step. They also found that elemental sulfur formed on the alumina surface accelerates the reaction rate. In a series of experiments performed in our laboratory it was found that α-Al_2O_3 and α-Al_2O_3 impregnated with sodium carbonate catalyzed reaction 12 at 700-800°C producing a mixture of COS and S_2 (Weston, 1985). At 800°C the product composition was at equilibrium according to reaction 12. Evidently Brönsted sites are not essential at temperatures above 700°C, for α-Al_2O_3 and aluminate do not contain such sites. The formation of COS from CO and S_2, reaction 13, and its

reverse are known to be catalyzed by several refractory oxides such as Al_2O_3 and SiO_2 (Haas and Khalafalla, 1973; Akimoto *et al.*, 1984).

With the above background information we proceed to interpret the two distinct periods in sulfate reduction experiments.

The Two Stages of Sulfate Reduction

For all sorbents and experimental conditions employed the reduction progressed in two stages, the first characterized by SO_2 release, the second by COS and S_2 release, Figures 3, 4, and 6. Comparison of Figures 3 and 7 and Figures 4 and 8 shows that the stage of SO_2 production is also characterized by fast removal of oxygen and slow removal of sulfur from the sorbent. During the stage of COS production, the removal of oxygen slows while that of sulfur accelerates. Removal of sulfur during the first stage is solely in the form of SO_2, while removal during the second stage involves release of S_2 as well as COS. The release of S_2 during the second stage is inferred from the TGA measurements by comparison of COS release and sulfur removal.

The product SO_2 during the first stage of reduction derives from reactions 6 and 9 in sequence, where 6 is catalyzed by the alumina surface. Part of the SO_2 produced escapes to the gas phase, the other part remains chemisorbed subject to further reduction by reactions 12 and 13. The sulfite produced by reaction 6 reacts with alumina 9 or disproportionates by the homogeneous reaction 7. Sulfur dioxide production during reduction of unsupported sulfate was observed to be negligible.

The switching from SO_2 production to COS and S_2 production cannot

be explained solely by the consecutive nature of reactions 9 and 12, for COS production is essentially zero during the first stage. One possible explanation is the activation of reaction 12 by the elemental sulfur buildup on the surface, as reported by Khalafalla and Haas (1972), for catalysis by γ-Al_2O_3 at lower temperatures. Another possible explanation is offered by the reaction of S_2 or COS with the remaining sulfate to yield sulfite or sulfide and SO_2, e.g.,

$$\frac{1}{2}S_2 + 2SO_4^{2-} = 2SO_3^{2-} + SO_2 \tag{14}$$

$$S_2 + SO_4^{2-} = 2SO_2 + S^{2-} \tag{15}$$

Similar reactions could take place between COS and SO_4^{2-}. Assuming these reactions to be sufficiently rapid, no S_2 or COS could be released until all sulfate has been consumed.

This second explanation of the separate evolution of SO_2 and COS is supported by the infrared spectra of sorbent samples corresponding to different reduction times. Figure 9 shows that the sulfate band declines relatively rapidly and disappears altogether in less than 4 min. A sulfite band, absent from the fresh sulfated sorbent, appears after 1 min but again disappears within 4 min reduction time. The time required for disappearance of the sulfate ion is comparable to the time of changeover from SO_2 to COS production, consistent with the explanation based on reactions 14 and 15. The changeover time also increases with alkali loading providing further evidence in favor of reactions 14 and 15, inasmuch as the time for elemental sulfur buildup required for acceleration of reaction 12 would be independent of alkali loading.

The carbonyl sulfide released during the second stage could arise from the reaction of CO with elemental sulfur, reaction 13, or from the reaction of CO_2 with the sulfide ion,

$$S^{2-} + CO_2 + Al_2O_3 = 2AlO_2^- + COS \tag{16}$$

Figure 12 shows the free energy of reaction 16 for sodium sulfide and lithium sulfide. To explore the role of reaction 16, an experiment was performed in the TGA wherein the reactant gas was switched from CO to CO_2 at the onset of the COS production stage in the TGA. The weight curve obtained is compared with the uninterrupted reduction of the same sorbent in Figure 13. When CO_2 is introduced in the system, the production of COS ceases completely and the major gas product changes to SO_2. The reaction responsible for this product is

$$\frac{1}{2}S_2 + 2CO_2 = SO_2 + 2CO \tag{17}$$

which in spite of a standard free energy of +92 kJ/gmol at 800°C would proceed in the presence of 10% CO_2 and very low concentrations of CO. The elemental sulfur participating in this reaction could derive from chemisorbed sulfur produced earlier or from sulfide via reaction 16a, below. In the presence of large amounts of CO_2 and the absence of CO the latter reaction would produce S_2 rather than COS and carbonate rather than aluminate,

$$S^{2-} + 2CO_2 = CO_3^{2-} + CO + \frac{1}{2}S_2 \tag{16a}$$

so that the stoichiometric result of reactions 16a and 17 would be

$$S^{2-} + 4CO_2 = CO_3^{2-} + 3CO + SO_2 \tag{18}$$

The weight increase observed in section c of Figure 13 is due to this carbonate formation as well as to the aluminate conversion to carbonate in the presence of carbon dioxide.

The long tail in the rate of COS production in Figures 3 and 4 is probably due to the slow kinetics of reaction 16, in view of the low concentration of CO_2 in the reactant gas. Figure 14 assembles the various reactions discussed above into a highly-coupled reaction network.

The Effects of Alkali Loading and Operating Conditions

The effect of alkali loading is shown in Figure 5 and Table 2. As shown in Figure 5, the rate of weight loss increases markedly with decreasing alkali loading, i.e., with increasing surface area of alumina per unit mass of alkali. This effect of alumina is clearly due to the direct reaction 9 as well as to the catalytic reactions 12 and 13. Table 2 shows that sulfur removal at fixed temperature and reaction time increases with decreasing alkali loading, the effect being more pronounced for the mixed-alkali sorbents. These effects are explained by the competition between the homogeneous sulfite disproportionation, reaction 7, and reaction 9 and subsequent surface catalyzed reactions 12, 13, and 16.

At fixed alkali loading the pure lithium and sodium-lithium sorbents undergo faster reduction and more extensive sulfur removal than the pure sodium sorbent. This effect may be due to faster reaction 9 in the presence of the counterion Li^+. Evidence for the increased reactivity of lithium salts in aluminate formation is offered by the results of Figure 2, concerning the carbonate-alumina reaction.

Temperature has a strong effect on the reaction rate ,Figures 3 and 4, and the product distribution. In particular, the ratio of elemental sulfur to the total sulfur removed during reduction in the TGA is zero at $700°C$ and 0.2-0.4 at $800°C$. In the microreactor experiments, elemental sulfur production at $700°C$ was zero during reduction but substantial during subsequent purge by nitrogen. Measurements of sulfur chemisorption currently under way show that elemental sulfur is very strongly chemisorbed on α-Al_2O_3 (e.g., desorption time at $700°C$ is on the order of 5 h).

The concentration of carbon monoxide has a strong effect on the rate of weight loss and product distribution. Figure 6 shows the reaction time increasing twentyfold as the CO concentration is reduced from 10% to 2.5%. At the 2% CO level, the shift from SO_2 to COS is greatly delayed and the SO_2 yield is much higher. Similar trends were observed in the packed-bed reactor runs where decreasing the concentration of CO from 10% to 1% increased the yield of SO_2 and elemental sulfur at the cost of COS.

REFERENCES

[1] Ahlgren, P., S. Lemon and A. Leder, "Preparation of Sodium Polysulfides by Solid and Molten State Reactions",*Acta Chem. Scand.*, **21**, 1119, 1967.

[2] Akimoto, M., K. Yamagami and E. Echigoya, "A Mechanistic Study on Vapor-Phase Catalytic Oxidative Dehydrogenation of Ethylbenzene with Carbonyl Sulfide", *J. Catal.*, **86**, 205, 1984.

[3] Bienstock, D., L. W. Brunn, E. M. Murphy, and H. E. Benson, *BuMines Inf. Circ. 7836*, 1958, 96 pp.

[4] Birk, J. R., C. M. Larsen, W. G. Vaux and R. D. Oldenkamp, "Hydrogen Reduction of Alkali Sulfate", *Ind. Eng. Chem. Process Des. Develop.*, **10**(1), 7 1971.

[5] Cho, M. H. and W. K. Lee, "SO_2 Removal by CuO on γ-Alumina", *J. Chem. Eng. Japan*, **16**(2), 127, 1983.

[6] Dearnaley, R. I., D. H. Kerridge and D. J. Rogers, "Molten Lithium Sulfate Sodium Sulfate-Potassium Sulfate Eutectic: Reactions of Some Sulfur Compounds", *Inorg. Chem.*, **22**, 3242, 1983.

[7] Foerster, V. F. and K. Kubel, "Uber die Zersetzung der Schwefligsauren Salze in der Gluhhitze", *Z. Anorg. Allge. Chem.*, **139**, 261, 1924.

[8] Gavalas, G. R., T. A. Weston and M. F. Stephanopoulos, paper presented at the 8th International Conference on Fluidized Combustion, Houston, March 18-21, 1985.

[9] Groenendaal, W., J. E. Naber and J. B. Pohlenz, "The Shell Flue Gas Desulfurization Process: Demonstration on Oil and Coal Fired Boilers", *AIChE Symposium Series*, **72**(156) 12, 1976.

[10] Haas, L. A. and S. E. Khalafalla, "Catalytic Thermal Decomposition of Carbonyl Sulfide and its Reactions with Sulfur Dioxide", *J. Catal.*, **30**, 451, 1973.

[11] *JANAF Thermochemical Tables*, 2nd Ed., NSRDS-NS-37, 1971.

[12] Khalafalla, S. E., E. F. Foerster and L. A. Haas, "Catalytic Reduction of Sulfur Dioxide on Iron-Alumina Bifunctional Catalysts", *Ind. Eng. Chem. Prod. Res. Develop.*, **10**(2), 133, 1971.

[13] Khalafalla, S. E. and L. A. Haas, "Active Sites for Catalytic Reduction of SO_2 with CO on Alumina", *J. Catal.*, **24**, 115, 1972.

[14] Manring, W. H., D. D. Billings, A. R. Conroy and W. C. Bauer, "Reduced Sulfur Compounds", *The Glass Industry*, 374, 1967.

[15] McCrea, D. H., A. J. Forney and J. G. Myers, *J. Air Pollut. Control Assoc.*, bf 20(12), 819, 1970.

[16] Oldenkamp, R. D. and E. D. Margolin, "The Molten Carbonate Process for Sulfur Oxide Emissions", *Chem. Eng. Prog.*, **65**(11), 73, 1969.

[17] Schlesinger, M. D. and E. G. Illig, "The Regeneration of Alkalized Alumina", *Chem. Eng. Prog. Symposium Series*, **67**(115), 46, 1971.

[18] Town, J. W., J. I. Paige and J. H. Russell, "Sorption of Sulfur Dioxide by Alkalized Alumina in a Fluidized-Bed Reactor", *Chem. Eng. Progress Symposium Series*, **66**(105), 260, 1970.

[19] Wall, J. D., "Control FCC SO_x Emissions", *Hydrocarbon Processing*, 45, October 1984.

[20] Weston, T. A., "The Regeneration of High Temperature Sulfur Dioxide Sorbents: The CO Reduction of Supported Alkali Sulfates", Ph.D. Dissertation, California Institute of Technology, 1985.

[21] Yang, R. T. and M. S. Shen, "Calcium Silicates: A New Class of Highly Regenerative Sorbents for Hot Gas Desulfurization", *AIChE J.*, **25**, 5, 1979.

Table 1. Composition of Sorbents

Sorbent	Composition	Sorbent Loading (mmol M^+/m^2)	(mg M_2SO_4/g)
Nα1	$Na_2SO_4/\alpha\text{-}Al_2O_3$	0.236	83.8
Nα2	$Na_2SO_4/\alpha\text{-}AL_2O_3$	0.476	169.0
Nα3	$Na_2SO_4/\alpha\text{-}Al_2O_3$	0.274	97.3
Nα4	$Na_2SO_4/\alpha\text{-}AL_2O_3$	0.044	15.6
NY	$Na_2SO_4/Y\text{-}AL_2O_3$	0.037	235.0
NLα1	$NaLiSO_4/\alpha\text{-}Al_2O_3$	0.506	111.2
NLα2	$NaLiSO_4/\alpha\text{-}Al_2O_3$	0.435	112.4
NLα3	$NaLiSO_4/\alpha\text{-}Al_2O_3$	1.235	319.1
NLY	$NaLiSO_4/Y\text{-}Al_2O_3$	0.018	107.3
NLZ	$NaLiSO_4/ZrO_2$	0.112	114.2
NLS	$NaLiSO_4/SiO_2$	0.118	153.0
Lα	$Li_2SO_4/\alpha\text{-}Al_2O_3$	0.373	82.0

Table 2. Product Selectivity After 20 Minutes Reduction with 10% CO in the TGA

Sorbent (Alkali Loading) (mmol M^+/m^2)	T (°C)	$S_{in\ sorbent}$	$\frac{S}{S + COS + SO_2}$	$\frac{COS}{S + COS + SO_2}$	$\frac{SO_2}{S + COS + SO_2}$
Nα3 (0.274)	800	.620	.224	.701	.075
Nα3 (0.274)	700	.934	0	.726	.274
Nα4 (0.044)	800	.115	.305	.502	.193
Nα4 (0.044)	700	.802	0	.727	.273
NLα1 (0.506)	800	.285	.351	.497	.152
NLα1 (0.506)	700	.426	.082	.730	.188
NLα2 (0.435)	800	.214	.240	.585	.174
NLα3 (1.235)	800	.311	.080	.561	.358
Lα (0.373)	800	.216	.271	.630	.098
Lα (0.373)	700	.560	0	.885	.115
Nγ (0.037)	800	.687	.079	.748	.173
Nγ (0.037)	700	.902	0	.612	.388
NLγ (0.018)	800	.730	0	.452	.548
NLγ (0.018)	700	.876	0	.516	.484

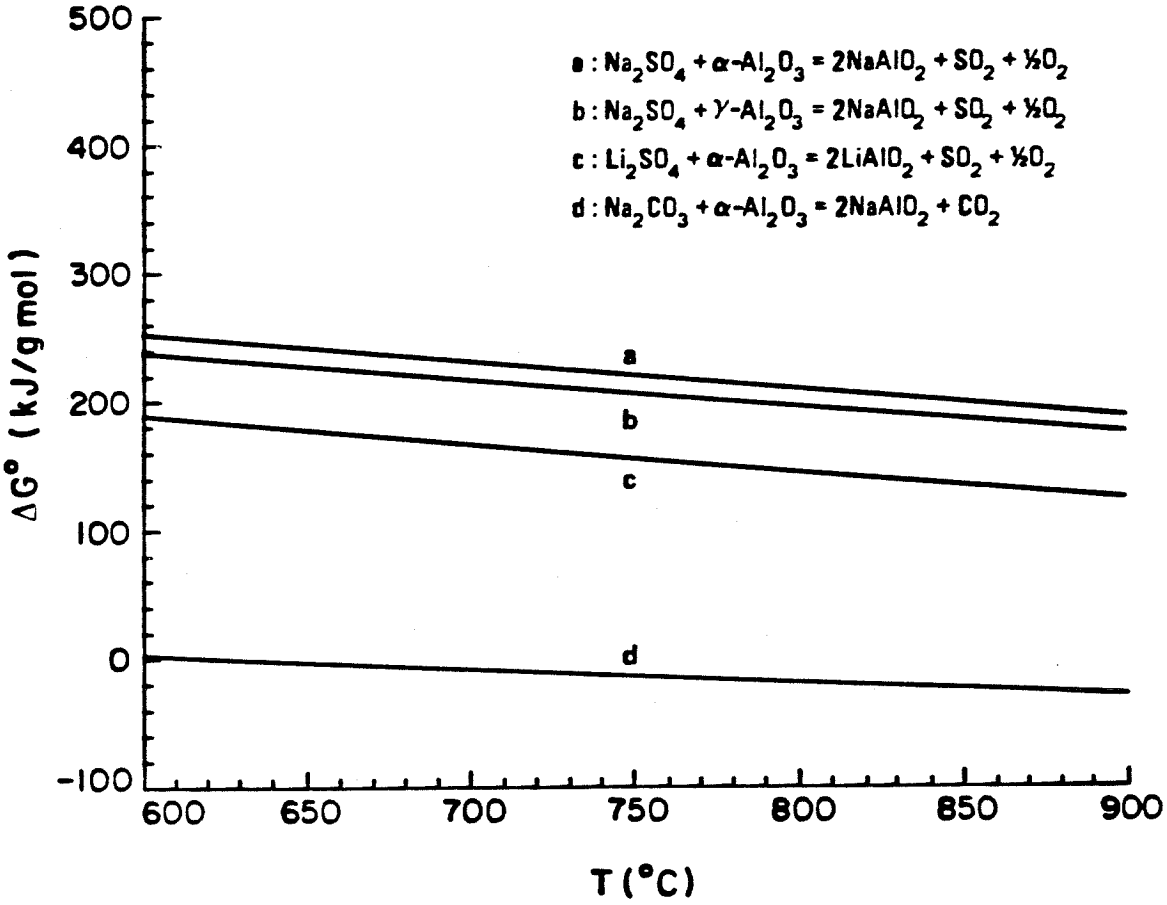

Figure 1. Standard Free Energy for the Decomposition of Alkali Sulfates and Carbonate (Data from JANAF, 1971).

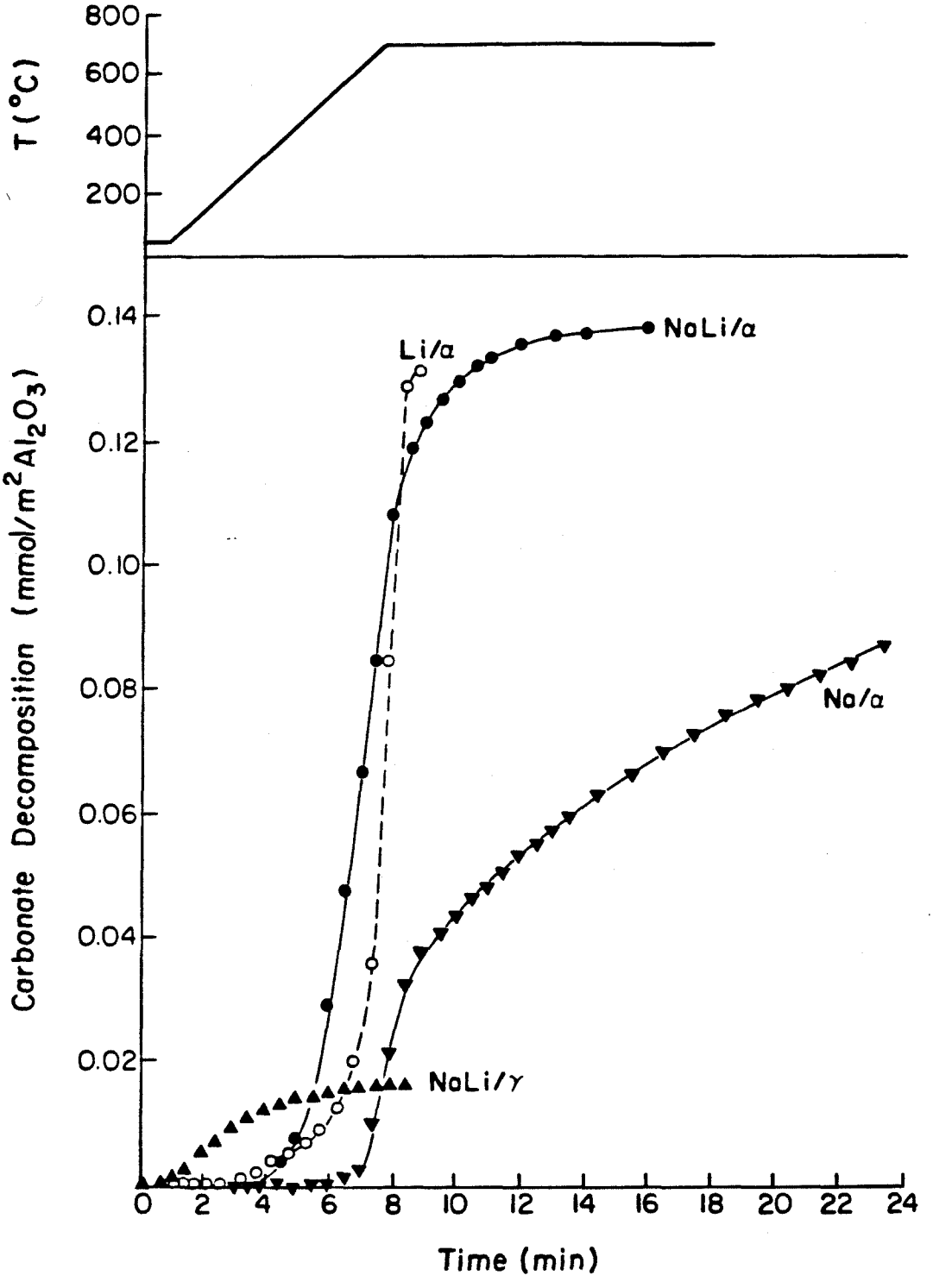

Figure 2. Alkali Carbonate Decomposition on Different Supports.

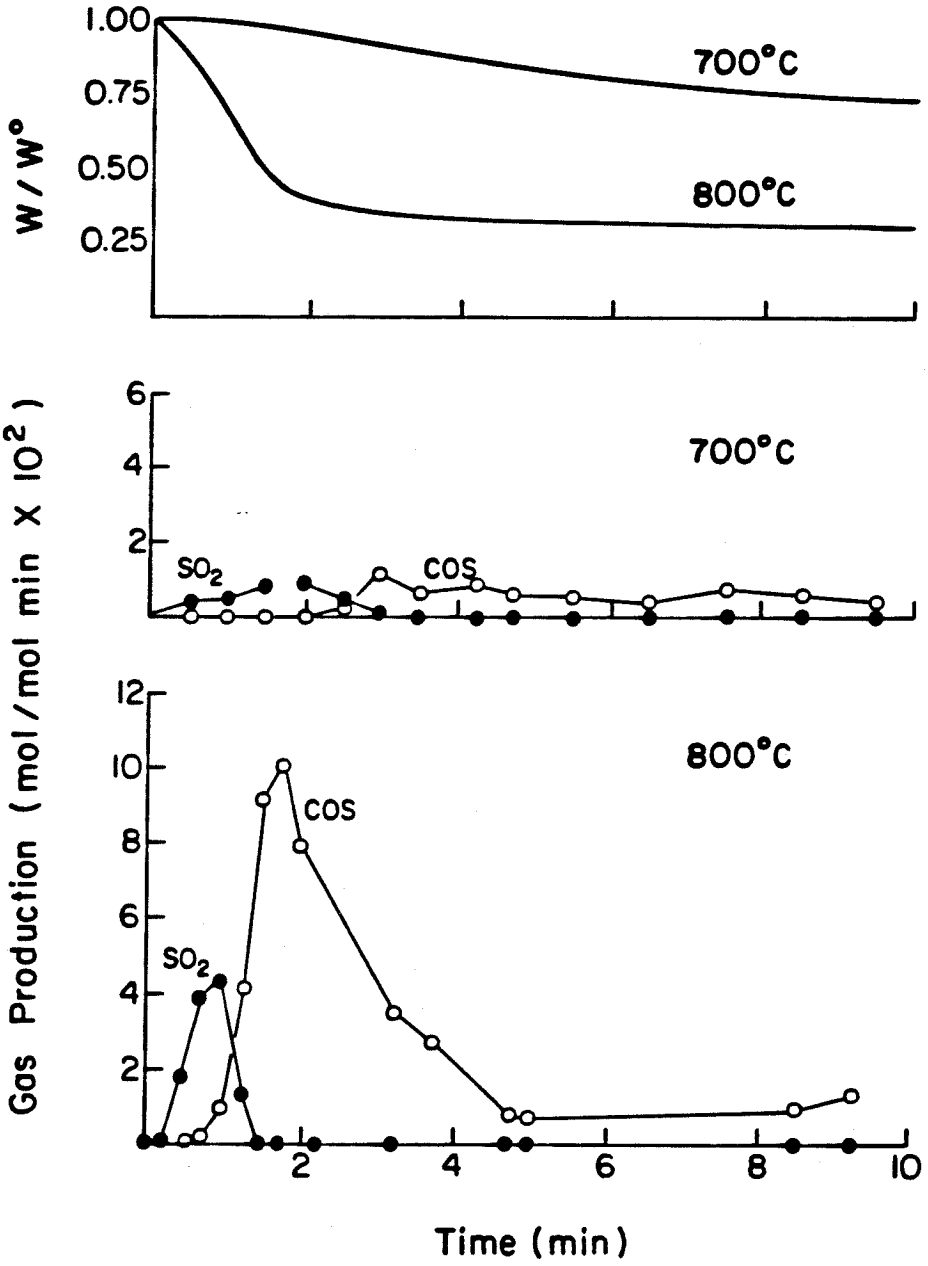

Figure 3. Reduction of $Na_2SO_4/\alpha\text{-}Al_2O_3$ (Nα3) with 10% CO in the TGA; Gas Production in Mols Per Initial Mol of Sulfate.

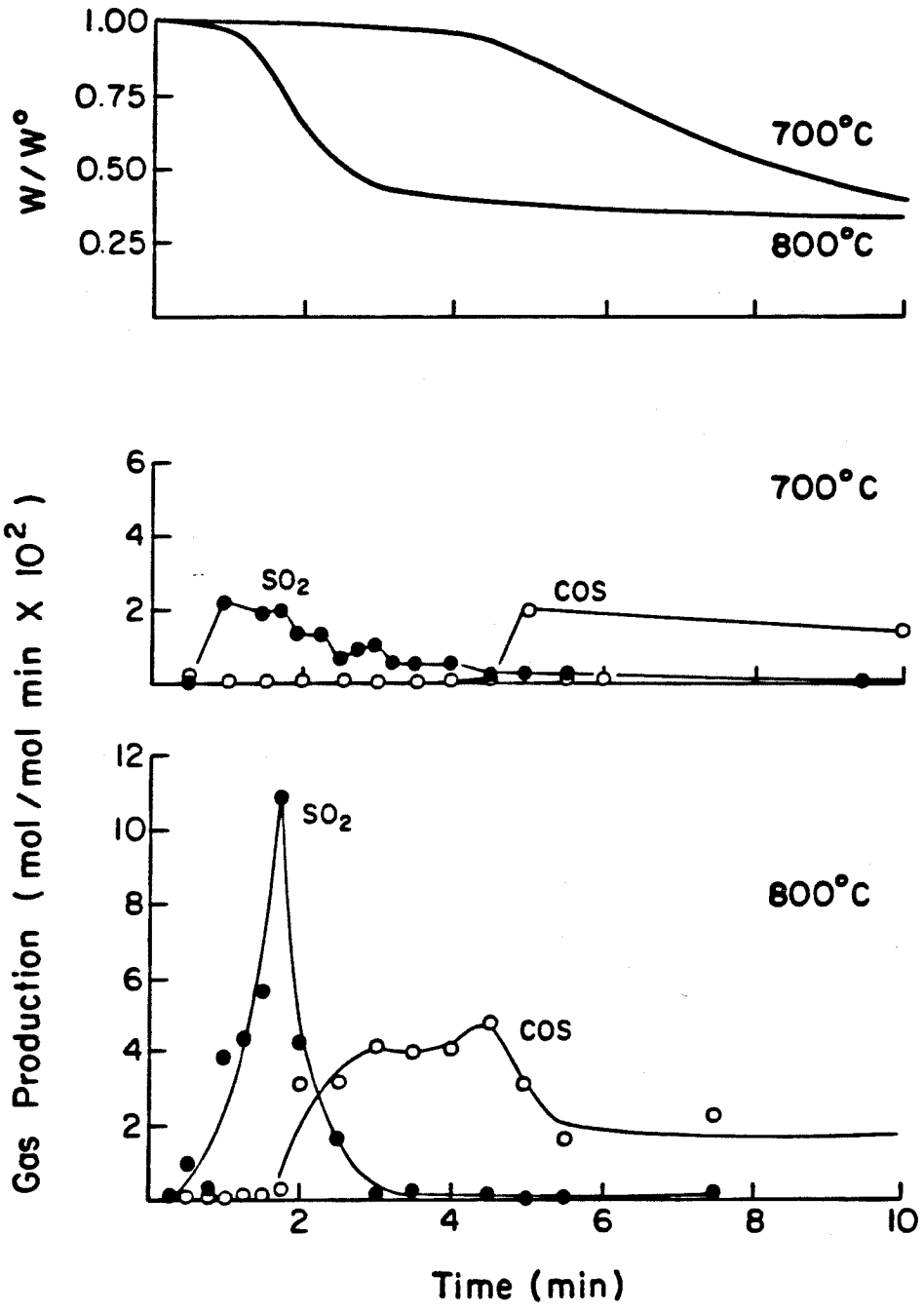

Figure 4. Reduction of $NaLiSO_4/\alpha\text{-}Al_2O_3$ (NLα1) with 10% CO in the TGA; Gas Production in Mols Per Initial Mol of Sulfate.

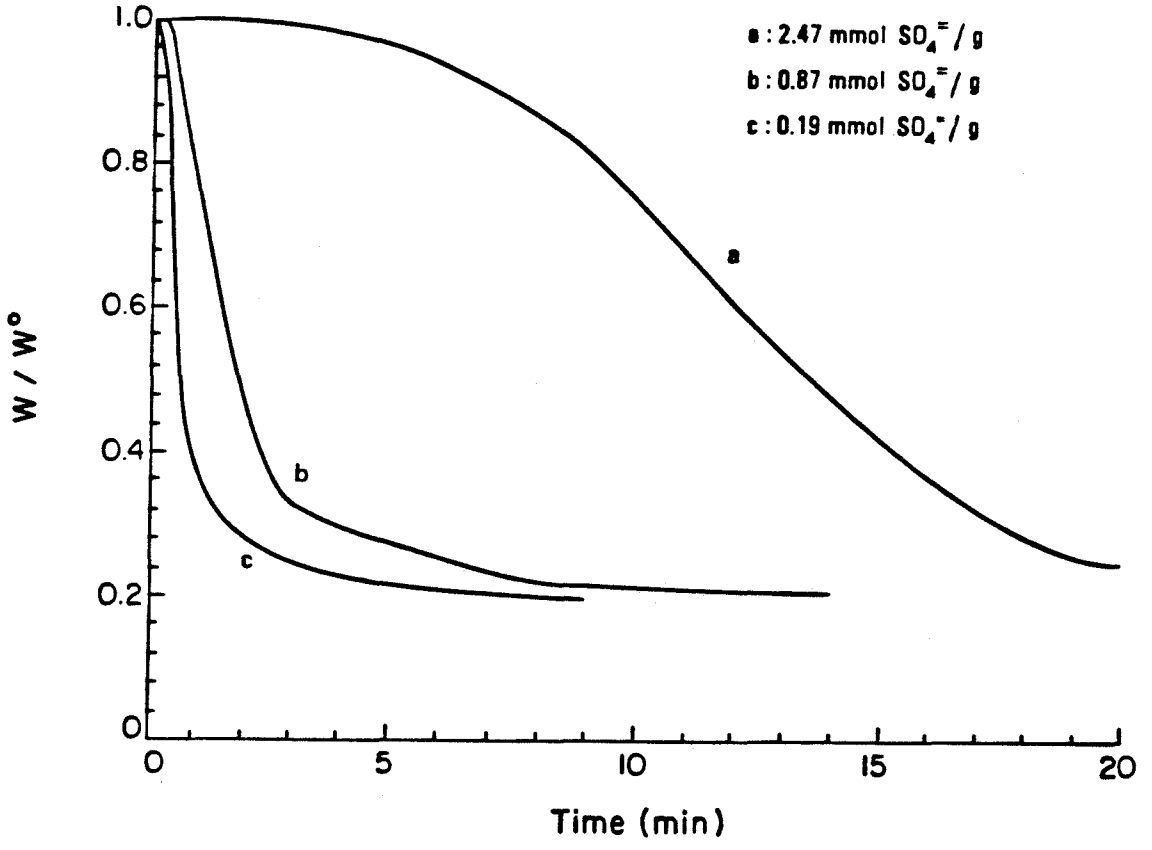

Figure 5. The Effect of Sorbent Loading on the Reduction of $NaLiSO_4/\alpha\text{-}Al_2O_3$ at 800°C with 10% CO in the TGA.

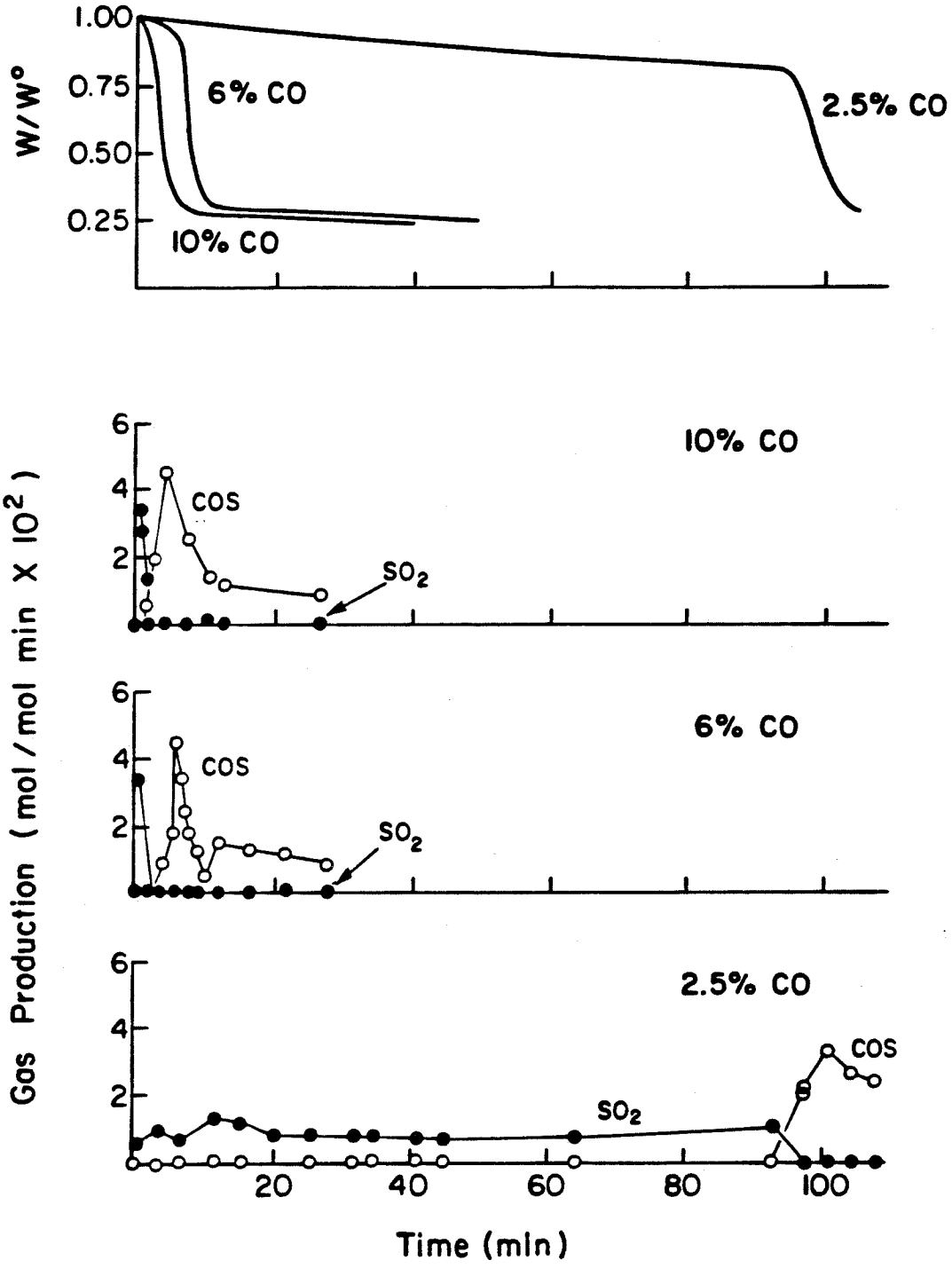

Figure 6. The Effect of CO Concentration on the Reduction of $NaLiSO_4/\alpha\text{-}Al_2O_3$ (NLα2) at 750°C in the TGA; Gas Production in Mols Per Initial Mol of Sulfate.

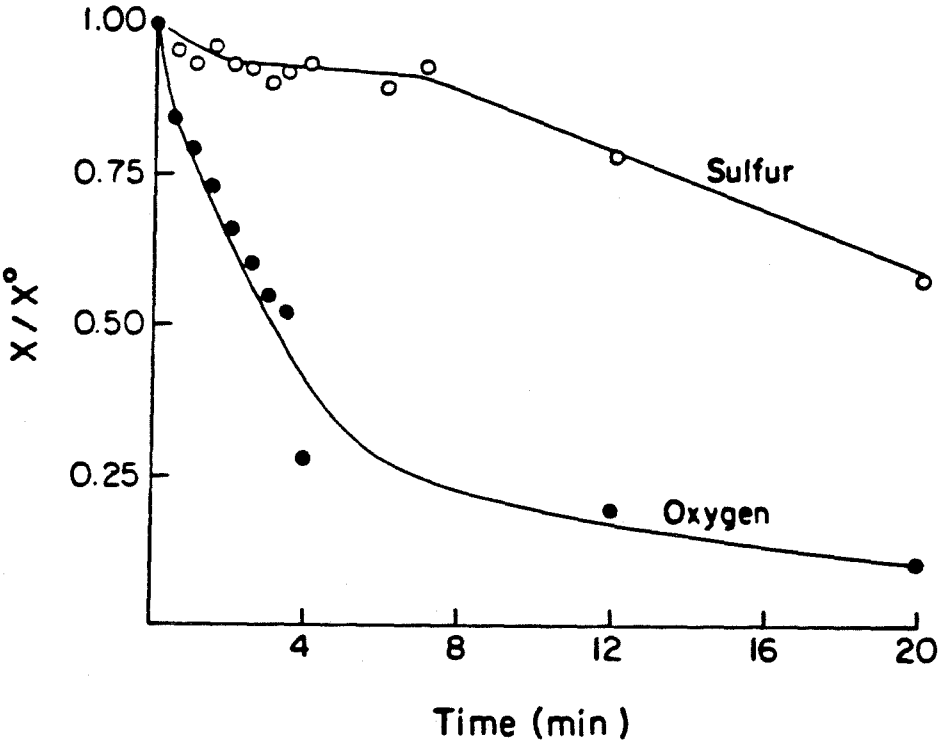

Figure 7. Sorbent Elemental Composition During Reduction of $Na_2SO_4/\alpha\text{-}Al_2O_3$ (Nα1) at 800°C with 10% CO.

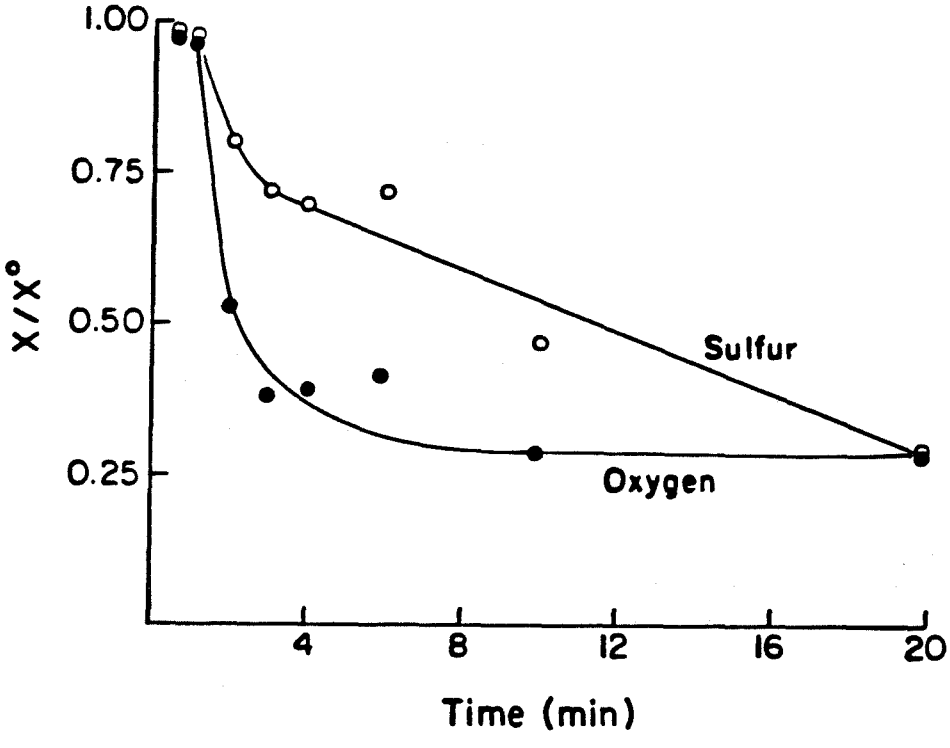

Figure 8. Sorbent Elemental Composition During Reduction of $NaLiSO_4/\alpha\text{-}Al_2O_3$ (NLα1) at 800°C with 10% CO.

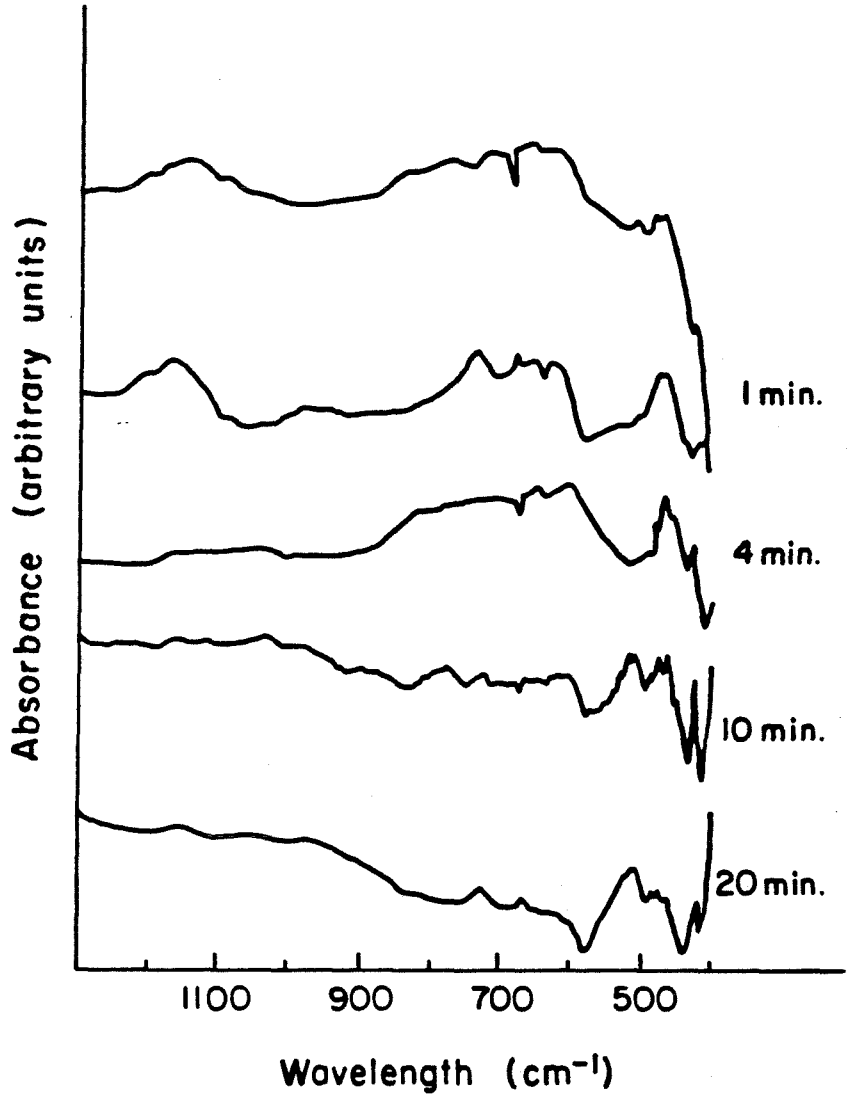

Figure 9. Infrared Absorption Spectra of $NaLiSO_4/\alpha\text{-}Al_2O_3$ (NLα1) Reduced at 800°C with 10% CO for Different Times.

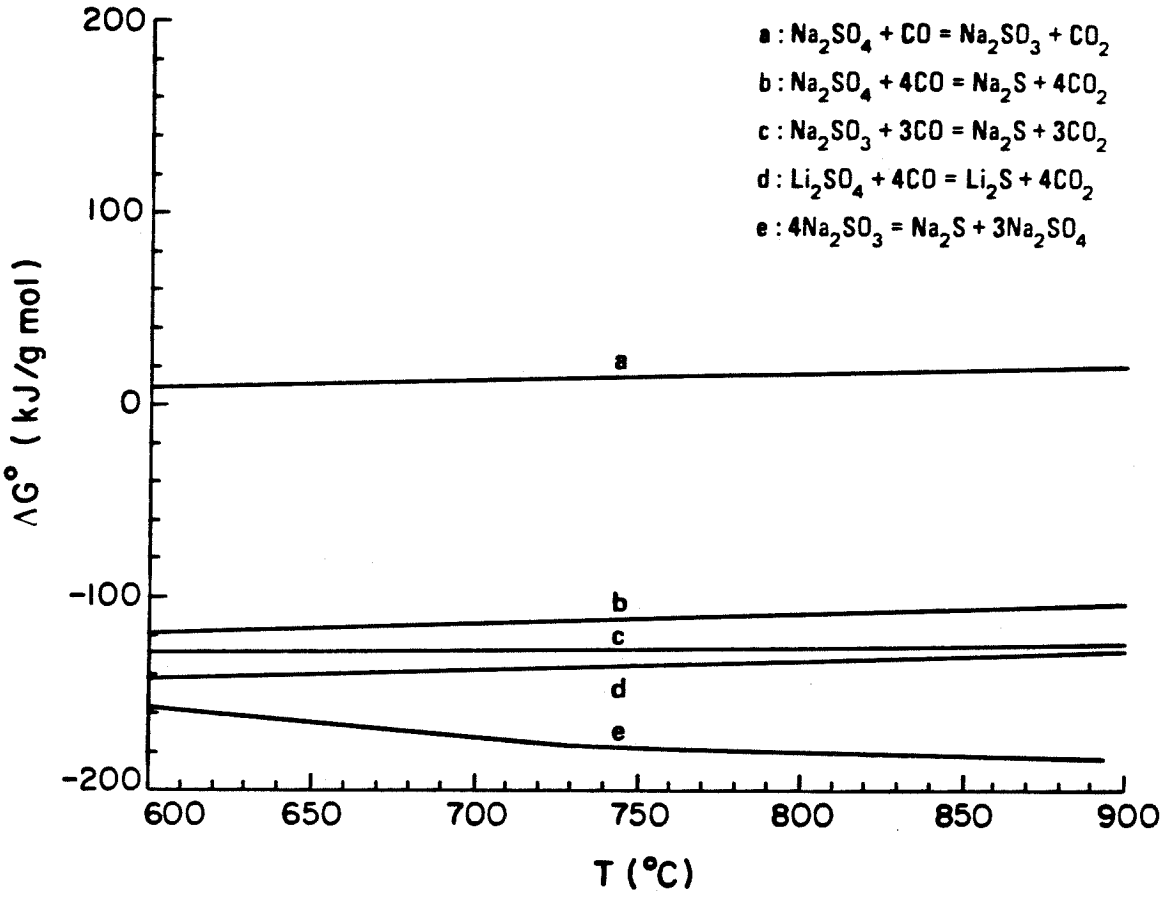

Figure 10. Standard Free Energy for the Reduction of Alkali Sulfate to Sulfite and Sulfide (Data from JANAF, 1971).

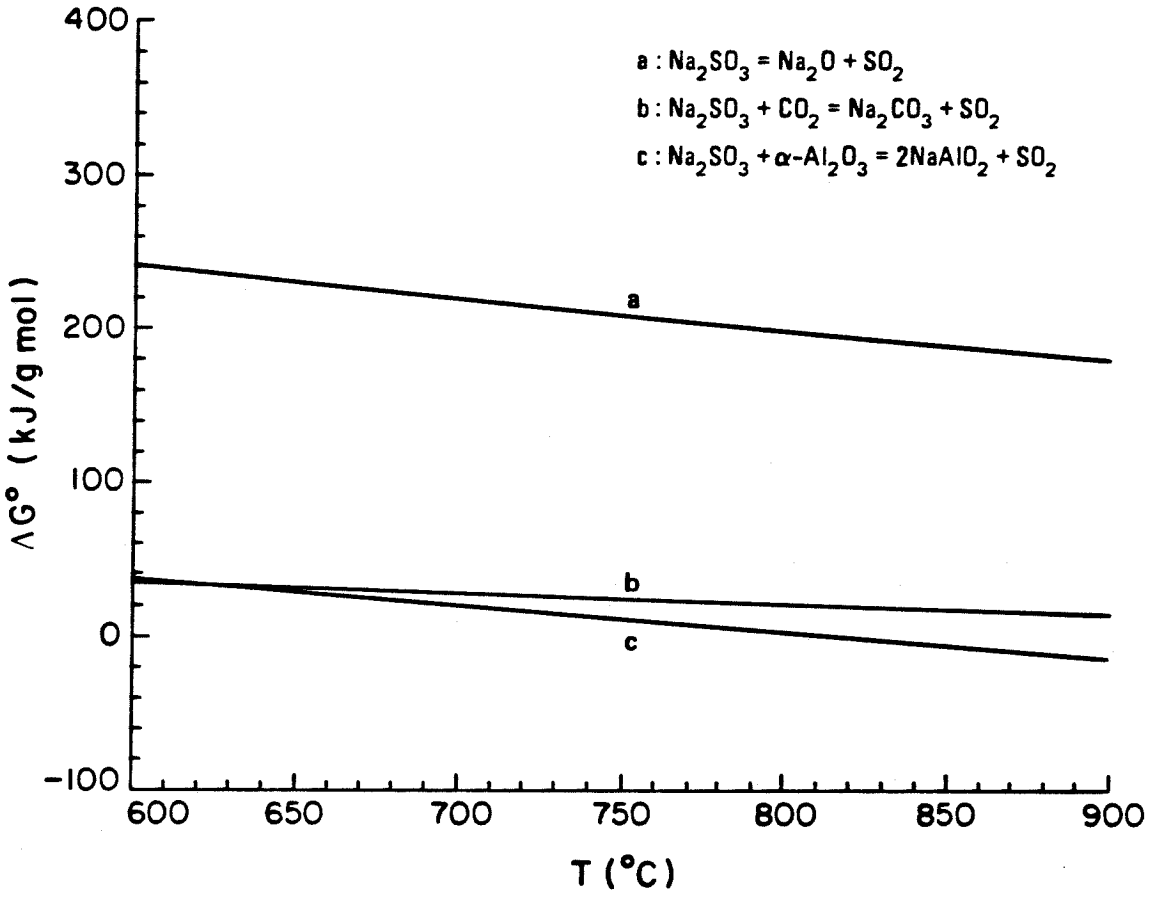

Figure 11. Standard Free Energy for the Decomposition of Sodium Sulfite (Data from JANAF, 1971).

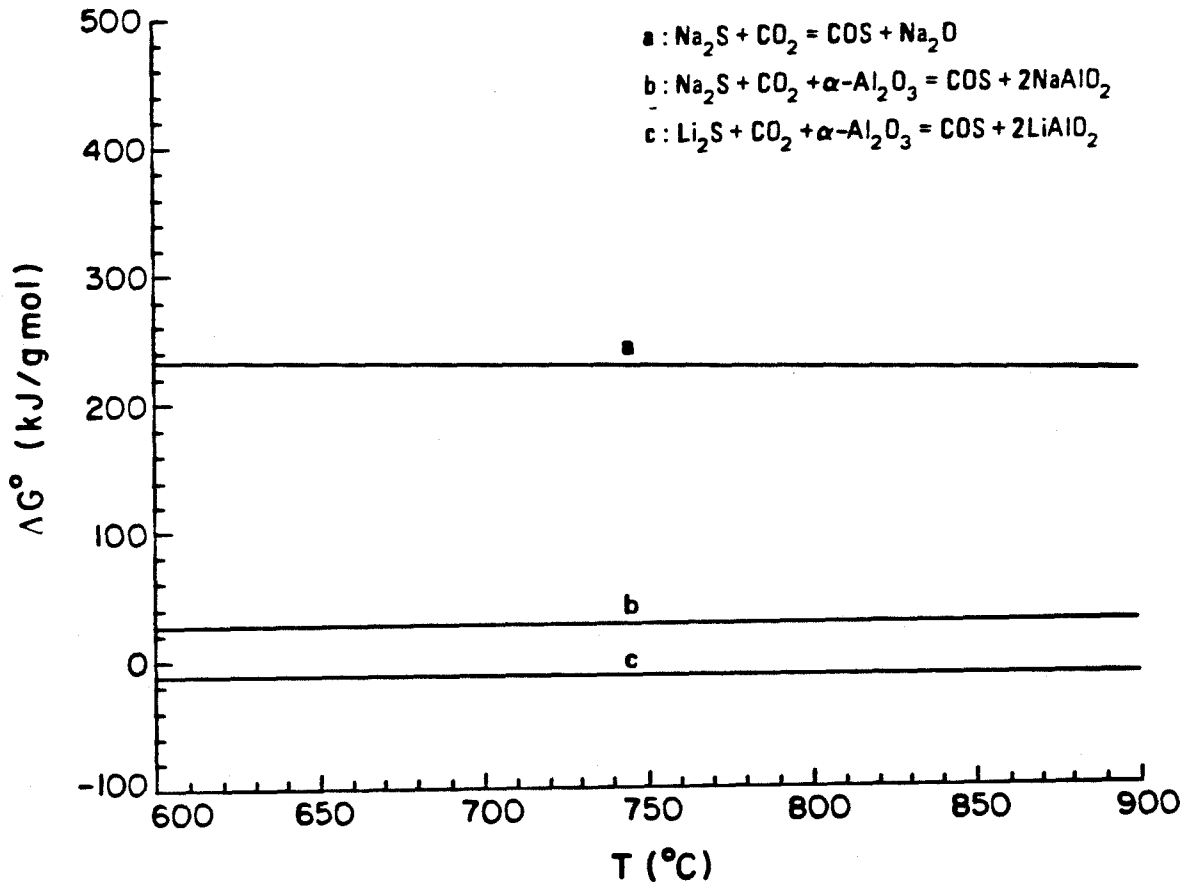

Figure 12. Standard Free Energy for the Reaction Between Alkali Sulfide and CO_2 (Data from JANAF, 1971).

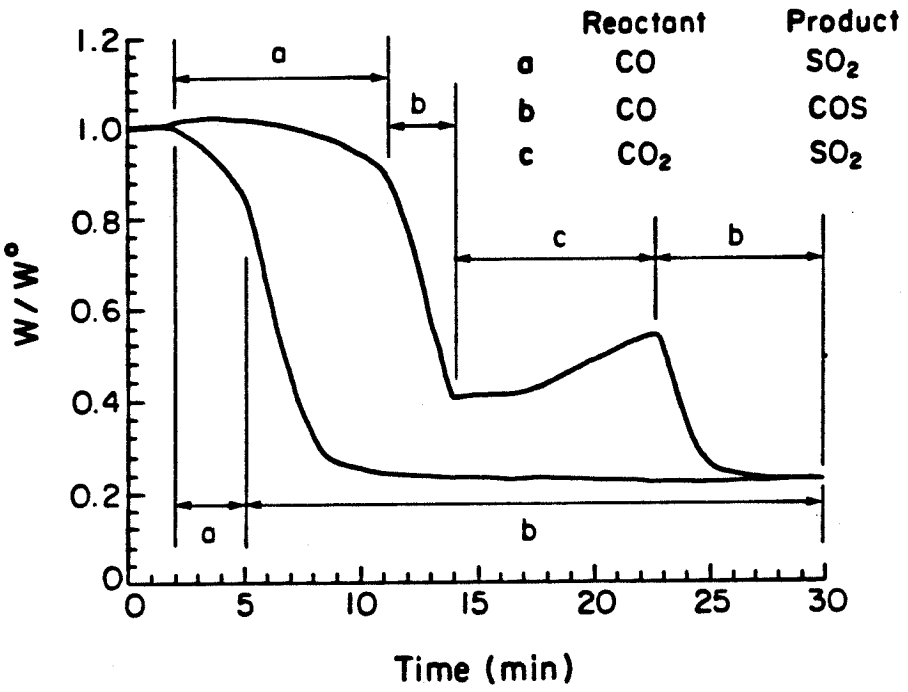

Figure 13. The Effect of CO_2 on the Weight Loss and Gas Production During Reduction of a $NaLiSO_4/\alpha\text{-}Al_2O_3$ Sorbent (NLα2) at 750°C with 5% CO.

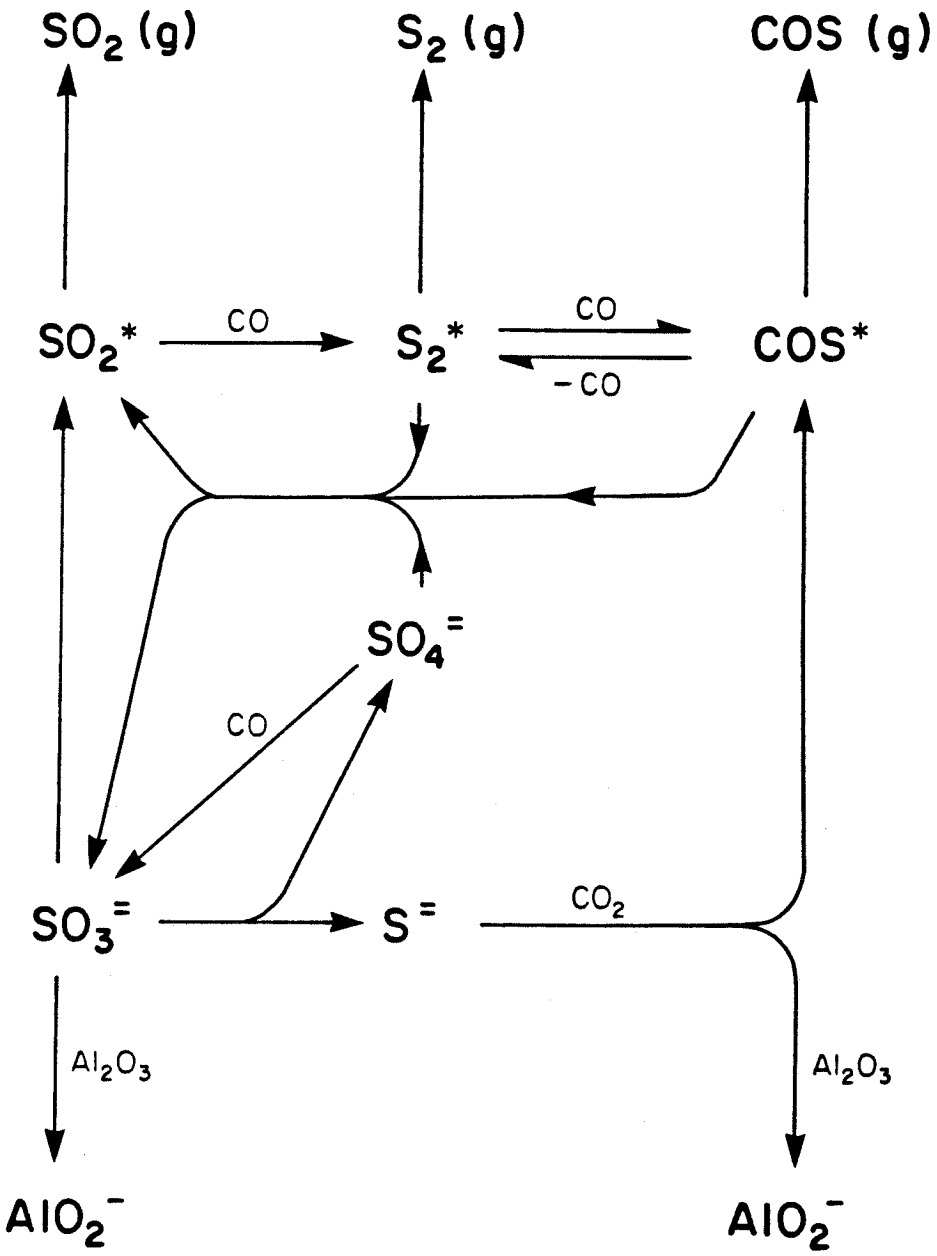

Figure 14. Proposed Reaction Network (* Denotes Chemisorbed Species).

10.2. Nature of the Remaining Sulfur

Reduction of the $NaLiSO_4/\alpha\text{-}Al_2O_3$ sorbents by CO for 30 minutes at $800°C$ removes over 80% of the sulfur. Reduction of the remaining sulfur by CO or H_2 is very slow : after a 90-minute exposure to CO at $800°C$, for example, almost 10% of the sulfur still remains in the sorbent.

That residual sulfur can be oxidized to sulfate by exposure to O_2 at the operating temperature of the sorbent. The behavior of that sulfate upon reduction by CO is, however, different from that of the completely sulfated sorbent. Reduction is fast, leading to the production of small quantities of COS and no SO_2.

Temperature-programmed oxidation curves of reduced sorbent $ST\alpha 1$ (Table 8.1) and of supported alkali sulfides ($SD\alpha$) are shown in Fig. 10.15. Oxidation of the residual sulfur begins at temperatures above $400°C$, reaching a maximum rate at $600°C$. Oxidation of the supported sulfides, on the other hand, takes place at lower temperatures. The higher resistance to oxidation exhibited by the reduced sulfur remaining in the sorbent after regeneration indicates that its chemical nature is different from that of the alkali sulfides. This stabilization may be caused by strong interaction with the aluminate or with active surface sites.

Fig. 10.16 shows SEM micrographs of the pore surface of sorbent $AC\alpha 1$ before and after reduction with CO for 30 minutes at $800°C$. Although the general texture of the surface has not been affected, thin crevices between particles, approximately 1 μm long, have been filled in as a result of the reduction.

10.2.1. X-Ray Photoelectron Spectroscopy The composition of alumina-supported alkali sulfates and their reduction products was further explored with X-ray photoelectron spectroscopy (XPS). This method, also known as *Electron Spectroscopy for Chemical Analysis* (ESCA), is a high-resolution spectroscopic technique based on a magnetic or electrical analysis of the core electrons which are emitted from a substance on irradiation with X-rays. Accurate measurement of the kinetic energy of the emitted photoelectrons makes it possible to calculate the binding energy of the electrons in the atomic orbitals. Typical sampling depths (i.e., electron mean free paths) are in the range of 5-100 Å. A particularly useful feature of this technique is the occurence of *chemical shifts* that result from changes in the chemical environment of the atom. Craig et al. [3] found that it was possible to distinguish up to seven different sulfur species present in ambient particulate matter from the position of the corresponding S 2p peaks.

An initial attempt using the sorbent in the particulate form resulted in loss of resolution by peak broadening caused by electric charging of the individual particles. These samples were also found to be very difficult to mount. A second set of samples was then prepared using Al_2O_3 film as a substrate (Sec. 8.1). The samples containing supported alkali sulfates ($ST2$) were calcined, while those containing alkali acetates ($AC1$) were first calcined and then sulfated with $SO_2 + O_2$ at $800°C$. The average thickness of the sulfate layer was approximately the same as in the impregnated particles (Table 8.1). Some of the sulfated samples were exposed to 10% CO at $800°C$ for various periods of time, and cooled down under CO.

SEM micrographs of this material (Fig. 10.17) reveals a somewhat different

texture from that of porous α-Al_2O_3 (Fig. 8.1). The surface appears to be non-porous and granular. As in the case of porous α-Al_2O_3, small crystallites are observed on the surface after impregnation, but in this case they do not disappear after calcination (Fig. 10.17 (d)).

Figs. 10.18 and 10.19 show the sulfur 2p region of the XPS spectra of samples $ST2$ and $AC1$, respectively. Since the peak heights varied from run to run due to the varying number of spectra recorded and the local surface concentration, the peak heights were normalized with respect to Na 1p. In both cases the sulfur appears as SO_4^{2-}, both before and after reduction. No reduced sulfur species such as S^o or S^{2-} is present after reduction, indicating a different behavior from the porous sorbents. The peak heights are greater in the case of sorbent $AC1$, possibly due to the presence of sodium in the substrate material. The amount of SO_4^{2-} decreases during the first minutes of reduction, and some still remains after 30 minutes of exposure to CO. As in the case of porous α-Al_2O_3, sulfur removal is accomplished through the sequence of reactions :

$$SO_4^{2-}/Al_2O_3 + CO \rightarrow SO_3^{2-}/Al_2O_3 + CO_2$$

$$SO_3^{2-}/Al_2O_3 \rightarrow 2AlO_2^- + SO_2.$$

The disproportionation reaction :

$$4SO_3^{2-} \rightarrow 3SO_4^{2-} + S^{2-}$$

does not appear to take place in this case. If any SO_2 is reduced, the elemental sulfur formed does not adsorb on the surface. Thus, the existence and

properties of reduced sulfur in the sorbent are closely tied to the properties of the alumina surface. It is possible that this species consists of elemental sulfur strongly coordinated to defect sites on the alumina surface. Since these sites are formed by dehydroxylation from hydrated aluminas, they would be present in the porous material but not in the Al_2O_3 films. This explanation is also consistent with the temperature-programmed oxidation experiments (Fig. 10.15). Oxidation of this species would lead to strongly chemisorbed SO_2. This is consistent with the observed behavior of this oxidized species upon reduction with CO.

10.3. Kinetic Model

The following reaction scheme will be used as a basis to describe the reduction process :

$$SO_4^{2-} + CO \xrightarrow{\bar{k}_1} SO_3^{2-} + CO_2 \tag{10.1}$$

$$SO_3^{2-} \xrightarrow{\bar{k}_2} \frac{3}{4}SO_4^{2-} + \frac{1}{4}S^{2-} \tag{10.2}$$

$$SO_3^{2-} \xrightarrow{\bar{k}_3} O^{2-} + SO_2^* \tag{10.3}$$

$$SO_2^* + 2CO \xrightarrow{\bar{k}_4} S^* + 2CO_2 \tag{10.4}$$

$$SO_4^{2-} + \frac{1}{2}S^* \xrightarrow{\bar{k}_5} SO_3^{2-} + \frac{1}{2}SO_2^* \tag{10.5}$$

$$CO + S^* \xrightarrow{\bar{k}_6} COS^* \tag{10.6}$$

$$S^{2-} + CO_2 \xrightarrow{\bar{k}_7} COS^* + O^{2-} \tag{10.7}$$

$$SO_2^* \xrightarrow{\bar{k}_8} SO_2 \tag{10.8}$$

$$COS^* \xrightarrow{\bar{k}_9} COS \tag{10.9}$$

$$S^* \xrightarrow{\bar{k}_{10}} \frac{1}{2}S_2. \tag{10.10}$$

The superscript * denotes chemisorbed species, and O^{2-} represents AlO_2^-.

Reactions 10.1, 10.3 and 10.8 are responsible for the SO_2 formation during the first stage of the reduction. Although elemental sulfur is formed on the surface during that stage via reaction 10.4, it is rapidly consumed by reaction 10.5. When SO_4^{2-} is depleted reactions 10.1 and 10.5 cease, signaling the beginning of the second stage. Reactions 10.3, 10.4 and 10.10 are responsible for the production of elemental sulfur during that stage. COS is produced either by reactions 10.6 and/or 10.7, and 10.9.

In the absence of alumina, the production of SO_2 encompasses the formation of alkali carbonate :

$$SO_4^{2-} + CO \longrightarrow SO_2 + CO_3^{2-}.$$

The SO_2 produced by CO reduction of sorbent $ST\alpha 1$ and of a molten mixture of Na_2SO_4-Li_2SO_4 containing traces of S^{2-} are compared in Fig. 10.20. The rate of SO_2 production is one order of magnitude higher in the case of the supported sulfates. In the absence of S^{2-} the difference is even greater. This result suggests that alumina may act as a catalyst for reaction 10.1. It will be assumed that reaction 10.1 takes place on the surface, involving sulfate ions present in the molten layer. The rate of reduction by carbon is proportional to the sulfate concentration on the carbon surface, given by [2] :

$$\left[SO_4^{2-}\right]^* = \frac{K\ \left[SO_4^{2-}\right]}{1 + K\ \left[SO_4^{2-}\right]}.$$

The reaction is then of zero order during most of the reduction, and of first order at very low sulfate concentrations. The catalyzed reduction by hydrogen, on the other hand, is of zero order in $[SO_4^{2-}]$ [1]. On the basis of strong adsorption of SO_4^{2-} on Al_2O_3, reaction 10.1 will be assumed to be of zero order in sulfate.

Assuming that all other reactions are of first order in the reactants, and that the Al_2O_3 and AlO_2^- concentrations do not affect the reaction rates, the concentrations of the species are governed by the following set of first-order ODE's :

$$\frac{d[SO_4^{2-}]}{dt} = -\bar{k}_1[CO] + \frac{3}{4}\bar{k}_2[SO_3^{2-}] - \bar{k}_5[S^*][SO_4^{2-}]$$

$$\frac{d[SO_3^{2-}]}{dt} = \bar{k}_1[CO] - (\bar{k}_2 + \bar{k}_3)[SO_3^{2-}] + \bar{k}_5[S^*][SO_4^{2-}]$$

$$\frac{d[S^{2-}]}{dt} = \frac{1}{4}\bar{k}_2[SO_3^{2-}] - \bar{k}_7[S^{2-}][CO_2]$$

$$\frac{d[O^{2-}]}{dt} = \bar{k}_3[SO_3^{2-}] + \bar{k}_7[S^{2-}][CO_2]$$

$$\frac{d[SO_2^*]}{dt} = \bar{k}_3[SO_3^{2-}] - \bar{k}_4[SO_2^*][CO] + \frac{1}{2}\bar{k}_5[SO_4^{2-}][S^*] - \bar{k}_8[SO_2^*]$$

$$\frac{d[COS^*]}{dt} = \bar{k}_6[CO][S^*] + \bar{k}_7[CO_2][S^{2-}] - \bar{k}_9[COS^*]$$

$$\frac{d[S^*]}{dt} = \bar{k}_4[CO][SO_2^*] - \frac{1}{2}\bar{k}_5[SO_4^{2-}][S^*] - \bar{k}_6[CO][S^*] - \frac{1}{2}\bar{k}_{10}[S^*].$$

The gas concentrations are :

$$\frac{[\dot{SO_2}]}{\lambda} = \bar{k}_8 \frac{[SO_2^*]}{\lambda},$$

$$\frac{[\dot{COS}]}{\lambda} = \bar{k}_9 \frac{[COS^*]}{\lambda}.$$

where :

$$[\dot{SO_2}] \equiv \frac{d[SO_2]}{dt}, \quad [\dot{COS}] \equiv \frac{d[COS]}{dt}.$$

The weight is obtained from :

$$\frac{W}{W_0} = \frac{1}{96\lambda} \sum_{i=1}^{7} M_i C_i,$$

where C_i are the concentrations of the ionic and chemisorbed species, and M_i their molecular weights.

Approximate values of the kinetic constants were obtained from the literature, whenever available, or from measurements of the rates of individual reactions. Constant $\bar{k}_1$ was estimated from the duration of the SO_2 production step : $\bar{k}_1 = 1$ mmole/gram sorbent·min at $800°C$. For the catalyzed reduction of SO_2 we have : $\bar{k}_4 = 4.5 \times 10^3$ min^{-1} [5]. The rate of desorption of SO_2 can be approximated with the values obtained in Chapter 4 : $\bar{k}_8 = 0.1$ min^{-1}. From recent experiments on the desorption of elemental sulfur from alumina, we have : $\bar{k}_{10} \approx 0.01$ min^{-1}. Constant $\bar{k}_5$ can be considered to be infinitely large.

The system of differential equations was integrated numerically using a standard 4th order Runge-Kutta method, with initial conditions :

$$[SO_4^{2-}] = \lambda, \quad [SO_3^{2-}] = \ldots = 0 \quad (\text{at } t = 0).$$

The effect of the values of the kinetic constants on the SO_2 and COS productions, weight, and sulfur and oxygen removal as a function of time was observed qualitatively, and compared with the experimental observations described in Sec. 10.1. As a result of the comparison, the following general conclusions can be drawn :

(i) The small weight loss observed experimentally during the first stage of the reduction can only be explained if all the sulfur remaining in the sorbent at the end of that stage (i.e., $\approx 90\%$) is in the form of sulfite or chemisorbed SO_2. The presence of significant amounts of S^{2-} or S^* would cause greater weight losses than observed. This means that the disproportionation reaction (10.2) does not take place to any significant extent during the first stage. Since reaction 10.2 is known to take place at the operating temperatures of the sorbent [4], sulfite may be present as a more stable surface species produced by surface reaction 10.1.

(ii) The fact that the oxygen content of the sorbent remains constant during the last stage of the reduction, while sulfur is removed as COS (Fig. 10.8), can only be accounted for by neglecting reaction 10.7. If this reaction was a significant source of COS, then the oxygen content in the sorbent would increase noticeably. Although reaction 10.7 is thermodynamically favorable (Fig. 10.12), the reduced sulfur species may in this case be less reactive than pure sulfide (Sec. 10.2). Therefore, reaction 10.6 is the main source of COS.

(iii) The rapid weight loss, accompanied by a burst of COS, at the beginning

of the second stage of reduction requires a rapid reduction to elemental sulfur (reactions 10.3 and 10.4), and fast desorption of COS (i.e., a large value of $\bar{k}_9$).

These considerations lead to the following reduced set of reactions :

$$SO_4^{2-} + CO \xrightarrow{k_1} SO_3^{2-} + CO_2 \tag{10.11}$$

$$SO_3^{2-} \xrightarrow{k_2} O^{2-} + SO_2 \tag{10.12}$$

$$SO_3^{2-} + 2CO \xrightarrow{k_3} O^{2-} + S^* + 2CO_2 \tag{10.13}$$

$$S^* \xrightarrow{k_4} \frac{1}{2} S_2 \tag{10.14}$$

$$CO + S^* \xrightarrow{k_5} COS. \tag{10.15}$$

During the first stage, only reactions 10.11 and 10.12 take place. Any elemental sulfur formed at that time would be consumed immediately via reaction 10.5. This scheme predicts a linear decrease in sulfate concentration :

$$\frac{d\left[SO_4^{2-}\right]}{dt} = -k_1 \left[CO\right] \;\Rightarrow\; \left[SO_4^{2-}\right] = \lambda - k_1 \left[CO\right] t$$

The kinetic constant k_1 can be obtained from the duration of the first stage, t_1 :

$$k_1 = \frac{\lambda}{[CO]\, t_1}. \tag{10.16}$$

The SO_2 concentration in the gas during this stage is obtained from the sulfite concentration in the sorbent :

$$\frac{d\left[SO_3^{2-}\right]}{dt} = k_1 \left[CO\right] - k_2 \left[SO_3^{2-}\right] \;\Rightarrow\; \left[SO_3^{2-}\right] = \left(\frac{k_1}{k_2}\right) \left[CO\right] \left\{1 - e^{-k_2 t}\right\}.$$

Hence,

$$[\dot{SO_2}] = k_2 \left[SO_3^{2-}\right] = k_1 [CO] \left\{1 - e^{-k_2 t}\right\}.$$

At low CO concentrations, or longer SO_2 production periods (eq. 10.16), the sulfite concentration may reach steady state, leading to a constant rate of SO_2 generation (Fig. 10.6, 2.5%). At $[CO] = 0.10$ the rate of SO_2 production rises rapidly :

$$\frac{[\dot{SO_2}]}{\lambda} \approx \frac{k_1 k_2}{\lambda} [CO] t = k_2 \left(\frac{t}{t_1}\right). \tag{10.17}$$

The fraction of sulfur remaining in the sorbent at the end of the first stage is given by :

$$r = 1 - \int_0^{t_1} \frac{[\dot{SO_2}]}{\lambda} dt = 1 - \left\{\frac{\lambda k_2}{2 [CO] k_1}\right\}. \tag{10.18}$$

At time $t = t_1$ the sulfate is depleted and reaction 10.11 ceases. The rate of production of SO_2 then begins to decrease. The remaining sulfur is in the form of chemisorbed SO_2, or sulfite, accounting for the small weight loss at $t \leq t_1$. During the second stage ($t > t_1$) reactions 10.12, 13, 14 and 15 proceed. Reactions 10.13 and 10.15 are fast, causing a sudden weight loss and production of COS. Reaction 10.14 is slower, accounting for the longer COS tail. Sulfite is consumed by reactions 10.12 and 10.13. As shown in Part I, SO_2 may actually adsorb with a wide range of binding energies. For simplicity, it will be assumed that k_2 is constant :

$$\frac{d\left[SO_3^{2-}\right]}{dt} = -\left(k_2 + k_3 [CO]\right) \left[SO_3^{2-}\right] \Rightarrow \left[SO_3^{2-}\right] = r\ \lambda\ e^{-k_{23}\tau},$$

where $k_{23} \equiv k_2 + k_3 [CO]$, and $\tau \equiv t - t_1$. The SO_2 production during this

stage is then :

$$\frac{[\dot{SO_2}]}{\lambda} = r\ k_2\ e^{-k_{23}\tau}$$

$$\Rightarrow\ ln\left\{\frac{[\dot{SO_2}]}{\lambda}\right\} = ln\{r\ k_2\} - k_{23}\tau. \tag{10.19}$$

The kinetic constants k_2 and k_3 can be obtained by regression of the SO_2 production data, from eqs. 10.17 and 10.19. At high temperatures and CO concentrations, the reduction of chemisorbed SO_2 is much faster than its desorption (i.e., $k_{23} \approx [CO]\,k_3$), and therefore the SO_2 concentration in the gas decreases rapidly (Figs. 10.3, 4 and 6).

The fraction of sulfur converted to SO_2 is :

$$\frac{[SO_2]}{\lambda} = \int_0^\infty \frac{[\dot{SO_2}]}{\lambda} dt = 1 - r + \left(\frac{k_2}{k_{23}}\right) r.$$

The concentration of chemisorbed sulfur is governed by :

$$\frac{d[S^*]}{dt} + k_{45}\,[S^*] = k_3\,[CO]\,r\ \lambda\ exp\{-k_{23}\tau\},$$

where $k_{45} \equiv k_4 + [CO]\,k_5$. The solution of this differential equation is :

$$[S^*] = \frac{k_3\,[CO]\,r\lambda}{k_{23} - k_{45}}\left[exp\{-k_{45}\tau\} - exp\{-k_{23}\tau\}\right].$$

The concentrations of elemental sulfur and COS in the gas are given by :

$$\frac{[\dot{S_2}]}{\lambda} = \frac{k_4\,[S^*]}{2\lambda} = \frac{k_3 k_4\,[CO]\,r}{2\,(k_{23} - k_{45})}\left[exp\{-k_{45}\tau\} - exp\{-k_{23}\tau\}\right],$$

$$\frac{[\dot{COS}]}{\lambda} = \frac{k_5\,[CO]\,[S^*]}{\lambda} = \frac{k_3 k_5\,[CO]^2\,r}{k_{23} - k_{45}}\left[exp\{-k_{45}\tau\} - exp\{-k_{23}\tau\}\right].$$

According to this model, the ratio $[S_2]/[COS]$ is constant at all times. The productions of COS and S_2 increase first as a result of reaction 10.13 (k_3) and decrease later due to reactions 10.14 and 10.15 (k_{45}).

The total productions of S_2 and COS at time $t = t_2$ are :

$$\frac{[S_2]}{\lambda} = \int_{t_1}^{t_2} \frac{[\dot{S_2}]}{\lambda} dt =$$

$$= \frac{k_3 k_4 [CO] r}{2(k_{23} - k_{45})} \left[\frac{1 - exp\{-k_{45}\Delta t\}}{k_{45}} - \frac{1 - exp\{-k_{23}\Delta t\}}{k_{23}} \right],$$

$$\frac{[COS]}{\lambda} = \int_{t_1}^{t_2} \frac{[\dot{COS}]}{\lambda} dt = \tag{10.20}$$

$$= \frac{k_3 k_5 [CO]^2 r}{(k_{23} - k_{45})} \left[\frac{1 - exp\{-k_{45}\Delta t\}}{k_{45}} - \frac{1 - exp\{-k_{23}\Delta t\}}{k_{23}} \right],$$

where $\Delta t \equiv t_2 - t_1$. The selectivity towards elemental sulfur is determined by the ratio of the kinetic constants of reactions 10.14 and 10.15 :

$$\frac{[S_2]}{[COS]} = \frac{k_4}{2[CO]k_5}. \tag{10.21}$$

The values of k_4 and k_5 obtained from eqs. 10.20 and 10.21 using experimental values of the total COS production and $[S_2]/[COS]$ satisfy the overall sulfur balance. Once the kinetic constants have been found, the weight (W), the oxygen content (Ω), and the sulfur content (Σ) of the sorbent can be computed

from the concentrations of the ions and chemisorbed species :

$$\frac{W}{W_0} = \frac{96\left[SO_4^{2-}\right] + 80\left[SO_3^{2-}\right] + 16\left[O^{2-}\right] + 32\left[S^*\right]}{96\lambda} =$$

$$= 1 - \frac{1}{6}\left(\frac{t}{t_1}\right) - \frac{2}{3}(1-r)\left(\frac{t}{t_1}\right)^2 \qquad ;\ (t \le t_1)$$

$$= \frac{1}{6} + \frac{2}{3} r\ e^{-k_{23}\tau} + \frac{1}{3}\left(\frac{k_{23} r}{k_{23} - k_{45}}\right)\left[e^{-k_{45}\tau} - e^{-k_{23}\tau}\right] \quad ;\ (t \ge t_1)$$

$$\Omega = \frac{4\left[SO_4^{2-}\right] + 3\left[SO_3^{2-}\right] + \left[O^{2-}\right]}{4\lambda} =$$

$$= 1 - \frac{1}{4}\left(\frac{t}{t_1}\right) - \frac{1-r}{2}\left(\frac{t}{t_1}\right)^2 \qquad ;\ (t \le t_1)$$

$$= \frac{1}{4} + \frac{1}{2} r\ e^{-k_{23}\tau}, \qquad ;\ (t \ge t_1)$$

$$\Sigma = \frac{\left[SO_4^{2-}\right] + \left[SO_3^{2-}\right] + \left[S^*\right]}{\lambda} =$$

$$= 1 - (1-r)\left(\frac{t}{t_1}\right)^2 \qquad ;\ (t \le t_1)$$

$$= \frac{k_3\left[CO\right] r}{k_{23} - k_{45}} e^{-k_{45}\tau} + \frac{(k_2 - k_{45})\, r}{k_{23} - k_{45}} e^{-k_{23}\tau}. \qquad ;\ (t \ge t_1)$$

Example: In the case of the reduction of sorbent $NL\alpha$ at 800^oC with 10% CO (Fig. 10.4), we have :

$$\lambda = 0.86 \text{ mmole} \cdot \text{gram}^{-1}$$

$$t_1 = 1.45 \text{ min}$$

$$\Delta t = 20 - 1.45 = 18.55 \text{ min}$$

$$[COS]/\lambda = 0.355$$

$$[S_2]/\lambda = 0.125$$

From eqs. 10.16, 10.17, and 10.18 we obtain, respectively :

$$k_1 = 5.93 \text{ mmole} \cdot \text{gram}^{-1} \cdot \text{min}^{-1}$$

$$k_2 = 0.098 \text{ min}^{-1}$$

$$r = 0.929$$

Regression of the $[SO_2]$ data (eq. 10.19) yields :

$$k_{23} = 3.152 \text{ min}^{-1} \quad \Rightarrow$$

$$\Rightarrow \quad k_3 = 30.54 \text{ min}^{-1}.$$

In this case, $k_{23} \approx [CO]\, k_3$. Solving eqs. 10.20 and 10.21, we find the other constants :

$$k_4 = 0.026 \text{ min}^{-1},$$

$$k_5 = 0.368 \text{ min}^{-1}.$$

The predicted weight loss, gas composition, and elemental sorbent composition are compared with the experimental results in Figs. 10.21, 10.22, and 10.23, respectively. The model adequately predicts a rapid loss of oxygen from the sorbent at the onset of the second stage, and a slower decrease in the sulfur

content. The weight loss during the first stage of the reduction is overestimated, possibly due to experimental errors in the measurements of the SO_2 concentration, or to accumulation of alkali carbonate during the first minute of the reduction. Since the kinetic constants were obtained from gas composition measurements only, the agreement between the experimental and the predicted weight at the end of the reduction indicates that those measurements are consistent with the final weight of the sorbent.

The production of COS at the onset of the second stage is higher than the model prediction, as evidenced by the weight loss (Fig. 10.21), gas composition (Fig. 10.22), and sorbent composition (Fig. 10.23) measurements. This discrepancy is probably caused by the assumption of a constant binding energy for sulfur. Weakly bound sulfur first reacts with CO, causing a large initial COS production.

The model generally gives good descriptions of the data at low and medium sorbent loadings. In all cases it is found that $k_3 > k_5 > k_4$. At higher loadings (sorbent $AC\alpha 3$) the rate of regeneration is much lower than predicted. Three processes that have not been taken into account in the model may become significant at high sorbent loadings, decreasing the rate of sulfur removal. The first one is the deactivation of the alumina surface by accumulation of reduction products, such as chemisorbed sulfur, and by formation of alkali aluminate. The second process is the accumulation of reduction products in the molten layer. SO_2 is known to dissolve in molten sulfate (Sec. 9.1). While diffusion of SO_4^{2-} and SO_3^{2-} ions from the melt to the surface is fast, any elemental sulfur retained in the melt would decrease the rate of desorption from the surface. In

the case of low and medium loading sorbents this layer is only a few molecules thick and these effects become negligible. Finally, at high sorbent loadings the existence significant quantities of free sulfite ions in the molten layer becomes possible. In the derivation of the model all reactions were assumed to take place on the surface, and SO_3^{2-} was considered to be equivalent to SO_2^*/AlO_2^-. The possibility of homogenous reactions in the melt, such as the disproportionation of sulfite, introduces new complications that are not taken into account in this simple model.

REFERENCES

[1] Birk, J.R., Larsen, C.M., Vaux, W.G., and Oldenkamp, R.D., *Ind. Eng. Chem. Process Des. Develop.*, **10**(1), 7, 1971.

[2] Cameron, J.H., and Grace, M., *Ind. Eng. Chem. Fundam.*, **22**(4), 486, 1983.

[3] Craig, N.L., Harker, A.B., and Novakov, T., *Atmospheric Environment*, **8**, 15, 1974.

[4] Foerster, V.F., and Kubel, K., *Z. Anorg. Allge. Chem.*, **139**, 261, 1924.

[5] Khalafalla, S.E., and Haas, L.A., *J. Catal.*, **24**, 115, 1972.

[6] Lepsoe, R., *Ind. Eng. Chem.*, **32**(7), 910, 1940.

[7] Riggs, W.M., and Parker, M.J., *Methods of Surface Analysis*, Vol. 1, A.W. Czanderna (Ed.), Elsevier, 1975.

[8] Wagner, C.D. *Handbook of X-Ray Photoelectron Spectroscopy*, New York, 1975.

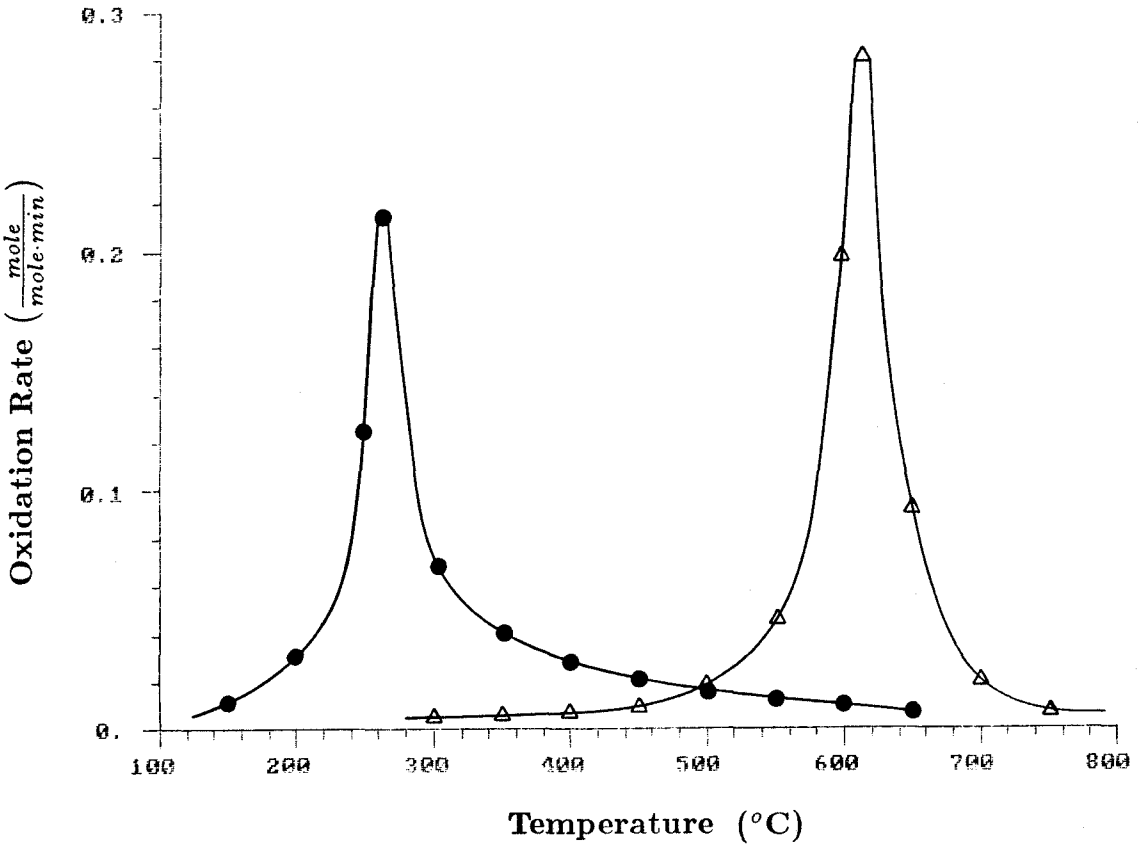

Figure 10.15. Temperature-Programmed Oxidation of Reduced Sorbent $ST\alpha 1$ (△) and Supported Sulfides (●).

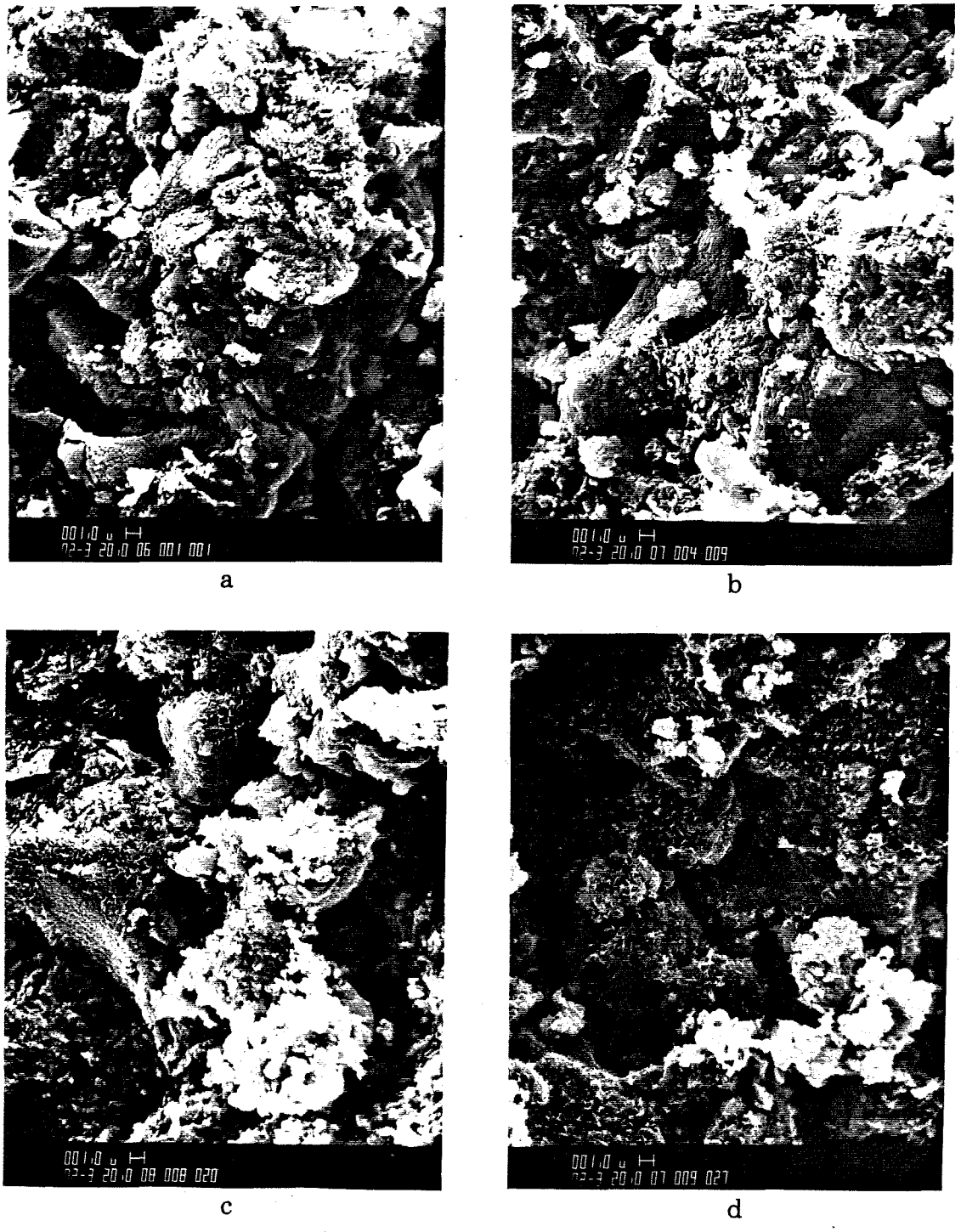

Figure 10.16. Scanning Electron Micrographs of α-Al_2O_3 Sorbent (a,b) Before, and (c,d) After Reduction; 1800X.

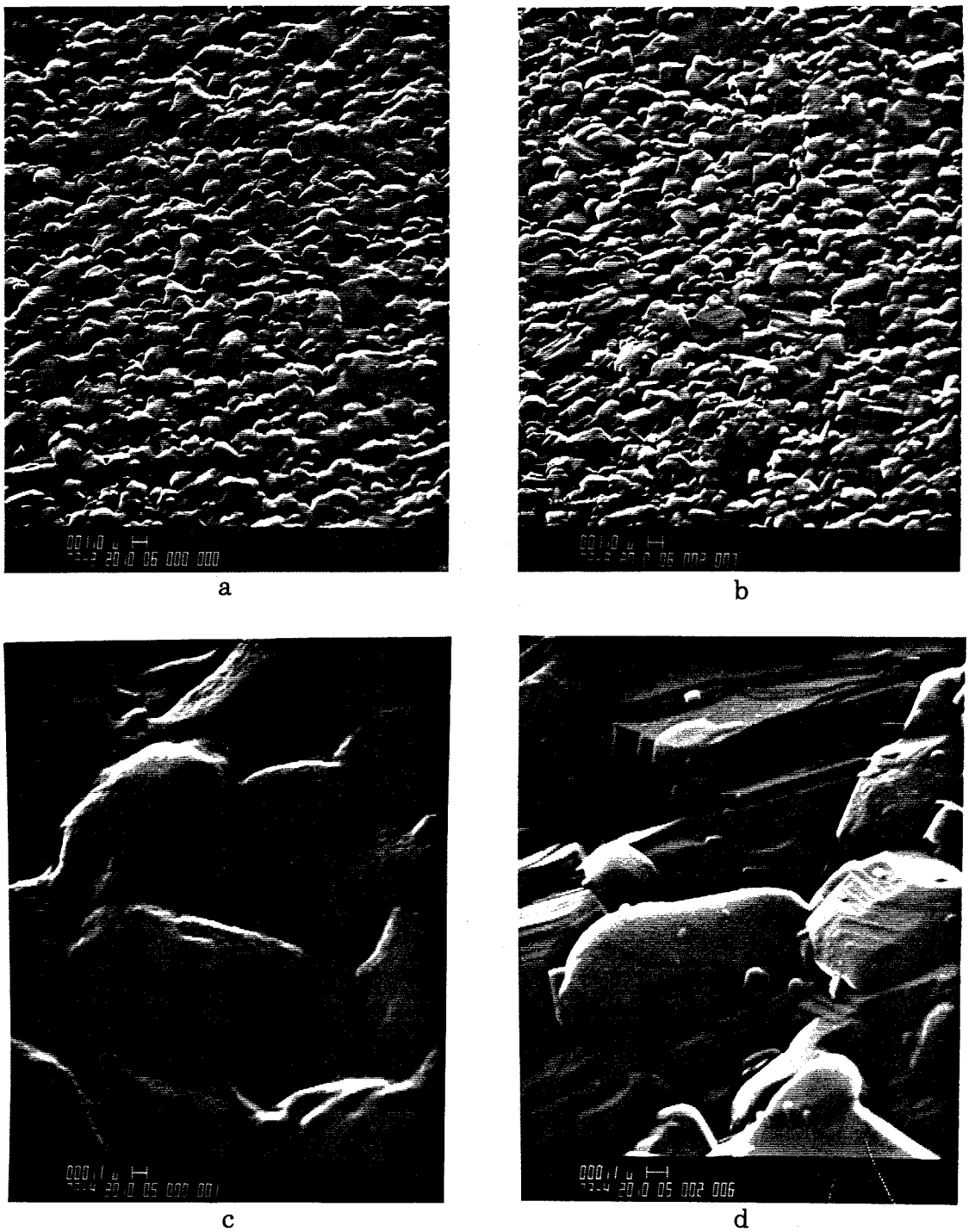

Figure 10.17. Scanning Electron Micrographs of (a,c) Al_2O_3 Film, and of (b,d) Sample ST2; (a,b) 1800X, (c,d) 18000X.

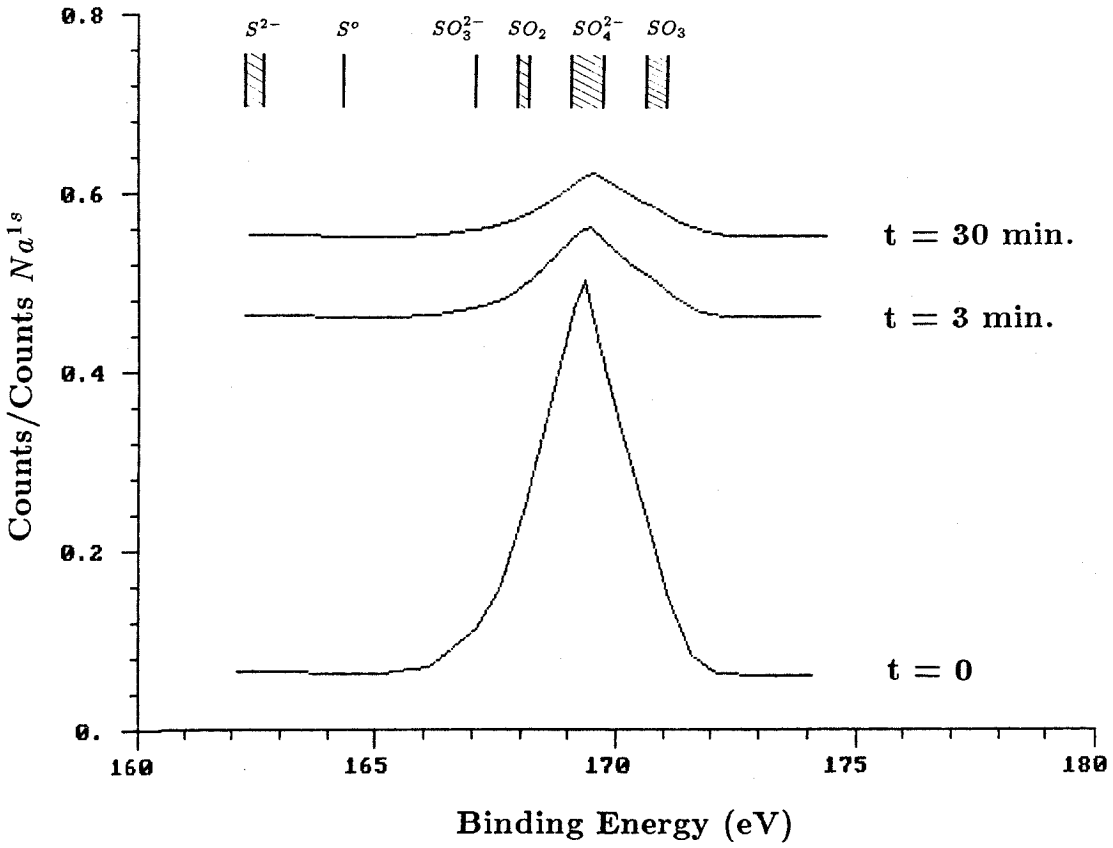

Figure 10.18. Sulfur 2p XPS Spectra of Sample *ST2* at Various Stages of Reduction.

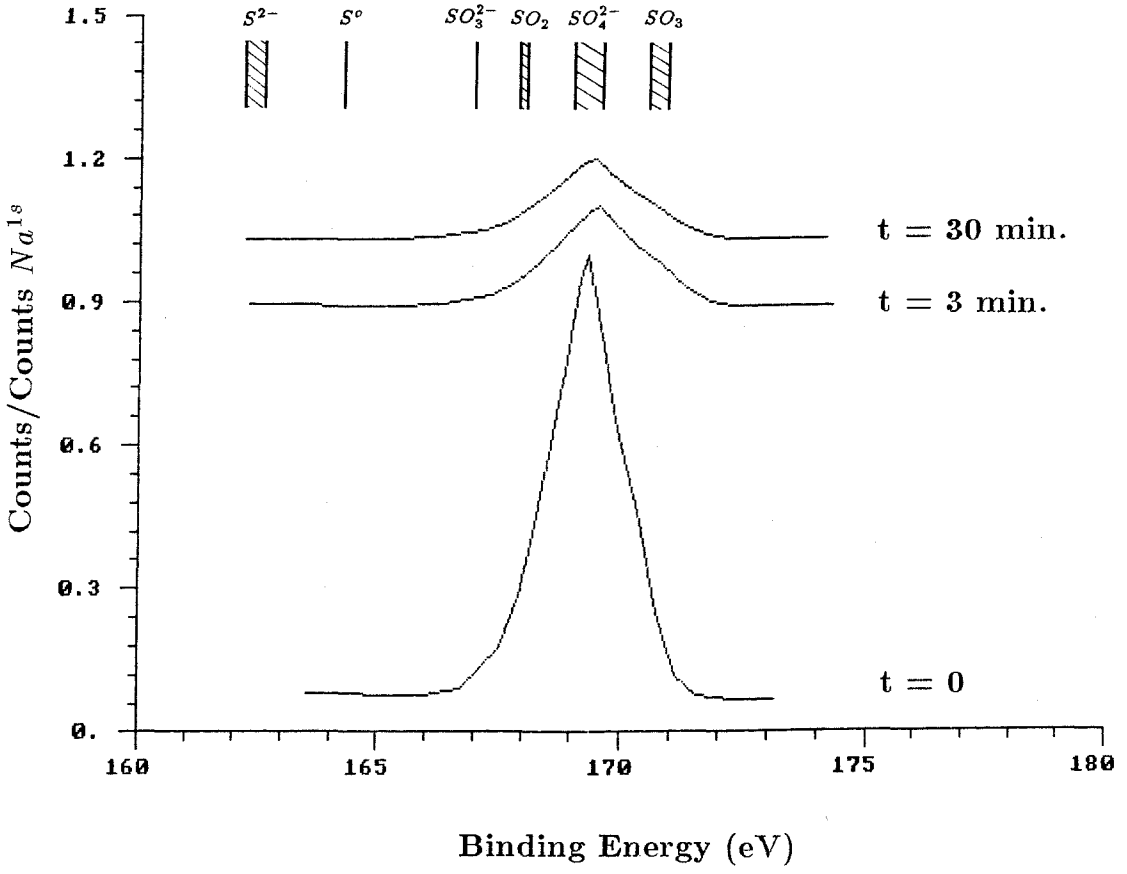

Figure 10.19. Sulfur 2p XPS Spectra of Sample *AC*1 at Various Stages of Reduction.

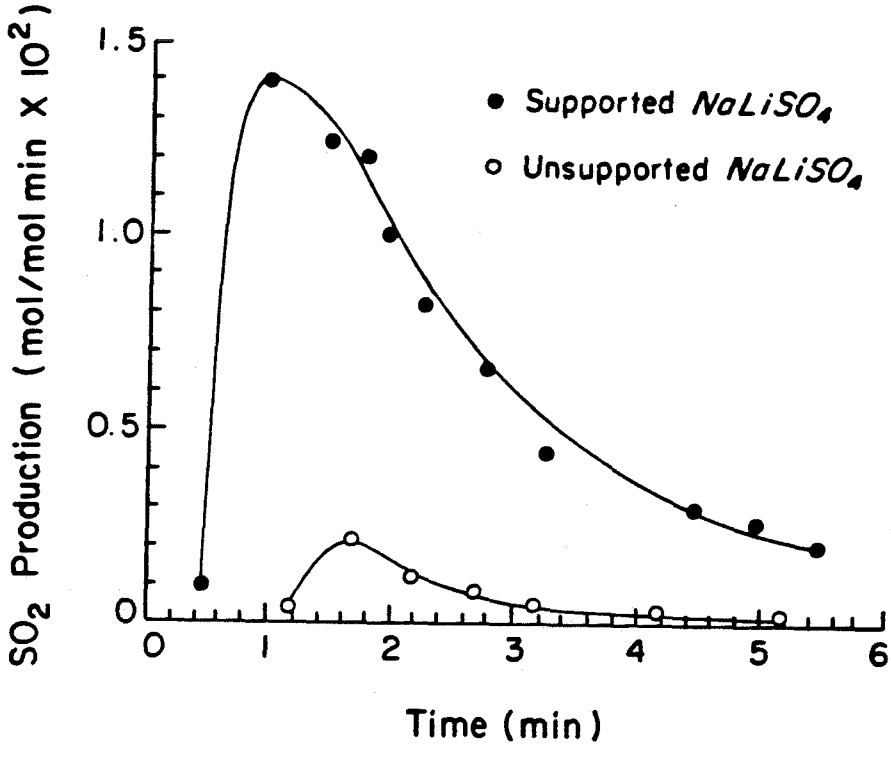

Figure 10.20. Effect of the Alumina Surface on the Rate of Production of SO_2.

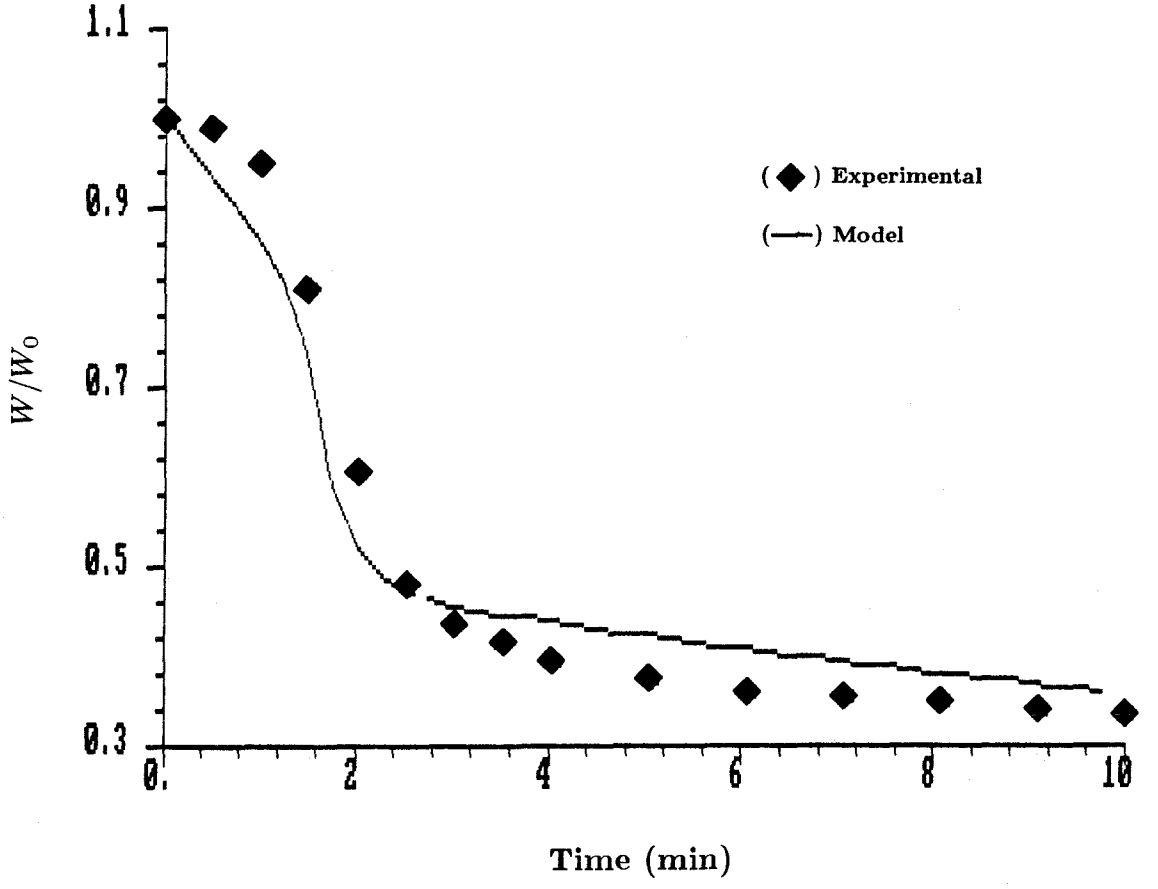

Figure 10.21. Kinetic Model I: Weight Loss.

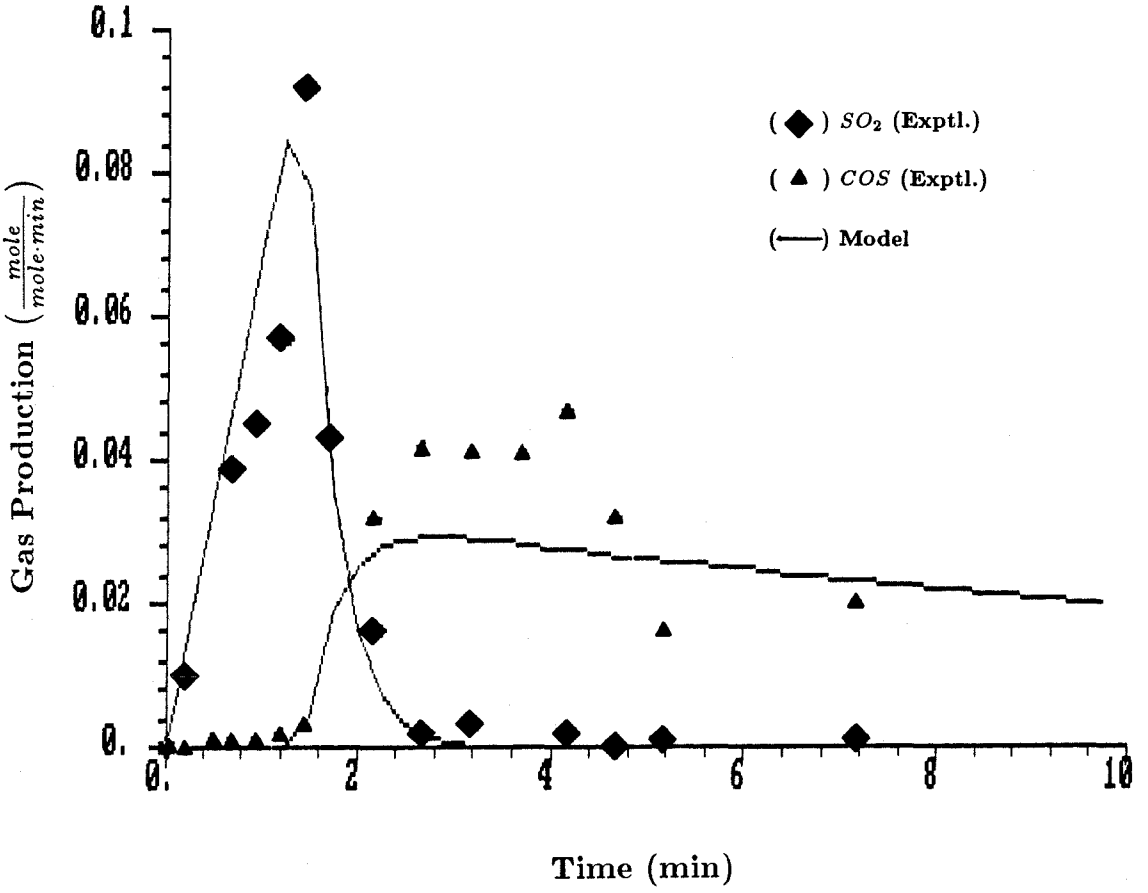

Figure 10.22. Kinetic Model II: Gas Production.

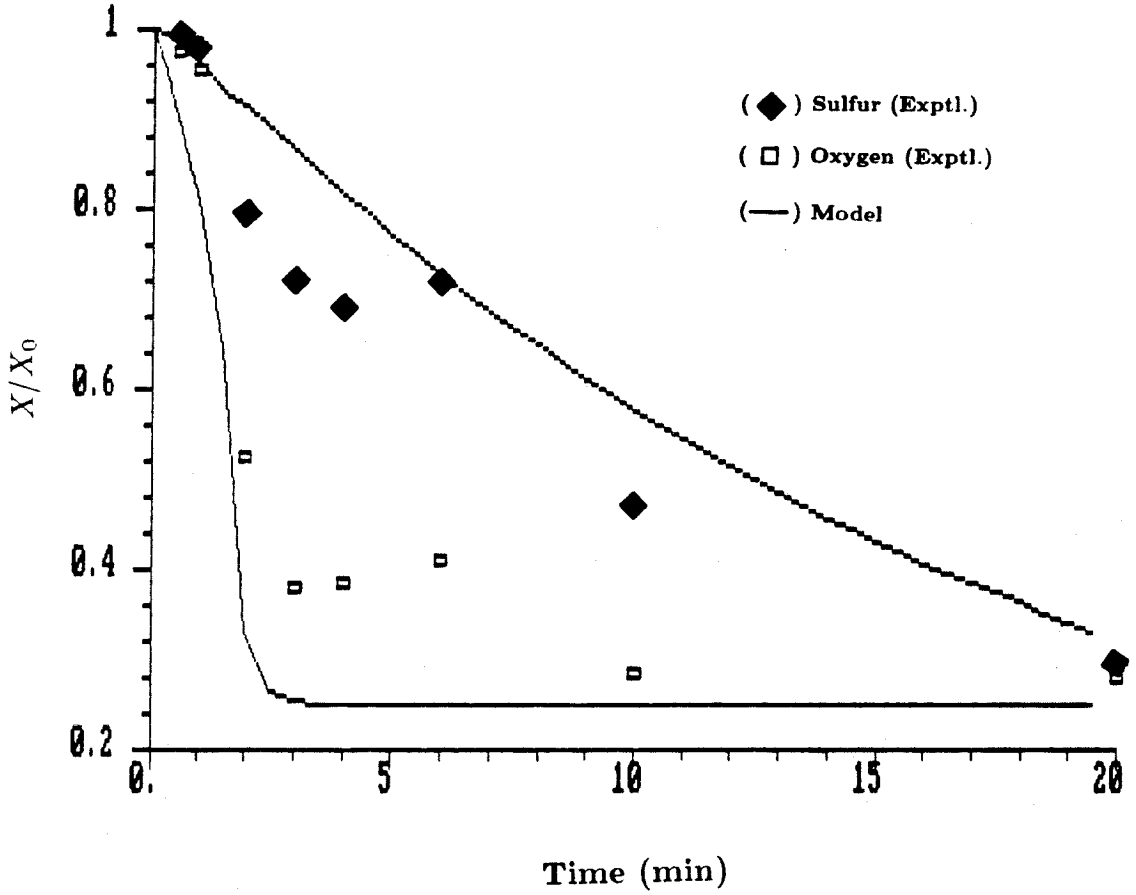

Figure 10.23. Kinetic Model III: Elemental Composition.

11. CONCLUSIONS AND SUGGESTIONS FOR FUTURE RESEARCH

11.1. Conclusions

1. The sorbent studied consists of a thin layer of sodium and lithium aluminate, supported on alumina. This layer reacts readily with SO_2 at 700-800^oC, but not with CO_2. Any alkali carbonate formed would decompose rapidly to form aluminate.

2. Sorbents prepared by calcination of alkali carbonates or alkali acetates, or by reduction of alkali sulfates behave identically with respect to sulfation and regeneration.

3. Sulfation proceeds to completion, at higher rates than bulk materials under similar conditions. The rate is proportional to the concentration of SO_2 in the gas, up to $[SO_2] \approx 5000$ ppm. Since all diffusion processes are fast, the overall rate is limited by the rate of reaction, which has an activation energy $E = 21.6$ kcal/mole.

4. The sorbent can be repeatedly regenerated. Regeneration leads to the recovery of the alkali aluminate, and some residual sulfur.

5. Although α-Al_2O_3 has lower surface area than γ- and χ-Al_2O_3, it constitutes a better support from the point of view of regenerability and rate of sulfur removal.

6. The rate of sulfur removal increases with increasing temperature, alkali to alumina ratio, and carbon monoxide concentration, and is higher when-

α-Al_2O_3 is used as a support. The selectivity towards elemental sulfur also increases with temperature and the ratio of alkali to alumina. but decreases with CO concentration.

7. Regeneration proceeds in two stages, through a complex network of highly coupled reactions. The main reactions that take place during those stages are :

   7.1. Reduction of the sulfate to sulfite and sulfur dioxide, which consitutes the only gaseous product during the first stage. This reaction is catalyzed by the alumina surface.

   7.2. Upon depletion of the sulfate, gaseous elemental sulfur and COS are formed by reduction of sulfite and chemisorbed SO_2, and further reaction with CO. Both reactions are catalyzed by Al_2O_3. This stage is characterized by rapid loss of oxygen due to the reduction of sulfite and chemisorbed SO_2. Weakly held elemental sulfur desorbs and reacts with CO. More strongly held sulfur is slowly removed as COS.

8. The residual sulfur consists of a reduced surface species, strongly coordinated to sites present in porous Al_2O_3, or to the aluminate. This species is more stable to oxidation than alkali sulfides. The properties of this species are closely tied to the properties of the alumina.

9. The effect of the support on the regeneration can be summarized as follows :

   9.1. The formation of aluminate makes the regeneration thermodynamically favorable, and precludes the formation of carbonates.

   9.2. It catalyzes the sulfate reduction during the first stage.

9.3. It catalyzes the reduction to elemental sulfur and the formation of COS during the second stage.

9.4. It acts as an adsorbent for reaction products, such as SO_2 and elemental sulfur.

9.5. By forming surface compounds, it alters the properties of reaction intermediates, such as alkali sulfite.

10. A simplified kinetic model adequately describes the regeneration at moderate sorbent loadings.

11.2. Suggestions for Future Research

Several areas remain open for further investigation :

1. The interaction between elemental sulfur and alumina needs to be studied in greater detail. This problem is relevant both to the direct catalytic reduction of SO_2 (Part I) and to the mechanism of sorbent regeneration (Part II). In particular, two aspects of this problem should be explored :

   1.1. *The effect of the active surface sites on the binding energy*: As suggested by the SO_2 adsorption experiments (Part I), it is possible that sulfur chemisorbs with varying strengths. Novel techniques are being developed to grow alumina films by oxidation of aluminum, with similar physical and chemical properties to commercial catalysts [1,2]. These films could be used in conjunction with sensitive surface techniques such as FTIR spectroscopy and XPS to study the adsorptive

behavior of elemental sulfur.

1.2. *The adsorptive properties of sulfur obtained by reduction of SO_2*: Information about the reduction of SO_2 to elemental sulfur, and the adsorption/desorption of both species could be obtained using a temporal analysis technique, wherein a small number of molecules (i.e., 10^{10}-10^{30}) is pulsed into a bed of alumina particles, and the composition of the effluent followed using mass spectrometry. This technique would also be useful to study the gas compostion during sorbent regeneration.

2. The effect of the alumina structure and the alkali to alumina ratio on the composition of the sorbent during reduction requires further study. Due to the presence of sulfur compounds with varying oxidation states, XPS would probably be the most suitable technique to identify reaction intermediates.

3. In order to extend the kinetic model to predict the behavior of a regeneration reactor, it is necessary to study the readsorption and reaction of the gaseous products. The progression of these products through a packed bed of sorbent can be followed using mass spectrometric temporal analysis.

REFERENCES

[1] Cocke, D.L., Johnson, E.D., and Merrill, R.P., *Catal. Rev.-Sci. Eng.*, **26**(2), 163, 1984.

[2] Hansma, P.K., Hickson, D.A., and Schwartz, J.A., *J. Catal.*, **48**, 237, 1977.

APPENDIX A: DATA ACQUISITION SYSTEM

An *ad hoc* microprocessor-based system was assembled to carry out the data acquisition and manipulation. This Appendix provides a brief description of the system and related software.

A.1. Hardware

The system consists of a modular S-100 unit equipped with seven plug-in Compupro boards. An 8-bit Z-80 microprocessor board, running at 4 MHz, was used for data acquisition and most of the data processing. The board allows vectored interrupt operation. A 16-bit 8086 microprocessor board equipped with a 8087 high-speed math coprocessor was also used for long calculations and memory- demanding tasks. The CPU was interfaced to a keyboard, CRT monitor and printer through an Interfacer-4 board, to a pair of Qume Datatrack 8" disk drives through a Disk-1A controller, and to 256 kilobytes of random-access memory.

The analog-to-digital conversion and timing are performed by a set of Tecmar S-100 AD212 boards. A plug-in mother board has the S-100 bus interface, an AM9513 timer containing five 16-bit cascadable counters and two alarm comparators, and the associated control logic. This board was configured to operate with input/output-mapped, 8 or 16-bit transfers, although memory-mapped operation is also possible. A remote daughter board connected to the mother board by a ribbon cable contains the data acquisition subsystem, consisting of a DT5712-PGL module from Data Translation, Inc., and associated

circuitry and jumpering. This module has eight true differential analog inputs, 12-bit accuracy, a 30 KHz conversion rate, and an instrumentation amplifier with programmable gains up to 500. The CPU communicates to these boards through a set of read/write registers for counter arming and reading, channel selection, A/D conversion strobing, etc.

The instruments were interfaced to the daughter board through a set of BCD connectors and RC filters located in a shielded box. Both the box and the daughter board were installed near the instruments, to minimize noise pickup. Proper grounding and shielding of each component were critical to ensure low noise level at gains higher than 100. A block diagram of the system is shown in Fig. A.1.

A.2. Software

A line editor, Pascal compiler, assembler, debugger, and CP/M operating system were available for both microprocessors. A set of programs was developed to carry out real time data acquisition and further processing. A list of the programs, procedures, and functions is given in table A.1. Routines P1, P2, P3, P4, P5, P53, P54, P55, P59, P60, and P61 carry out basic communication tasks, such as setting the timer counter modes, loading and arming the counters, reading the timer, selecting the analog channel, trigger A/D conversions, etc. These simple tasks that are performed a large number of times were written in assembly language. The main data acquisition programs P17, P20, P22, P42, P44, P68, P69, P70, P71, P72, and P73 that make use of those procedures were

written in Pascal. The procedures and functions utilized by the main programs were grouped in separate modules, designated M–FILENAME. The inverted tree programming structure is illustrated in Fig. A.2.

At the beginning of each session the A/D converter was calibrated using P6. In most cases, the offset error was not very significant. Zeroing of the TGA and initial weight measurements were done prior to each run using P8. The GC was calibrated by washing out a stirred tank containing known initial concentrations of SO_2 and COS, and recording the exit concentrations with program P7. Calibration constants are obtained with P37 and P57 after the calibration run. Program P20 duplicates some of the functions of a standard chromatografic integrator. The GC data reduction programs were written to handle inputs from a separate integrator.

After the experiments the data were reduced (P30, P31, P32, P64), and then printed (P15, P18, P19, P52), plotted (P13, P14, P33, P34, P46, P47, P48, P49, P51), or reformatted and sent to a mainframe computer (P56). Detailed program descriptions and listings with comments are available at the Caltech Chemical Engineering Laboratory, Room 338A.

REFERENCES

[1] Cassel, R.B., and Gray, A.P., "Microprocessor-Controlled Thermogravimetric Separations," *Thermochimica Acta*, **36**, 265, 1980.

[2] Osborne, A., "An Introduction to Microcomputers," Adam Osborne and Associates, Berkeley, 1978.

[3] Sargent, M., and Shoemaker, R.L., "Interfacing Microcomputers to the Real World," Addison-Wesley, Massachusetts, 1981.

[4] Tseng, H.P., Christman, P.G., and Edgar, T.F., "Computer Control and Data Acquisition for a Thermogravimetric Analyzer," *Chem., Biomed., and Environ. Instrumentation*, **11**(5 & 6), 377, 1981.

[5] Wilson, I.R., and Addyman, A.M., "Pascal, An Introduction," Springer-Verlag, New York, 1978.

Table A.1. List of Programs.

P#	Name	Description
P1	AD01	Generates wait loop, converts and input voltage from any channel
P2	AD02	Converts and inputs voltage from any channel
P3	AD03	Scans channels, converts and inputs voltage
P4	AD04	Generates wait loop, scans channels, converts and inputs voltage
P5	ADC	Converts and inputs voltage from any channel, gain=1
P6	CAL–AD	Finds A/D converter calibration constants to correct offset error
P7	CAL–GC	Collects GC calibration data, generates GC calibration file
P8	CAL–TGA	Interactively zeroes the TGA and measures initial sample weight
P9	CRCK	Finds file code to detect possible file changes
P10	CONST	Prints A/D converter calibration constants
P11	CONV–HEX	Converts timer output to Hex
P12	DISPLAY	A/D converter diagnosis program
P13	DRAW	Plots data files on the CRT monitor
P14	DRAW–TGA	Plots weight vs time data on the CRT monitor
P15	GAS–CONC	Prints gas concentration data from the GC
P16	GC–CONST	Prints the GC calibration constants

Table A.1. List of Programs (continued).

P#	Name	Description
P17	GC–DET	Outputs concentration from the GC flame-photometric detector
P18	GETDATA	Prints out time, weight, rate of weight change and temperature files
P19	GET–WT	Prints initial sample weight
P20	INT–GC	Detects GC peaks, separates fused peaks, does baseline correction and peak integration
P21	KEY	Boolean function, returns program to main menu
P22	LAB	Collects, displays, stores and processes data from TGA and GC
P23	LOOPS	Prints contents of file LOOPS.DAT (see MAKELOOP)
P24	LSQ	Performs least squares regression of gas concentration data
P25	MAKELOOP	Generates file LOOPS.DAT with volume of GC loops and tubing
P26	M–CALGC	Procedures and functions for program CAL–GC
P27	M–CALTGA	Procedures and functions for program CAL–TGA
P28	M–INTGC	Procedures and functions for program INT–GC
P29	MKGCCONS	Creates file containing GC calibration constants
P30	MKGCDAT	Creates a plottable file with gas concentration vs. time data
P31	MKTGADAT	Reduces TGA data files into plottable file TGADATA.ijk
P32	MKTGAIR	Reduces TGA and IR spectrometer data into a plottable file

Table A.1. List of Programs (continued).

P#	Name	Description
P33	MKPLOT1	Plots TGA data vs. time on the Bausch & Lomb plotter
P34	MKPLOT2	Plots TGA and GC data vs. time on the Bausch & Lomb plotter
P35	M–LAB	Procedures and functions for program LAB
P36	M–MODI	Procedures and functions for program MODIFY
P37	MODIFY	Plots and processes GC calibration data, calculates calibration constants
P38	M–OUT–AD	Procedures and functions for program OUT–AD
P39	M–NOISE	Procedures and functions for program NOISE
P40	M–THERMO	Procedures and functions for program THERMO
P41	NOISE	Performs statistical analysis of A/D converter noise
P42	OUT–GC	Outputs voltage from GC flame-photometric detector
P43	OUTIME	Saves and inputs contents of time of day registers
P44	OUT–TGA	Outputs the weight, rate of weight change and temperature of the TGA
P45	PATCH	Links data files from different or interrupted TGA runs
P46	PLOT	Plots TGA, IR, and GC data on the CRT monitor
P47	PLOTDERV	Plots the rate of weight change on the Bausch & Lomb plotter
P48	PLOTGC	Plots the gas concentration data on the Bausch & Lomb plotter

Table A.1. List of Programs (continued).

P#	Name	Description
P49	PLOTEMP	Plots the TGA temperature on the Bausch & Lomb plotter
P50	PLOTLIB	Procedures and functions to drive the Bausch & Lomb plotter
P51	PLOTWT	Plots the sample weight on the Bausch & Lomb plotter
P52	PRINT–GC	Prints out the gas concentration data
P53	READ–HSECS	Saves the contents of the 1/100 sec. timer counter
P54	READ–SECS	Saves the contents of the seconds timer counter
P55	READ–TIME	Saves and inputs the contents of the time of day registers
P56	REFM	Reformats CP/M-formatted disks to the PDP-11 format
P57	REGRESS	Finds GC calibration constants by linear regression
P58	SCOMPARE	Compares data files
P59	SET–AUTO	Sets board for auto-incrementing mode (channel scanning)
P60	SETIME0	Sets the AMD 9513 timer for time of day operation, initial time = 0
P61	SETIME1	Sets the AMD 9513 timer for time of day operation, arbitrary time
P62	SHOW	Interactively reads and writes from and to A/D and timer registers

Table A.1. List of Programs (continued).

P#	Name	Description
P63	SHOW–AD	Prints output of and A/D channel in binary form, for diagnosis
P64	SMOOTHNG	Smooths data and computes derivative using a weighed average method
P65	SPEED	Determines rate of conversion of A/D module
P66	SWEEP	Data file manager
P67	TEMP	Converts voltage from TGA thermocouple to temperature (^oC)
P68	TGA	Continuously collects, displays and stores TGA data
P69	TGA1	Continuously collects, displays and prints TGA data
P70	TGA2	Continuously collects, displays, prints and stores TGA data
P71	TGA3	Continuously collects, displays and prints TGA data storing at the end
P72	TGA–GC	Continuously collects, displays and stores TGA and GC data
P73	TGA–IR	Continuously collects, displays and stores TGA and IR spectrometer data
P74	THERMO	Continuously outputs the TGA temperature
P75	WT–SECS	Generates a waiting loop of arbitrary duration

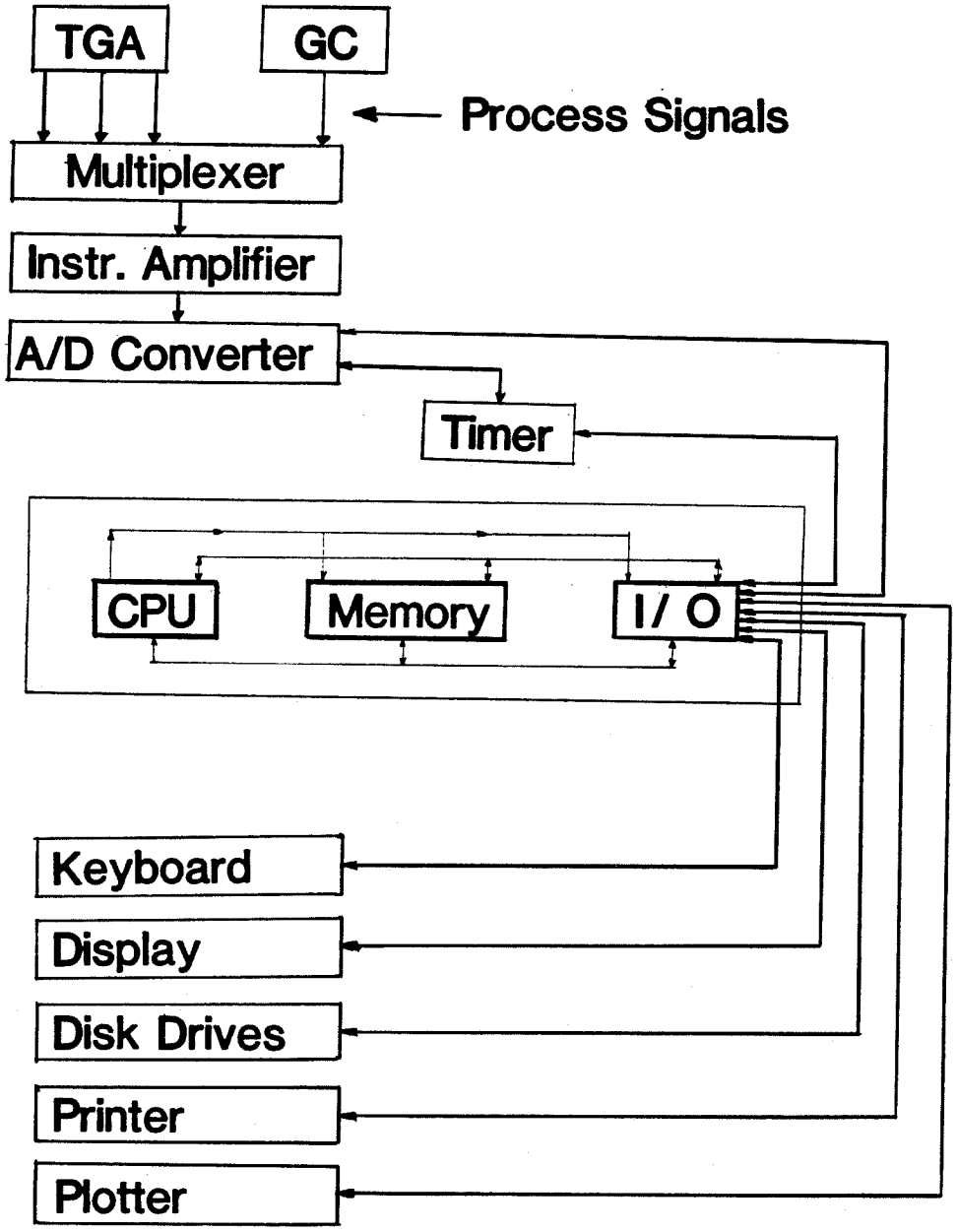

Figure A.1. Block Diagram of the Data Acquisition System

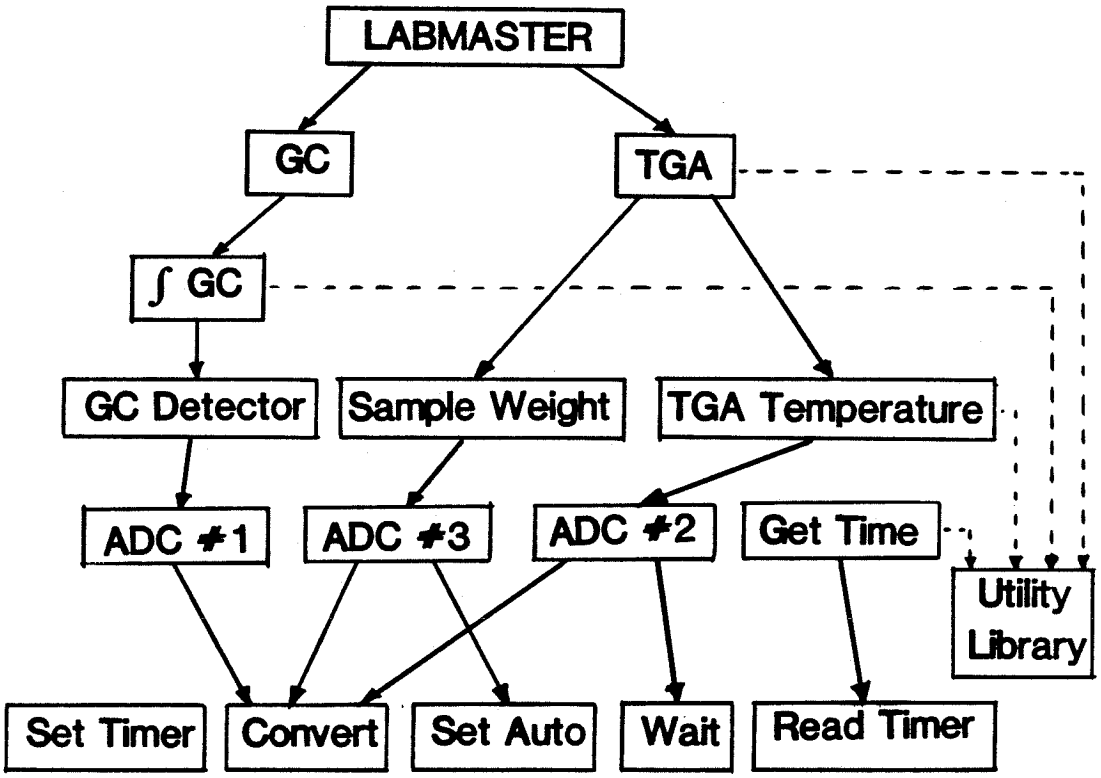

Figure A.2. Data Acquisition Software

APPENDIX B: TGA TEMPERATURE PROGRAMMER

A microprocessor-based temperature programmer and controller (TPC) was designed and assembled to program the heating and control the temperature of the TGA reaction chamber. The TPC generates a digital version of the temperature in the reaction chamber which is further processed to send a heating pattern to an electric furnace via a solid-state relay. Interaction with the system is provided by a set of seven-segment displays, a keypad and a set of LED's. A serial port is also provided to interface the controller to the data-acquisition system described in Appendix A.

B.1. Hardware

The heart of the controller is a 6802 microprocessor, running at 1 MHz. The microprocessor is interfaced to a MC6850 ACIA, a 2716 EPROM, a ADC0802 A/D converter, a set of six LED's, a keypad, four multiplexed seven-segment displays, and an optically isolated triac through suitable buffers.

Since only about 90 bytes of RAM are required, the internal RAM available in the 6802 was sufficient. A MC14411 bit-rate generator is used both for the ACIA and as an interrupt-signal generator that can be latched by means of a D-Q flip-flop. Interrupts are generated at a rate of 600 Hz. for scanning the displays and keypad and also for timing the heating process. Four seven-segment displays were used to display the temperature and the heating parameters. Since no BCD to 7-segment decoders were used this conversion is

done by the program.

The temperature of the furnace is measured with a chromel-alumel thermocouple. The signal from the thermocouple is amplified to the ADC range (0 to +5VDC) by means of a AD595 instrumentation amplifier, which also provides cold junction compensation. The temperature is digitized by an 8-bit ADC0802 analog-to-digital converter, limiting the accuracy to $4°C$ in a 0-1100$°C$ range.

Power to the furnace is supplied through an optically isolated triac with zero-crossing detection, rated for 25 A at 240 VAC. The triac was mounted on a thick aluminum slab to dissipate the heat. Finally, one 2-kilobyte EPROM was used to store the control program.

B.2. Software

The TPC programs were developed in a Hewlett Packard 68000 system and downloaded onto a set of 2 kbyte EPROM's. Upon reset, the system strobes the ADC and displays the temperature of the furnace, in $°C$. Both the keypad and the seven-segment displays are scanned continuously by the interrupt routines. When a key is pressed, the final temperature ($°C$) and the heating rate ($°C$/min) are entered and displayed. If maximum values of 1200$°C$ and 100$°C$/min are exceded, an error message is diplayed and the parameters can be re-entered. Otherwise, the heating process starts.

Pulses are sent to the heater at a rate of 6 sec^{-1}. The pulse width is determined according to a proportional-integral control algorithm. The error is calculated as the difference between the set-point temperature, determined from

the heating pattern, and the measured temperature. Since the response of the furnace was very fast, a proportional control was satisfactory for all practical purposes.

During the heating the set-point temperature is increased linearly at the desired rate. Once the final temperature is attained, the set-point remains constant. A program is also available to handle an arbitrary change of the set-point temperature from the data-acquisition computer through the serial port. A manual containing a detailed description of the controller, its program, memory map, flow diagram, operation, and program listing with comments is available at the Caltech Chemical Engineering Laboratory, Room 338A, or from the author.